Inaugural dissertation

for

obtaining the doctoral degree

of the

Combined Faculty of Mathematics, Engineering and Natural Sciences

of the

Ruprecht - Karls - University Heidelberg

Presented by

M.Sc. Valerie Griesche

born in: Ingolstadt, Germany

Oral examination: September 15th 2025

The Impact of Adenosine mRNA Modifications on Macrophage Function

Referees: Prof. Dr. Nina Papavasiliou

Prof. Dr. Dr. Georg Stoecklin

ACKNOWLEDGMENTS

I deeply appreciate the help and support from everybody who made my PhD studies possible and accompanied me along the journey.

First and foremost, I would like to give a huge thank you to my supervisor Nina. Thank you for giving me the opportunity to do my PhD in your lab, to provide guidance, advice, and support, for believing and trusting in me throughout my PhD, to be so approachable and to always make time for a meeting when needed (despite your crazy schedule), supporting my travel to many great conferences and encouraging my personal growth also beyond the science. Thank you for being the best supervisor that I could have asked for.

I would like to thank my thesis examination and thesis advisory committee members Prof. Dr. Dr. Georg Stoecklin, Prof. Dr. Martina Muckenthaler, and Prof. Dr. Alexander Dalpke. Thank you for immediately agreeing to be part of my committees and taking the time to justly evaluate my dissertation. Thank you for the engaged discussions and support during my TAC meetings and the fruitful collaborations that contributed to the success of my PhD.

I would like to thank Christina and Maria for providing murine bone marrow cells and advice in BMDM differentiation, Chih for the nice collaboration and ribosome sequencing, Martina and Martin for your help in LC-MS/MS, Steffen for cell sorting and the next generation sequencing core facility for library preparation and Illumina sequencing.

A warm thank you to every member of D150, D160 and Panosome, and every student who joined the group during the course of my PhD. Thank you so much for being amazing lab mates and friends throughout and beyond my PhD journey. Thank you for all the help, advice, scientific and mental support, the laughter, scientific and non-scientific discussions inside and outside the lab, and for making me enjoying the time in the lab even when experiments were not going the way I hoped for. My PhD would not have been the same without you as my lab family.

Among the people from my lab, I would like to give a special thanks to Ricca: Thank you for always being available for providing advice, help and discussions that crucially contributed to the success of my PhD, thank you for reviewing my manuscript and my thesis. You truly acted as deputy group leader already years before your official nomination. A huge

thank you goes to Salvo: What would I have done without all your dedication to the bioinformatic analysis of my data? Thank you for all the time and energy you invested in this project. I really enjoyed working together with you and I am looking forward to share a publication with you! Thank you to Laura and Caterina to provide the best company in the girl's office. Sadly we are missing a seat in the office for Eliana! Sharing the struggles but also great achievements and memories with you can only make life better. A big thank you also goes to Annette, the good soul of the lab. Thank you for keeping the lab running, taking care of last-minute orders and for any advice on lab protocols and other lab-related issues!

I am very grateful for the amazing support from my family. Thank you to my parents who are without doubt my biggest supporters in anything I do, for making my studies in the US and in Germany possible, for raising and shaping me into the person I became and for giving me the courage to make bold decisions. Thank you to my brother Christian for setting an example by obtaining the first PhD in the family, for providing help and guidance in everything that is outside my skillset and comfort zone without any hesitation. A big thank you to my sister Cornelia for sharing my passion for sports and outdoor activities, regular cat-content, endless stories and laughter, and for being the person I can talk to about anything that is on my mind.

I would also like to express my huge gratefulness for my boyfriend Jaime. Thank you for accompanying me throughout my Master, PhD and beyond. For sharing my struggles and listening to my complains and worries, but also for sharing my excitement and all of the great moments and experiences in life. Thank you for letting me wake you up every weekend, for always accommodating my usually busy (sports) schedule, and for doing all the things that make me happy and let me smile every day. Having somebody by my side who understands, supports and believes in me throughout my PhD means a lot to me. I could not have imagined this journey without you.

Thank you to everybody else who was part of my PhD journey. I am grateful for every friend, colleague and collaborator, for every shared experience, and every memory that forms part of my time in Heidelberg and made my PhD experience unique and enjoyable.

ABSTRACT

Macrophages are innate immune cells characterized by a high level of plasticity, which enables their quick adaptation to a changing environment required for initiating, promoting, and resolving inflammatory processes to protect from external threats and maintain tissue homeostasis. Such reprogramming cannot be achieved via transcriptional changes alone, and therefore RNA modifications on macrophages' transcripts play a crucial role in allowing such versatility needed for a fast and adaptive response. Utilizing the mouse macrophage cell line RAW 264.7 (RAW) as a model system, I investigated the impact of METTL3-mediated m6A and ADAR1-mediated adenosine-to-inosine (A-to-I) editing on macrophage pro-inflammatory activation and immune function. Mapping A-to-I editing sites using short-read Illumina sequencing and m6A using single molecule Nanopore sequencing in RAW macrophages with wild-type genotype or genetic defects in *Adar1* or *Mettl3*, I identified RNA modification sites on more than half of the genes that are involved in macrophages' immunological functions. Gene expression analysis revealed that loss of m6A induced innate immune sensing, whereas loss of A-to-I editing dampened innate immune activation in macrophages. Additionally, transcriptomic analysis identified ADAR1's and METTL3's crucial role in macrophage activation in response to pro-inflammatory stimuli. Using functional assays, I confirmed METTL3's and ADAR1's impact on macrophage activation such as the upregulation and presentation of immunostimulatory cell surface markers and phagocytosis activity. While m6A levels remained mostly stable upon ADAR1 depletion, loss of METTL3 globally decreased A-to-I editing levels after pro-inflammatory stimulation. Besides the regulatory effect of some m6A sites on the *Adar1* transcript that impact *Adar1*'s splicing and translation into protein, I found a positive association between A-to-I and m6A sites in transcripts where the modifications were placed at a distance above 139 nucleotides, suggesting a role of m6A in supporting ADAR1-mediated editing. Using a reporter assay for targeted ADAR1 editing, I observed increased ADAR1 recruitment and editing when ADAR1-engaging guide RNAs contained m6A modifications as compared to unmodified guide RNAs. Collectively, the demonstrated interdependency between m6A and A-to-I RNA modifications holds potential to advance therapeutic RNA editing strategies in the future.

ZUSAMMENFASSUNG

Makrophagen sind Zellen des angeborenen Immunsystems, die sich durch ihr hohes Maß an Plastizität auszeichnen. Diese ermöglicht ihre schnelle Anpassung an eine sich verändernde Umgebung, was erforderlich ist, um Entzündungsprozesse zu initiieren, voranzutreiben und zu beheben - zum Schutz vor äußeren Bedrohungen und zur Aufrechterhaltung der Gewebehomöostase. Diese Umprogrammierung von Makrophagen kann nicht allein durch transkriptionelle Veränderungen hervorgerufen werden. Daher spielen RNA-Modifikationen in den Transkripten von Makrophagen eine entscheidende Rolle, um die nötige Vielseitigkeit für eine schnelle und anpassungsfähige Reaktion zu ermöglichen. Unter Verwendung der murinen Makrophagen-Zelllinie RAW 264.7 (RAW) als Modellsystem untersuchte ich die Auswirkungen der METTL3-vermittelten m6A Modifizierung und der ADAR1-vermittelten Adenosin-zu-Inosin (A-zu-I)-Editierung auf die proinflammatorische Aktivierung und die Immunfunktion von Makrophagen. Durch die Katalogisierung von A-zu-I-Editierungspositionen mittels Kurzlese-Illumina-Sequenzierung und m6A Positionen mittels Einzelmolekül-Nanopore-Sequenzierung in RAW-Makrophagen mit Wildtyp-Genotyp oder Gendefekten in *Adar1* oder Mettl3 identifizierte ich RNA-Modifikationspositionen in mehr als der Hälfte der Gene, die an der immunologischen Funktion von Makrophagen beteiligt sind. Eine Genexpressionsanalyse in Makrophagen ergab, dass der Verlust von m6A die angeborene Immunerkennung aktiviert, während der Verlust der A-zu-I-Editierung die angeborene Immunaktivierung abschwächt. Darüber hinaus identifizierte die Transkriptomanalyse die entscheidende Rolle von ADAR1 und METTL3 bei der Makrophagenaktivierung als Reaktion auf proinflammatorische Stimuli. In funktionellen Untersuchungen bestätigte ich den Einfluss von METTL3 und ADAR1 auf die Makrophagenaktivierung, insbesondere auf die Hochregulierung und Präsentation von immunstimulierenden Zelloberflächenmarkern und die Phagozytoseaktivität. Während die m6A-Konzentrationen nach Verlust von ADAR1 weitgehend konstant blieben, führte der Verlust von METTL3 zu einem globalen Rückgang der A-zu-I-Editierung. Ich identifizierte eine regulierende Wirkung einiger m6A-Modifikationen auf dem *Adar1*-Transkript, die sich auf das Spleißen und die Proteintranslation von *Adar1* auswirken. Außerdem stellte ich eine

positive Assoziation zwischen A-zu-I- und m6A-Positionen fest, wenn sich diese in einem Abstand von mehr als 139 Nukleotiden befanden. Dies weist auf eine förderende Rolle von m6A bei der ADAR1-vermittelten RNA-Editierung hin. Mit einem Reporterassay zur gezielten ADAR1-Editierung konnte ich eine verstärkte ADAR1-Rekrutierung und -Editierung beobachten, wenn ADAR1-aktivierende Leit-RNAs m6A-Modifikationen anstelle von unmodifizierten Adenosinen beinhalteten. Zusammenfassend besitzt diese herausgestellte Wechselwirkung zwischen m6A- und A-zu-I-RNA-Modifikationen das Potenzial zukünfitge therapeutische RNA-Editierungsstrategien voranzutreiben.

TABLE OF CONTENTS

ABBREVIATIONS

Abbreviation	Name
3' UTR	3' untranslated region
A	Adenosine
A-to-I	adenosine-to-inosine
ADAR	adenosine deaminase RNA specific
ALKBH5	AlkB homolog 5, RNA demethylase
AP-1	activating protein-1
APC	antigen-presenting cell
ARG1	Arginase 1
ASO	antisense oligonucleotides
ATPase	Adenosine triphosphatase
b2M	beta-2-microglobulin
BMDM	bone marrow-derived macrophage
Cas9	CRISPR-associated protein 9
CD	cluster of differentiation
CPH	carboxypeptidase H
CPM	counts per million reads
CRISPR	clustered regularly interspaced short palindromic repeats
CTLA4	cytotoxic T-lymphocyte associated protein 4
ctrl	control
Cx3cr1	CX3C motif chemokine receptor 1
DAMP	damage-associated molecular pattern
DES	differentially editing sites
DM	differential methylation
DROSHA	double-stranded RNA-specific endoribonuclease
dsRNA	double-stranded RNA
E. coli	Escherichia coli
eGFP	enhanced green fluorescent protein
eIF3	eukaryotic initiation factor 3
FACS	fluorescence-activated cell sorting
FcγR	fragment crystallizable γ receptor
Fmr1	fragile X messenger ribonucleoprotein 1
FTO	fat mass and obesity-associated protein
G	guanosine
GFP	green fluorescent protein

GO	gene ontology
gRNA	guide RNAs
HNRNP	heterogeneous nuclear ribonucleoprotein
I	inosine
IFN	interferon
IFN-γ	interferon-γ
IFNAR	interferon-α/β receptor
IFNAR	interferon-α/β receptor
Ifnb1	Interferon-β1
Ifngr	interferon-γ receptor
IGF2BP	insulin-like growth factor mRNA-binding protein
IgG	immunoglobulin G
IKK	IκB kinase
IL	interleukin
Il1rl1	interleukin 1 receptor-like 1
indels	insertion-deletion mutations
iNOS	inducible nitric oxide synthase
IRF	interferon regulatory factor
IRF2BP	IRF2 assisted by interferon regulatory factor 2 binding protein
ISG	interferon stimulated gene
IVT	in-vitro transcribed
JAK	janus kinase
KO	knockout
LC-MS/MS	liquid chromatography with tandem mass spectrometry
LEAPER	leveraging endogenous ADAR for programmable editing of RNA
LINE	long interspersed nuclear element
Log2FC	log 2-fold-change
LPS	lipopolysaccharide
LRPPRC	leucine rich pentatricopeptide repeat containing
M-AAT	M-Alpha-1 antitrypsin
M-CSF	macrophage-colony stimulating factor
m5C	5-methylcytosine
m5U	5-methyluridine
m6A	N6-Methyladenosine
MAPK	mitogen-activated protein kinase
MARCO	macrophage receptor with collagenous structure
MAVS	mitochondrial antiviral signaling protein
MDA5	melanoma differentiation-associated protein 5

MedFI	median fluorescent intensity
METTL	methyltransferase
MHC II	major histocompatibility complex class II
miRNA	microRNA
mRNA	messenger RNA
MyD88	myeloid differentiation primary response 88
NF-κB	nuclear factor κB
NGS	Next Generation Sequencing
NK cells	natural killer cells
NKRF	NFKB repressing factor
NOD	nucleotide binding oligomerization domain containing
Nr4a1	nuclear receptor subfamily 4 group A member 1
nt	nucleotides
Oas	2′-5′-oligoadenylate synthetase
OasI	2'-5'-oligoadenylate synthetase like
ONT	Oxford Nanopore Technology
PAMP	pathogen-associated molecular pattern
PBS	phosphatebuffered saline
PCA	principal component analysis
PCR	polymerase chain reaction
PD1	programmed cell death 1
PKR	protein kinase RNA-activated
poly-A	poly-adenylated
Pparg	peroxisome proliferator activated receptor-γ
PRR	pattern recognition receptors
PS	lipid phosphatidylserine
Q	quartiles
RAW	RAW 264.7
RESTORE	Recruiting Endogenous ADAR to Specific Transcripts for Oligonucleotide-mediated RNA Editing
RIGI	retinoic acid-inducible gene I
RLR	RIG-I-like receptors
RNA	ribonucleic acid
rRNA	ribosomal RNA
RT-qPCR	reverse transcription quantitative PCR
S. aureus	Staphylococcus aureus
s2U	2-thiouridine

SAM	S-adenosylmethionine
sgRNA	single guide RNA
SINE	short interspersed nuclear elements
Snd1	staphylococcal nuclease and tudor domain containing 1
SR	scavenger receptor
ssRNA	single-stranded RNA
ssRNA	single-stranded RNA
STAT	signal transducer and the transcription
TAM	tumor-associated macrophage
TBK1	TANK-binding kinase 1
TCR	T cell receptor
TGF-β	transforming growth factor β
Th	helper T
TIR	toll/interleukin-1 receptor
TIRAP	TIR domain-containing adaptor protein
TLR	toll-like-receptor
TNF-α	tumor necrosis factor-α
Tor1aip2	torsin 1A-interacting protein 2
TRAF6	TNF receptor associated factor 6
Trem2	triggering receptor expressed on myeloid cells 2
TRIF	TIR domain-containing adaptor protein inducing interferon beta
tRNA	transfer RNA
Tsc1	tuberous sclerosis complex 1
TSS	transcription start site
TTS	transcription termination site
U	uracil
W	tryptophan
WT	wild type
WTAP	wilms' tumor 1-associating protein
YTHDC1	YTH N6-Methyladenosine RNA Binding Protein C1
YTHDF1	YTH domain-containing family protein 1
YTHDF2	YTH domain-containing family protein 2
Zbp1	Z-DNA binding protein 1
Ψ	pseudouridine

LIST OF FIGURES

LIST OF TABLES

Supplementary data

Appendix A

1. Introduction

1.1 RNA modifications

Since the first discovery of naturally formed chemical Ribonucleic acid (RNA) modifications in 1958[1], more than 150 different RNA modifications, mostly on rRNA and tRNA, have been reported up-to-date[2]. While most classes of RNA are modified throughout their life cycle, the effect of the modification on RNA metabolism is best understood for messenger RNA (mRNA), transfer RNA (tRNA), and ribosomal RNA (rRNA) such as their influence on transcription, stability, splicing, cellular localization, and translation[3]. RNA modifications enable a rapid and adaptable response to various stimuli, including oxidative stress, DNA damage, and anticancer treatments. In response to external stress, RNA-modifying enzymes regulate RNA stability to promptly modulate the proteome even before changes in transcription can occur. Hence, they are crucial for a cell to rapidly adapt to a changing environment[4].

1.1.1 m6A mRNA modification

Among a minimum of ten different mRNA modifications, N6-Methyladenosine (m6A) is the most prominent internal mRNA modification[3]. Catalytic methyltransferase 3 (METTL3), METTL14 and wilms' tumor 1-associating protein (WTAP) constitute the core of the m6A writer complex that is almost exclusively responsible for the m6A deposition in eukaryotic mRNA[5]. Together with additional associated proteins, the complex facilitates methylation of adenosines (A) under consumption of S-adenosylmethionine (SAM)[6]. METTL16 was reported to methylate at least one transcript independently from METTL3, but it plays a negligible role in global m6A levels in mRNA[7,8]. METTL3 predominantly deposits m6A in the consensus DRACH motif (with D = G/A/U, R = G/A, H = A/U/C)[9]. Despite its sequence preference, DRACH motifs are not always methylated. Further, m6A is also frequently found in the GGACG motif, corresponding to an expanded DRACN motif (with N being any base)[10,11]. On the transcript level, m6A predominantly occurs after the last exonic splice site as well as in the 3' untranslated region (3'UTR) proximal to the stop codon[12].

Based on the intracellular localization of a transcript, m6A is recognized by different "reader proteins" that facilitate m6A's divergent roles in mRNA metabolism. For instance, YTH domain-containing family protein 2 (YTHDF2) induces mRNA degradation, insulin-like growth factor mRNA-binding proteins (IGF2BPs), leucine rich pentatricopeptide repeat containing (LRPPRC), and fragile X messenger ribonucleoprotein 1 (FMR1), staphylococcal nuclease and tudor domain containing 1 (SND1) stabilize mRNA, YTH domain-containing family protein 1 (YTHDF1) and eukaryotic initiation factor 3 (eIF3) promote translation, YTH N6-methyladenosine RNA binding protein C1 (YTHDC1) and various heterogeneous nuclear ribonucleoprotein (HNRNP) members assist in splicing, and YTHDC1 mediates nuclear export[13–23]. m6A was reported to also exert a direct role on RNA secondary structure by thermodynamically stabilizing single-stranded RNA (ssRNA) while destabilizing double-stranded RNA (dsRNA) structures[24]. This mechanism counteracts folding of m6A-modified endogenous and viral RNA into dsRNA duplexes, thereby preventing innate immune activation[25,26]. A third group of m6A-associated genes are so-called "eraser proteins". AlkB homolog 5, RNA demethylase (ALKBH5) and fat mass and obesity-associated protein (FTO) can remove preinstalled m6A marks on their target transcripts (Fig. 1)[27,28].

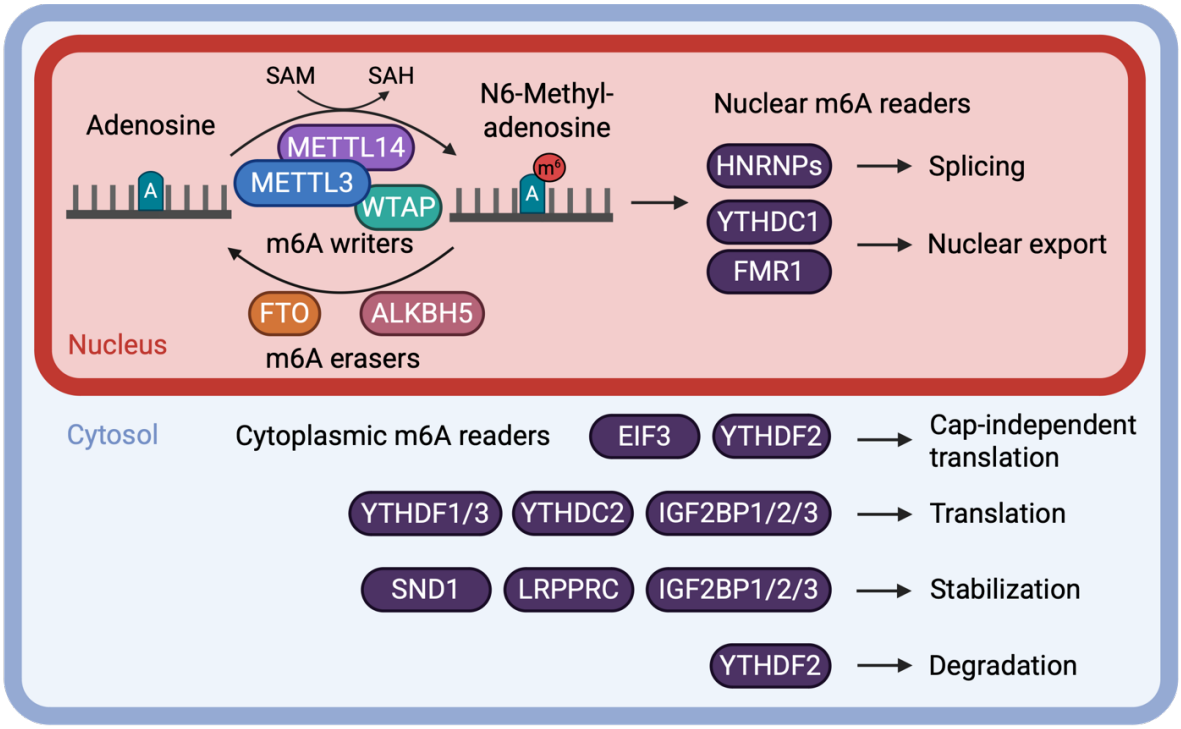

Figure 1. m6A writers, readers and erasers.

1.1.2 A-to-I RNA editing

Adenosine-to-inosine (A-to-I) RNA editing, catalyzed by members of the adenosine deaminase RNA specific (ADAR) protein family, is another prominent modification found in eukaryotic mRNA. ADARs bind to dsRNA to deaminate adenosine (A) to inosine (I), which is recognized as a guanosine (G) during translation. As inosine no longer base pairs with uracil (U), RNA editing disrupts the original dsRNA structure[29]. ADAR1 is ubiquitously expressed and typically edits non-coding regions of transcripts. In contrast, ADAR2 is highly expressed in the brain, where it induces recoding events in coding regions of mRNA. ADAR3 is catalytically inactive and dampens editing[30].

ADAR1 possesses two distinct isoforms: the shorter and ubiquitously expressed p110 isoform, predominantly localized in the nucleus, and the longer, interferon-inducible p150 isoform, mostly found in the cytoplasm, playing a role during development, homeostasis and viral infection[29,31]. ADAR1 typically edits repetitive elements as they are prone to form double-stranded structures, i.e. Alu-elements (which are present in humans but absent in mice), short interspersed nuclear elements (SINE), long interspersed nuclear elements (LINEs), or intronic regions, and 3' UTR[32]. ADAR1's association and modification of endogenous dsRNAs avoids their recognition by innate immune sensing pathways[33,34].

1.1.3 Targeted RNA editing

Due to ADAR's ability to cause single base substitution, targeted RNA is of interest for therapeutic applications, such as correcting disease-causing mutations on the RNA level. Unlike DNA editing approaches, RNA editing is transient and does not alter the genome[35]. Different tools have been developed that deliver exogenous ADAR deaminase domains or full ADAR proteins fused with targeting domains. A simultaneously delivered guide RNA complementary to the target sequence recruits the exogenous ADAR-fusion protein for targeted RNA editing[36–41]. A new generation of tools no longer requires delivery of an editing protein. Instead, delivery of only a guide RNA that is typically imperfectly complementary to and forms a dsRNA structure with the targeted region, allows recruitment of endogenous ADAR and site-specific RNA editing. The RESTORE (Recruiting Endogenous ADAR to Specific Transcripts for Oligonucleotide-mediated RNA Editing) system is utilizing chemically

modified antisense oligonucleotides (ASOs) containing an invariant ADAR recruitment domain (an imperfect hairpin) and a sequence complementary to the target transcript[42]. The LEAPER (leveraging endogenous ADAR for programmable editing of RNA) system uses an unmodified, encodable long linear guide RNA almost complementary to its target region[43]. In the meantime, the first RNA therapeutics using the new technologies for recruitment of endogenous ADAR entered the first clinical trial. Preliminary results indicate successful restoration of wild-type M-Alpha-1 antitrypsin (M-AAT) by targeted editing in treated AAT deficiency patients[44,45]. This evidence of successful RNA editing therapy in patients provides a promising avenue for future clinical applications.

1.1.4 RNA sensing pathways

The innate immune system has developed many mechanisms to defend the cell from external and internal threats. Different pattern recognition receptors (PRR) can recognize pathogen-associated molecular patterns (PAMPs) and damage-associated molecular patterns (DAMPs). While toll-like-receptors (TLRs) reside on cellular membranes, retinoic acid-inducible gene I (RIGI)-like receptors (RLRs) and nucleotide binding oligomerization domain containing (NOD)-like receptors reside in the cytoplasm. Activation of the receptors contributes to inflammation through the production of cytokines and chemokines[46].

Immunostimulatory RNA serves as a potent stimulus for various innate immune receptors. TLRs localized in the endosome include ssRNA-sensing TLR7, TLR8 (which only senses RNA in humans), and TLR13 (which is only present in mice), as well as dsRNA-sensing TLR3. In the cytosol, the RLRs RIGI and melanoma differentiation-associated protein 5 (MDA5) recognize distinct types of dsRNAs. Once these receptors recognize RNAs, their partially overlapping downstream signaling leads to the production of type I interferons (IFNs). TLRs (not TLR3) lead to myeloid differentiation primary response 88 (MyD88) recruitment, inducing downstream IκB kinases (IKKs) and mitogen-activated protein kinases (MAPKs), that in turn trigger nuclear factor κB (NF-κB) and activating protein-1 (AP-1) for pro-inflammatory cytokine production. Simultaneously, MyD88 activates interferon regulatory factor (IRF) 5 and IRF7 for type I IFN production. TLR3 activates toll-interleukin-1 receptor (TIR) domain-containing adaptor protein inducing IFN-β (TRIF),

stimulating TANK-binding kinase 1 (TBK1) and IKK-i/ε. Activation of downstream IRF3 and IRF7 induces type I IFNs. Activated MDA5 and RIGI associate with mitochondrial antiviral signaling protein (MAVS) at the mitochondrial membrane to induce TBK1-IKK-i/ε and downstream IRF3 and IRF7 for type I IFN production (Fig. 2)[46].

Type I IFNs play a crucial role in the antiviral response. Their binding to interferon-α/β receptor (IFNAR) initiate the janus kinase (JAK)–signal transducer and the transcription (STAT) signaling pathway, and downstream interferon stimulated gene (ISG) expression. ISGs include hundreds of genes with anti-viral features that help the cell fight viral infection that include additional dsRNA sensors protein kinase RNA-activated (PKR) and 2′-5′-oligoadenylate synthetases (OASs). Upon dsRNA sensing PKR dimerizes and autophosphorylates to promote translational shutdown and apoptosis. OASs sense and cleave dsRNA into 2′-5′-oligoadenylate that is required for cytoplasmic ribonuclease RNase L's activity to degrade viral RNAs. Resulting dsRNA cleavage products can in return activate RLRs[46].

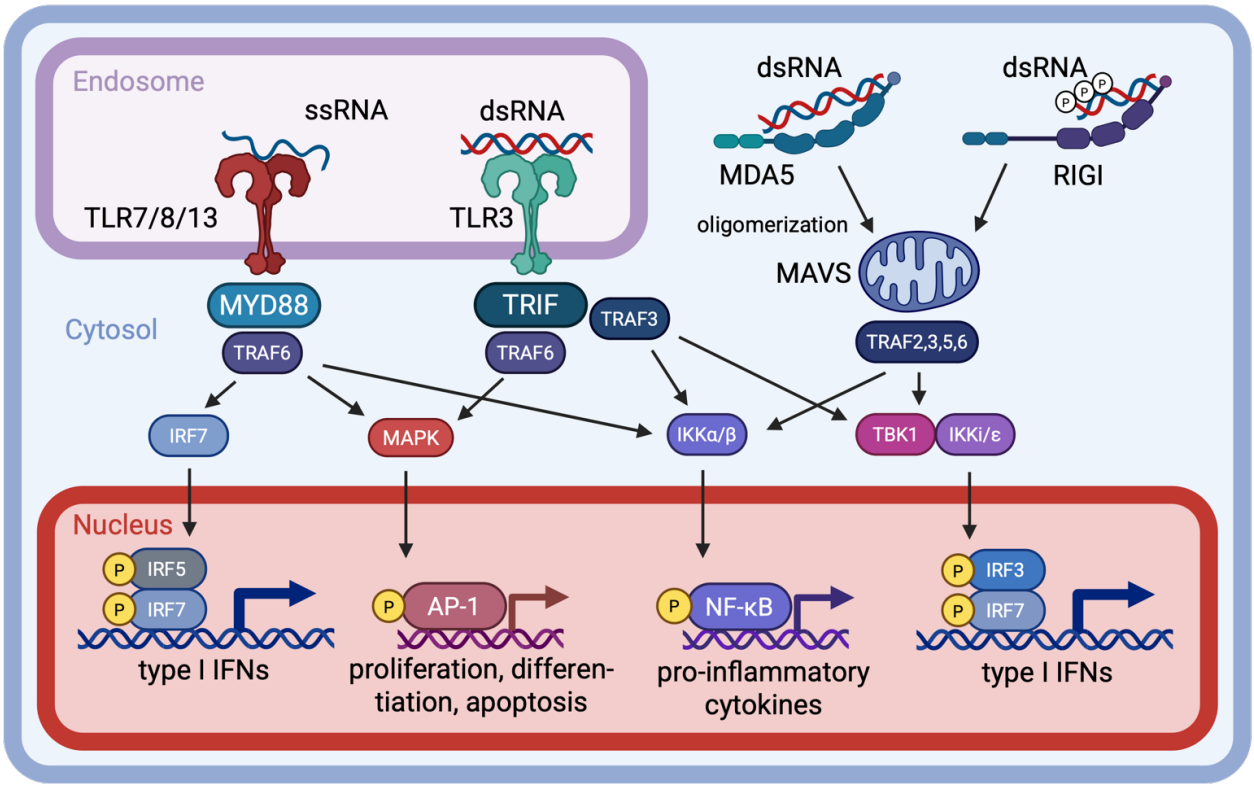

Figure 2. Innate immune RNA sensing pathways.

1.1.5 RNA modifications help distinguish self and non-self RNA

RNA modifications are an important marker to distinguish self- from non-self RNA and regulate innate immune recognition and activation of RNA sensors. The base for this distinction is the existence of different RNA modifications and patterns in foreign and endogenous RNAs. Indeed, increased levels of RNA modifications were detected in eucaryotic rRNA and tRNA as compared to respective RNA species of procaryotic origin. Additionally, some RNA modifications are uniquely found in organisms belonging to distinct biological domains[47,48].

Immunostimulatory unmodified in-vitro transcribed (IVT) RNA was found to activate TLR3 by double-strand formation[49,50]. In turn, delivery of m6A-, 5-methylcytosine (m5C)-, 5-methyluridine (m5U)-, 2-thiouridine (s2U)-, or pseudouridine (Ψ)-modified RNA reduced recognition by TLR3, TLR7, and TLR8, and consecutive innate immune activation as compared to delivery of unmodified RNAs[51]. Further, m6A and A-to-I editing of endogenous RNAs disrupt dsRNA structures, thereby preventing their recognition by dsRNA sensors and immune activation[25,33,34,52]. While depletion of METTL3-mediated m6A on endogenous transcripts was found to activate PKR, RNase L, and MAVS signaling pathways, the mechanism and the contributions of individual RNA sensors remains not fully solved[25]. ADAR1 edits endogenous dsRNA to disrupt their dsRNA structure and prevent their recognition by MDA5 and downstream interferon production[33,34,52]. Additionally, ADAR1 inhibits RIGI activity by binding self-dsRNA[53], while suppressing PKR by both editing-dependent and editing-independent mechanisms[54].

1.2 Macrophages

Macrophages are a subset of innate immune cells that reside within all types of mammalian tissues. While precursors of tissue resident macrophages locate to their niche during the early embryonic state, monocyte-derived macrophages are differentiated from bone marrow progenitors throughout life. Macrophages play a crucial role in development, tissue homeostasis, tissue repair, and the immune response. Thereby, exhibiting different transcriptional and functional characteristics. As a reaction to a changing tissue physiology

or to exogenous stimuli, macrophages can quickly modulate their phenotypic and functional characteristics[55].

1.2.1 Macrophage polarization

Based on their inflammatory phenotype, macrophages can be classified into different groups. Naïve (M0) macrophages have not yet encountered pro- or anti-inflammatory stimuli and can polarize into different phenotypes. Macrophages exposed to pro-inflammatory stimuli, e.g., TLR-ligand lipopolysaccharide (LPS), or cytokines, e.g., interferon-γ (IFN-γ), polarize towards a pro-inflammatory, so-called classically activated, M1-like state[56]. These macrophages are essential during the acute phase of infection and injury. Their high level of antigen presentation, reactive oxygen species, and pro-inflammatory cytokine production recruits and activates other immune cells, promoting inflammatory, antimicrobial, and anti-tumor capacities[55,56]. In contrast, anti-inflammatory stimuli, such as interleukin 4 (IL-4) and IL-13, drive macrophages into an anti-inflammatory, so-called alternatively activated, M2-like state. Anti-inflammatory macrophages play a crucial role during the resolution phase of an infection, driving tissue repair (Fig. 3). The M1 and M2 states can be further divided into many subcategories, based on the specific stimulus and characteristics of the polarized macrophages. Despite this classification, polarization is not limited to strictly defined stages, but occurs within a dynamic range that allows for continuous changes in macrophages' phenotype, underscoring their plasticity. Particularly *in vivo*, macrophages exhibit a large transcriptional diversity, indicating the existence of many different macrophage subpopulations that are specialized to fulfill their specific function[55].

1.2.2 Phagocytosis

Macrophages act in the first line of defense to protect the body from infection. Using a variety of different cell surface receptors, macrophages recognize PAMPs and DAMPs and initiate rapid immune responses[57,58]. A key function in this process is their high phagocytic activity. While known for the engulfment of bacteria and other large antigens, macrophages

also clear cellular debris, senescent, dying and cancerous cells, thereby promoting immune homeostasis[57].

To initiate phagocytosis, macrophages' receptors recognize pathogenic surface antigens and form membrane protrusions, known as pseudopodia, around the pathogen to initiate the engulfment into a phagosome. A variety of receptors mediate phagocytosis with varying substrate specificities. For instance, mannose receptor (cluster of differentiation 206 [CD206]) and Dectin 1 recognize fungal polysaccharides, while scavenger receptors (SRs) such as SR-A and macrophage receptor with collagenous structure (MARCO) mediate phagocytosis of Gram–positive and Gram-negative bacteria. Opsonins can also mark the surface of pathogens for clearance. For instance, immunoglobulin G (IgG) can act as an opsonin, recognized via fragment crystallizable receptors (FcγRs). Similarly, molecules of the complement system, as well as linker-proteins bound to lipid phosphatidylserine (PS) on the outer cell membrane of apoptotic cells, are sensed for initiation of phagocytosis[58].

Quickly after engulfment, sterilization products (reactive oxygen species and free fatty acids) are produced in the phagosome, followed by delivery of hydrolases and lysosomes. Decreasing the endo-lysosomal pH by the proton adenosine triphosphatase (ATPase) pump activates the degradation system[58].

Phagocytosis is not only a means of removing unwanted particles from the extracellular space, but also provides a source of additional immune stimulation. For instance, cell-surface receptors such as TLR2, TLR4, and TLR5 not only contribute to phagocytosis but also initiate downstream inflammatory signaling. The same applies to TLR3, TLR7, TLR8, and TLR9, which are recruited to the phagosome to sense pathogenic nucleic acids. Moreover, processing of pathogenic antigens in the phagosome enables their presentation on the cell surface, thereby allowing activation of adaptive immune cells[58].

1.2.3 Cross-talk between macrophage and other immune cells

While fulfilling important innate immune functions, macrophages are crucial for the communication between the innate and the adaptive immune system. Particularly pro-inflammatory macrophages provide immunostimulatory signals to innate and adaptive immune cells. Upon pathogen recognition by PRRs, macrophages produce cytokines that

serve as an alert signal to promote inflammation and activation of other immune cells. For example, their secretion of IL-1 and tumor necrosis factor-α (TNF-α) contribute to dendritic cell (DC) maturation and activation. IFNs improve antigen presentation and effector and memory T cell formation. Also, $CD8^+$ T cell and helper T (Th) 1 cell effector function is driven by IL-12 that can be produced by macrophages (Fig. 3)[57].

Additionally, macrophages act as professional antigen-presenting cells (APCs) characterized by presenting exogenous antigens on the major histocompatibility complex class II (MHC II) on their cell surface. After phagocytosis, macrophages process the pathogen's antigens into peptides that are typically loaded on MHC II for presentation to $CD4^+$ helper T cells. Like non-APCs, macrophages also display intracellular antigens on MHC I, which increases during macrophage activation for more efficient presentation to $CD8^+$ T cells (Fig. 3)[57].

Recognition of the peptide-loaded MHC by an antigen-specific T cell receptor (TCR) provides the central first signal for T cell activation. Macrophages also provide the essential secondary signal to T cells by expressing co-stimulatory molecules CD80 and CD86, which engage the T cell co-receptor CD28. Macrophages upregulate their levels of co-stimulatory molecules during activation. As a third signal, macrophages secrete cytokines to further drive activation, proliferation, and differentiation of T cells (Fig. 3)[57].

In contrast, anti-inflammatory macrophages possess immunosuppressive functions that dampen the immune response[57]. Particularly in cancer, tumor-associated macrophages (TAMs) respond to tumor-secreted factors, promoting cancer growth by driving angiogenesis and tumor cell migration. Furthermore, immunosuppressive macrophages produce inhibitory molecules such as IL-10, transforming growth factor β (TGF-β), and arginase 1 (ARG1) and display programmed cell death 1 (PD1) and cytotoxic T-lymphocyte associated protein 4 (CTLA4) immune checkpoint ligands to suppress immune activity (Fig. 3)[59].

Besides sending signals, macrophages are also influenced by cues from other immune cells. IFN−γ secreted by activated T and natural killer (NK) cells enhances macrophages' anti-microbial function and pathogen clearance while inducing pro-inflammatory polarization. Conversely, IL-4 and IL-13 derived from Th2 cells drive anti-inflammatory macrophage polarization for tissue repair and antimicrobial responses[57].

Together, the cross-talk between the innate and adaptive immune system facilitates the coordination and integration of various signals and players within the immune system to enhance and optimize the immune response against pathogenic threats[57].

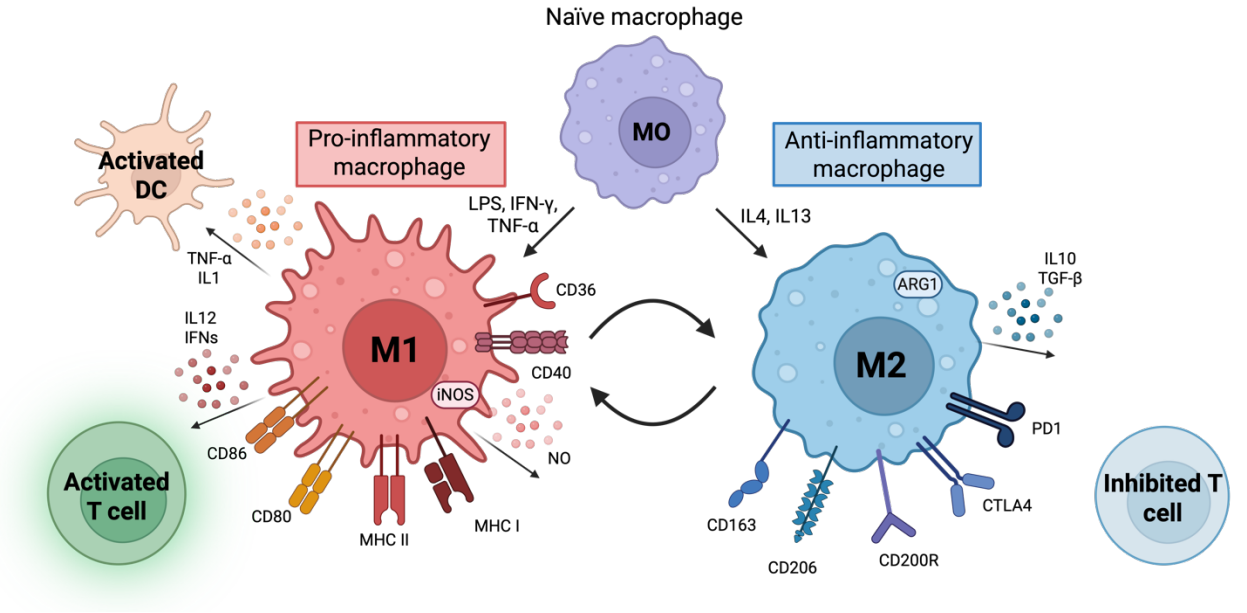

Figure 3. Pro- and anti-inflammatory macrophage polarization and phenotypic characteristics.

1.2.4 Role of m6A and A-to-I editing in macrophage function

Former studies have demonstrated the multifaceted roles of RNA modifications in the development, activation, polarization and migration of immune cells to modulate the immune reaction[60]. METTL3 is essential for the maintenance and differentiation of hematopoietic stem cells[61]. In macrophages, m6A increases the stability of *STAT1* transcript, promoting macrophage M1 polarization and phagocytosis[62]. TNF receptor associated factor 6 (*TRAF6)* mRNA methylation enhances NF-κB signaling and macrophage-mediated inflammation[63,64]. In DCs, m^{6}A sites on *CD40*, *CD80* and TIR domain-containing adaptor protein (*TIRAP)* mRNAs increased their translation and TLR4/NF-κB signaling mediated cytokine response[65]. As these genes are also expressed in macrophages, similar regulatory mechanism might apply. On the other side, m6A might also promote a M2 phenotype as observed in the context of m6A reader IGF2BP2's recognition and stabilization of m6A sites

on tuberous sclerosis complex 1 (*Tsc1*) and peroxisome proliferator activated receptor-γ (*Pparg*) driving alternative macrophage activation[66].

Recent papers demonstrated that ADAR1 promotes macrophage activation, yet, in an editing-independent manner. ADAR1 associates with miRNA processor double-stranded RNA-specific endoribonuclease (DROSHA) leading to DROSHA's degradation and limiting production of mature anti-inflammatory microRNAs (miRNAs)[67]. Additionally, ADAR1 promotes NF-κB phosphorylation and consecutive expression of the inflammatory mediators inducible nitric oxide synthase (iNOS) and IL-1β[68]. These findings indicate that RNA modifications and associated proteins play an important role in regulating macrophages' activity.

1.3 Interactions of m6A and A-to-I RNA editing

m6A and A-to-I RNA editing are two of the most common mRNA modifications, and both modify adenosines. Despite a lot of knowledge existing on the two RNA modifications individually, their interaction remains incompletely understood. Some research was performed on the relationship between METTL3-mediated m6A and ADAR1-mediated A-to-I editing in specific contexts. In breast cancer, a direct link between ADAR1 and METTL3 was established as ADAR1 A-to-I editing increased METTL3 expression and global m6A levels. Specifically, ADAR1 edits the 3' UTR of *METTL3* transcripts, thereby modifying a miRNA binding site to stabilize the mRNA and increasing its expression levels[69]. In glioblastoma, methylation of *ADAR1* transcript near the stop codon induces binding of m6A reader YTHDF1 that promotes *ADAR1* translation into protein[70]. Yet, a different group observed a negative association between A-to-I and m6A in human transcripts. While they identified A-to-I sites mostly within Alu-elements in the 3' UTR, they found m6A sites predominantly proximal to the stop codon, hence, in mostly non-overlapping locations. The study identified reduced ADAR1 binding and editing in the majority of methylated transcripts, while m6A writer knockdown, induced global changes in A-to-I editing with overall increased editing levels. Conversely, in a subset of methylated transcript they observed increased editing levels, however, this subset was not closer examined in the study[71].

2. Methods

“Cell culture

RAW 264.7 (RAW) macrophages were cultured in cell-culture treated vessels in DMEM (high glucose) supplemented with 10% FCS, 1% L-glutamine, and 1% penicillin/streptomycin at 37 °C, 5% CO2, and relative humidity 90%. […]

HEK293T cells (obtained from DKFZ, ATCC, Cat# CRL-3216, RRID: CVCL_0063) were cultured at 37°C, 5% CO2 in high-glucose DMEM (Sigma-Aldrich, Cat# D6429) supplemented with 10% FBS (PAN Biotech, Cat# P40-37100) and 1% penicillin/streptomycin (Sigma-Aldrich, Cat# P4333). The cell line was authenticated using Multiplex Cell Authentication by Multiplexion (Heidelberg, Germany). Additionally, the purity of both cell lines was validated using the Multiplex cell Contamination Test by Multiplexion (Heidelberg, Germany). No Mycoplasma, SMRV, or interspecies contamination was detected.”[72]

BMDMs were cultured in RPMI supplemented with 10% FCS, 1% penicillin/streptomycin, and 1 µg/ml Macrophage colony-stimulating factor (M-CSF) at 37 °C, 5% CO2, and relative humidity 90%.

For macrophage pro-inflammatory stimulation, macrophages were treated with LPS (100 ng/ml), IFN-γ (20 µg/ml), R848 (1µM), LTA (50µg/ml), and Motolimob (100 ng/ml) for 24 h or as indicated. For anti-inflammatory stimulation, macrophages were treated with 40 µg/ml IL-4 and 40 µg/ml IL-13 for 24 h. METTL3 inhibition used 10 µM of STM2457 for 24 h prior to pro-inflammatory stimulation by cytokines or TLR ligands and 48 h prior to co-culture with particles for phagocytosis or as indicated.

“Generation of RAW knockout and control cell lines

Guides targeting the genomic sequence of *Mettl3* (exon 1: GCGAGAGATTGCAGCGGCGA, exon 3: GGGCGGCAAATTTCTGGAGA), and *Adar1* (exon 2: ACTCTAACAACCCGCTGACA), as well as non-targeting control guides (GCTTTCACGGAGGTTCGACG, ATGTTGCAGTTCGGCT-CGAT)[73] were cloned into plasmid pSpCas9(BB)-2A-GFP (PX458, Addgene, #48138, a gift from Feng Zhang). RAW cells were nucleofected with plasmids using Amaxa’s Cell Line Nucleofector Kit V (Lonza, 10507935)

and the manufacturer's protocol for Nucleofector II Device. 48 h after nucleofection, cells were resuspended in cell sorting buffer (PBS supplemented with 2% FCS, 25 mM HEPES, and 2 mM EDTA), stained with Propidium iodide (Invitrogen, BMS500PI) for live/dead discrimination and GFP expressing clones were single-cell sorted for ADAR1- and METTL3-knockout (-KO) clones and sorted in bulk for the non-targeted control using the BD Aria 3 Cell Sorter.

Validation of KO cell lines

After expansion, clonal cell lines were screened for biallelic indels by amplification of the targeted gene region by polymerase chain reaction (PCR) using Q5 high-fidelity DNA polymerase (NEB, M0491L) with associated reagents according to NEB's standard protocol and Sanger Sequencing (Microsynth Seqlab GmbH)."[72] When distinct indels were induced in the two alleles in one clone, PCR products where cloned into plasmid vectors by TOPO TA PCR cloning (Invitrogen) and sequenced by *E. coli* NightSeq (Microsynth Seqlab GmbH). Oligos used to amplify targeted region for METTL3-KO: VG6_mMETTL3ex1_fw (GGCGTCCTCGTGAGAATTAGA) / VG7_mMETTL3ex1_rv (TTGGTGTGGTGTTACGCTTG) and VG8_mMETTL3ex3_fw (ATGGCAGACAGCTTGGAGTG) / VG9_mMETTL3ex3_rv (ACACTGAC-TGGACTGACCCT); for ADAR1: VG18_Adar1_ex2_fw (GACGGACAAGAAGCGTGAGA) / VG19_Adar1_in2-3_rv (ACCAAGACAGCGTAAGAGCC).

Successful knockout was validated by Western blot for absence of protein expression. For METTL3-KO clones, m6A-dependet splice isoforms of *Tor1aip2* were quantified by reverse transcription quantitative PCT (RT-qPCR) as described below."[72] For ADAR1-KO clones, RNA was harvested and reverse transcribed as described below. ADAR1-specific editing sites in *Exoc1* were PCR amplified (VG23_Exoc8_B1r2fw_ad1edit: GAAACTTAGTAACTGAGTAGAG; VG24_Exoc8_B1r2rv_ad1edit: CCCTACTCAACAACCTGAAG) and absence of editing in the ADAR1-KO samples were detected by Sanger sequencing.

"Flow cytometric analysis of cell surface markers

Unstimulated or cells stimulated for 24 h with 100 ng/ml LPS and 20 µg/ml IFN-γ [for pro-inflammatory stimulation or 40 µg/ml IL-4 and 40 µg/ml IL-13 for anti-inflammatory stimulation] were harvested in [Fluorescence-Activated Cell Sorting (FACS)] […] buffer (PBS

[phosphatebuffered saline] supplemented with 2% FCS), incubated for 10 minutes in homemade Fc blocking buffer, stained for 30 minutes with antibody staining cocktail in FACS buffer, followed by 30 min staining with violet live/dead fixable staining solution (Invitrogen, 34964, 1:1000 in PBS), and fixation for 10 minutes with 4% Paraformaldehyde (Thermo, 28908) in PBS. Between steps, cells were washed by adding […] excess FACS buffer and centrifugation for 5 minutes at 800 g at 4°C. Samples were analyzed using the BD Canto II flow cytometer.

Phagocytosis assay

For unstimulated samples, 100 000 cells were plated in flat-bottom 96-well plates in fresh medium and allowed to attach for 1 h. For stimulated samples, 10 000 cells were plated two days before [the] phagocytosis assay and treated for 24 h with 100 ng/ml LPS and 20 µg/ml IFN-γ. [Where applicable, STM2457 (10uM) or DMSO was added to the cells 48 h prior to the phagocytosis-co-culture. DMSO and STM2457 concentrations were maintained throughout the phagocytosis assay.] Cells were washed twice with non-supplemented DMEM (high glucose), followed by adding 5 µg pHrodo Green [E. coli,] S. aureus (Invitrogen, P35367) or Zymosan (Invitrogen, P35365) particles in 50 µl non-supplemented DMEM. Cells were incubated with particles for uptake for 1 h at 37°C. Cells were harvested, incubated for 30 minutes with violet live/dead fixable staining solution (1:1000 in PBS), and washed. Cells were analyzed at the BD Cytek Aurora Spectral Flow Cytometer using automated spectral unmixing"[72] based on median fluorescent intensity (MedFI) signals.

For bead-uptake, FITC-labeled beads (Sigma, L4655) were added in 50 µl at a final bead-to-cell ratio of 100:1 (bead stock diluted 1:136). For LPS-coating, beads were incubated with 30 ug/ml for 1h at RT, followed by six washes with FACS buffer and centrifugation at 10 000 g for 5 min. The bead-uptake assay followed the same procedure as described above but after staining for live/dead discrimination, cells were fixed in freshly thawed 4% paraformaldehyde in PBS for 10 minutes, cells were washed, centrifuged, and pellets were resuspended in fresh FACS buffer and analyzed using the Canto II flow cytometer.

“Next Generation Illumina Sequencing (NGS)

For NGS sequencing, RNA extraction was performed using the RNeasy Mini kit (Qiagen, 74104) according to the manufacturer. Contaminating DNA was removed using the Turbo DNase-free Kit (Invitrogen, AM1907) according to the manufacturer. RNA was quantified by Nanodrop and submitted to the DKFZ Core Facility for library preparation (rRNA depletion protocol) and sequenced using NovaSeq 6000 Sequencing System (Illumina).

Direct RNA sequencing using Oxford Nanopore Technology

Unstimulated and cells treated for 24 h with LPS and IFN-y treatment were lysed in Trizol and RNA was extracted using Zymo Direct-Zol Kit (Zymo, R2050) including DNase I treatment. Libraries were prepared from 2.5 µg total RNA using the Direct RNA Sequencing Kit (SQK-RNA004) according to the manufacturer. Libraries were loaded on the PromethION RNA Flow Cell (FLO-PRO004RA) on the promethION 24 sequencing device.

RNA LC-MS/MS

Unstimulated and cells treated for 24 h with LPS and IFN-y treatment were lysed in Trizol and RNA was extracted using Zymo Direct-Zol Kit (Zymo, R2050) including DNase I treatment. Poly-A enrichment was performed using the NEBNext Poly(A) mRNA Magnetic Isolation Module (NEB). RNA samples from three replicates were pooled and RNA was precipitated overnight at -70°C using ammonium acetate (Sigma, A2706) and ice-cold ethanol. RNA was digested and internal standards of 13C labeled yeast RNA was added. Calibration samples of unmodified and modified nucleotides were prepared. Samples were injected into the LC-MS/MS instrument for measurement. Data was analyzed using the Aligent Masshunter qualitative and quantitative software.

Reverse transcription (RT) and RT qPCR

RNA extraction for downstream reverse transcription was performed using the RNeasy Mini kit (Qiagen, 74104) according to the manufacturer. Contaminating DNA was removed using the Turbo DNase-freeKit (Invitrogen, AM1907) according to the manufacturer. Reverse transcription was performed using ProtoScript First Strand cDNA

Synthesis Kit (NEB, E6300L) according to the manufacturer. Quantitative PCR, was performed using iTaq Universal SYBR Green Supermix (Biorad, 1725121) according to the manufacturer using the CFX Connect Real-Time System (Bio-Rad). Samples were normalized by the amount of the housekeeper CPH [carboxypeptidase H] (CPH_fw: ATGGTCAACCCCACCGTG ; CPH_rv: TTCTTGCTGTCTTTGGAACTTTGTC) present in each sample. Oligos used to target transcripts: Tor1aip2_long_ex-junction_fw: TCTGGACCTATGGTTCCGTG; Tor1aip2_long_ex-junction_rv: GCTGGGCTGGGGAAGAATAG; Tor1aip2_short_ex3_fw: TGGGTCTGCTTCTGTGGTCT; Tor1aip2_short_ex3_rv: CAAGAGGGGCCAGGTAGTTC; Adar1_ex2_fw: GATGCCCTCCTTCTACAGCC; Adar1_ex3_rv: ATTCCCGCCCATTGATGACA; Adar1_in2-3_rv: TCTGGGCAGTCTCTTACCGA[; Ifnb_fw: CAGCTCCAAGAAAGGACGAAC; Ifnb_rv: GGCAGTGTAACTCTTCTGCAT].

Western blot

Cultured cells were washed with PBS and lysed in Cell Lysis Buffer (Cell signaling, 9803) containing cOmplete, Mini, EDTA-free Protease Inhibitor Cocktail (Roche, 11836170001) and 1 mM phenylmethylsulfonylfluoride (Sigma, 93482, 1:100) for 30 minutes on ice, followed by centrifugation for 15 min at 10 000 g at 4 °C. The protein in the supernatant was quantified using the Pierce BCA Protein Assay Kit (Thermo, 23225) according to the manufacturer, and was cooked with Laemmli buffer for 5 minutes at 95 °C. Samples were loaded on Mini-PROTEAN TGX Precast Gels (4-15%, Bio-Rad, 4561086) and run for 30 minutes at 70 V followed by 130 V until reaching desired separation. Proteins were transferred to a Nitrocellulose Blotting Membrane (Cytiva) using a wet blotting system for 70 minutes at 100 V. The nitrocellulose membrane was blocked for 1 h with 5% skim milk in TBS-T (1X TBS with 0.1% Tween-20). Membranes were incubated with primary antibodies (METTL3, Abcam, ab195352; ADAR 1, Santa cruz, sc-73408, beta-actin, Sigma, A5441; alpha Tubulin, Abcam, ab4074) in 5% milk - TBS-T overnight at 4 °C while rotating. Membranes were washed three times with TBS-T and incubated with corresponding horseradish peroxidase-coupled secondary antibodies (goat anti mouse - HRP (H+L), Biorad, 170-6516; goat anti rabbit-HRP (H+L), Biorad, 170-6515) in 5% skim milk - TBS-T for 1 h at room temperature while shaking. After three washes with TBS-T, membranes were incubated with chemiluminescence based detection reagent 1 and 2 at equal volumes (ECL

Start Western Blotting Detection Reagent, Cytiva, RPN3243, or SuperSignal West Pico PLUS Chemiluminescent Substrate, Thermo, 34095). Chemiluminescent signals were detected using the ChemiDoc Imaging System (BioRad). Densiometric quantification was performed using the ImageG software. Amount of protein was normalized against the amount of the housekeeper control in each sample.

Generation of reporter cell line for targeted RNA editing assay

In order to generate the reporter cell line for RNA editing, HEK293T cells were seeded in 24-well plates (~150,000 cells per well) to have a confluency of 70-90% the following day. After 24 h, cells were transfected with 2 µg of the mCherry-T2A-eGFP W58X reporter plasmid (a kind gift of Dr. Joshua Rosenthal, University of Chicago[74]) using Lipofectamine 2000 (ThermoFisher, Cat# 11668019). Then, 48 h after transfections, cells were diluted to single cells in 96-well plates and selected using puromycin (1.5 µg/ml) for two weeks. Clonality was validated by visual inspection with a microscope, and the clones were then screened for the presence of mCherry and absence of eGFP via flow cytometry analysis. The original mCherry-T2A-eGFP W58X was modified by inserting a puromycin resistance cassette within the BglII restriction site to allow selection.

In vitro transcription (IVT) of guide RNAs (gRNAs)

pENTER-U6 coding an optimized RESTORE gRNA[42] to target the eGFP W58X was used to prepare IVT template for gRNAs production. IVT template was generated by PCR using the following primers: forward (5'-AAGCTAATACGACTCACTATAGGTGAATAGTATAACAATA-TGC-3') and reverse (5'-AAACTACCTGTTCCATGG-3') primers. The forward primer contains the T7 promoter needed for the following IVT reaction. Q5 High-Fidelity DNA Polymerase (New England Biolabs, Cat# M0491) was used for amplification. The PCR product was then purified with the Nucleospin Gel and PCR cleanup kit (Macherey Nagel, Cat# 740609.50) and eluted in 25 µl DEPC-treated water. IVT was performed using the Takara IVTpro T7 mRNA Synthesis Kit (Cat#6144) according to manufacturer's instructions in 20 µl reaction containing 2 µl of 10X Transfection Buffer, 2 µl of 10x Enzyme mix, 2 µl of 100 mM ATP/UTP/CTP/GTP, 2 µl of 100 mM N6-Methyl-ATP (Jena Bioscience, Cat#NU-1101) in place of ATP, and 1 pmol of DNA template. In vitro transcription reaction was incubated at

37°C for 16 h. DNA template was removed by adding RNAse-free DNAse I (2000 Ul/mL; New England Biolabs, Cat# M0303) for 15 min at 37°C. DNA Dephosphorylation was performed by incubating the IVT product with 2 µl of QuickCip (5000 Ul/mL; New England Biolabs, Cat# M0525) at 37°C for 2 h. IVT gRNAs were purified from the solution by Monarch Clean UP RNA Kit (50 µg) (New England Biolabs, Cat# T2040), eluted in 100 µl DEPC-treated water, and quantified with nanodrop.

Targeted RNA editing assay

HEK293T mCherry-T2A-eGFP W58X cells were seeded in 24-well plates (~150,000 cells per well) to have a confluency of 70-90% the following day. 16 h prior to transfection, the HEK293T mCherry-T2A-eGFP W58X cells were treated with 500 U/mL [IFNα] […] to induce ADAR1 expression. The cells were then transfected with 20 pmol of gRNA, with and without m6A, using Lipofectamine 2000 (Thermo Fisher Scientific, Cat# 11668019). Flow cytometry analysis for eGFP+ cells was performed at 24h, 48h, 72h post-transfection (FACS Canto II at DKFZ Core Facility Flow Cytometry).

Ribosome profiling (Ribo-Seq)

One day before the experiment, RAW macrophages were seeded at a density of 2 × 10^6 or 3 × 10^6 cells per 10 cm dish for WT or METTL3-KO cells, respectively. At different time points after addition of 100 ng/ml LPS (Sigma, catalog no. L2630) + 20 ng/ml IFN-γ (PeproTech, catalog no. 315-05), cells were washed in ice-cold PBS supplemented with 100 µg/ml cycloheximide (Roth, Cat# 8682.3), and harvested by scraping in polysome lysis buffer (20 mM Tris-HCl buffer pH 7.4, 10 mM MgCl2, 200 mM KCl, 1% NP-40, 100 µg/ml cycloheximide, 2 mM DTT, 1 tablet EDTA-free Roche cOmplete Mini Protease Inhibitor per 10 ml). Lysates were rotated for 10 min and then centrifuged at 9,300g for 10 min at 4 °C. About 10% of the lysates were saved as input control. The remaining lysates were digested with RNase I (60 U per A260; Ambion, Cat# AM2294) for 20 min at 4 °C and followed 17.5–50% sucrose density gradient centrifugation for 1 h 45 min at 40,000 rpm at 4 °C. The monosomal fractions were collected from the gradients into urea buffer (10 mM Tris-HCl pH 7.5, 350 mM NaCl, 10 mM EDTA, 1% SDS, 7 M urea). RNA was purified by phenol extraction and precipitation in 50% isopropanol by using phenol: chloroform: isoamyl alcohol

(AppliChem, Cat# A0944) and GlycoBlue (Ambion, Cat# AM9515). rRNA was then depleted using the Human-Mouse-Rat riboPOOL Kit (siTOOLs, Cat# dp-K096-53). Input RNA was fragmented randomly by alkaline hydrolysis at pH 10.0 for 12 min at 95 °C. Both fragmented input (IN) and ribosome footprints (FP) were isolated by size-selection (25–35 nt) and extraction from a 15% polyacrylamide Tris-borate-EDTA-urea gel. Purified RNAs were phosphorylated at their 5' end with 10 U T4 PNK (NEB, Cat# M0201S), 40 U RNase OUT (Invitrogen, Cat# 10777019) and 1 mM ATP in T4 PNK reaction buffer for 1.5 h at 37 °C.

After end-repair, libraries were generated with the NEBNext Multiplex Small RNA Library Prep Kit (NEB, Cat# E7300) according to the manufacturer's manual. To determine the required number of PCR cycles, 1 µl of cDNA per sample was diluted 8 times and used for a qPCR reaction (forward primer: 5'-GTTCAGAGTTCTACAGTCCGA-3', reverse primer: 5'-CCTTGGCACCCGAGAATTCCA-3') using SybrGreen master mix (Applied Biosystems, Cat# A25742) on a QuantStudio Real-Time PCR System. The highest threshold cycle determined among all samples was used for library preparation. The resulting libraries were purified by 10% polyacrylamide Tris-borate-EDTA gels following the manufacturer's instructions and sequenced on a NextSeq550 device (Illumina) with SE75 mode, acquiring an average 8 million reads per sample.

Bioinformatic analysis of Ribo-Seq data

Sequences were demultiplexed and converted to fastq files using bcl2fastq v.2.20. Adapters were removed with the FASTX-toolkit v.0.0.13, retaining only sequences at least 28 nt long. The four random nucleotides at the beginning and the end of the reads were trimmed with an in-house-developed Perl script. The trimmed reads were mapped to tRNA and rRNA sequences (as downloaded from the UCSC Genome Browser) by bowtie v0.12.8, allowing a maximum of two mismatches and reporting all alignments in the best stratum (settings: -a --best --stratum -v 2). Reads that did not map to tRNA or rRNA sequences were aligned to the mouse transcriptome (Gencode VM18 as downloaded from the UCSC Genome Browser wgEncodeGencodeBasicVM18 table). Only reads between 25 and 35 nt long, and mapping to ORFs of isoforms arising from one specific gene (as defined by a common gene symbol) were counted. An offset of 12 nt upstream of the start codon and 15 nt upstream of the stop codon with respect to the 5' end of the read was assumed. Translation efficiencies for each

condition were calculated and compared between METTL3-KO and control cells using DESeq2[75]. The downstream analysis included only those genes for which DESeq2 could calculate adjusted P values (Wald test, Benjamini–Hochberg adjustment) for the fold change in translation efficiency [...].

Illumina RNA-seq data processing

Adapters were trimmed using Trimmomatic v0.38[76] ith follow command line:

```
"trimmomatic.sh PE -threads 15 /${S_name}_R1.fastq.gz /${S_name}_R2.fastq.gz
/Trimmed/${S_name}_R1_paired.fastq.gz /Trimmed/${S_name}_R1_unpaired.fastq.gz
/Trimmed/${S_name}_R2_paired.fastq.gz /Trimmed/${S_name}_R2_unpaired.fastq.gz
ILLUMINACLIP:/Illumina.fa:3:30:7 MINLEN:50"
```

Alignment of fastq files to the UCSC mm10 genome was performed using STAR 2 v.2.5.3.a[77] nd the parameters detailed below.

```
"STAR --runMode alignReads --readFilesCommand zcat --genomeDir
/UCSC_GRCm38/STAR_index_2.5.3a --readFilesIn ${S_name}R1_paired.fastq.gz
${S_name}_R2_paired.fastq.gz --outFileNamePrefix ${S_name} --runThreadN 10 --
outFilterMultimapNmax 1 --outSAMstrandField intronMotif --outSAMtype BAM
SortedByCoordinate".
```

Bams quality was checked using qualimap v2.2[78]. Output bam files were sorted and indexed using samtools v1.5[79].

Illumina RNA-editing calling and processing

RNA editing candidates were identified using REDItools v2.0[80], employing the reditools.py script with the following parameters:

```
"reditools.py -f ${S_name}_Aligned.sortedByCoord.out.sorted.dedup.bam -o
/REDITOOLED/${S_name}_Aligned.sorted_reditooled.txt -s 2 -T 2 -os 4 -m
/REDITOOLED/homopol/${S_name}_Aligned.sorted_homopol.txt -c
```

```
/REDITOOLED/homopol/${S_name}_Aligned.sorted_homopol.txt -r
/UCSC_GRCm38/mm10.fa -sf /UCSC_GRCm38/Splicesites/mm10_splicesites.ss -q 25 -
bq 35 -mbp 10 -Mbp 10"
```

Key parameter settings included a minimum read mapping quality of 25 (-q 25), a minimum base quality of 35 (-bq 35), and exclusion of the first and last 10 bases of each read (-mbp 10 -Mbp 10). Additional parameters specified were: strand-specific mode 2 (-s 2), strand confidence mode 2 (-T 2), and a minimum homopolymer length of 4 (-os 4).

The output files generated by Reditool were processed using a custom in-house script (1.Make_reditoolbackground.R). This script is designed to identify genomic regions that consistently exhibit no edits in the context of A-to-G transitions, representing A-to-I editing as detected by Illumina sequencing (Ctrl_Positions). The script executes the following steps:
Filtering: ADAR-KO Reditool output files are processed to discard sites with more than one substitution type. Only genomic positions with a minimum coverage of 10 reads and no substitutions reported (indicated by the AllSubs column = "-") are retained.
Replicate and Sample Type Selection: Genomic positions are required to be present in at least 2 out of 3 biological replicates and in at least 2 out of 4 sample conditions, ensuring a consistency threshold of 50%.

Aggregation: The script aggregates genomic positions by genomic region and sample type. For each site, the median values of read coverage and the frequency of the alternative allele (expected to approximate 0) are calculated.
These steps are designed to ensure the reliability and consistency of RNA editing calls across the studied samples, enhancing subsequent filtering of false positives and SNPs.

In the next step, the in-house script "2.0.0.RNA_editing_Filtering.R" utilizes the previously generated list of genomic positions (Ctrl_Positions) to identify overlapping sites in CTRL and METTL3-KO samples that exhibit A-to-G mutations, indicative of A-to-I editing as detected by Illumina sequencing. The filtering criteria for retaining candidate editing events involve two main stages.

1. Raw Editing Sites Database Creation

This step aims at reducing the file size and optimizing subsequent steps for faster processing. The criteria applied during this stage are as follows:

Filtering Covered Positions: Genomic positions (Ctrl_Positions) are filtered to keep only those with a median coverage of ≥10 across sample replicates.

Ctrl Positions Matching: Positions are cross-referenced with the previous filtered Ctrl_Positions, and only matching sites are retained.

Filtering Editing Candidates: Genomic positions with multiple substitution types are discarded, while positions exhibiting A-to-G substitutions and a coverage of ≥5 are retained.

2. Refining Candidate Edited Positions.

Replicate and Sample Group Consistency: Candidate edited positions must be present in at least 2 out of 3 biological replicates and in at least 2 out of 8 sample group conditions.

Coverage: Candidate edited positions with a median coverage of ≥10 within sample replicates are kept.

Editing Frequency Support: Candidate edited positions are further filtered based on the median count of read supporting the editing site of ≥5 across sample replicates.

The script produces three output files, each tailored for specific analyses in this study:

2.Editing_sites_db_Gt10_Al5_Mc10.txt.gz: This file contains a list of edited sites filtered according to the criteria outlined above. It will be referred to as DB1 in this study.

2.Editing_complete_db_Gt10_Al5_Mc5.rds: This database includes a comprehensive list of genomic positions with editing observed in some samples (DB1). It highlights the presence of unedited positions overlapping with edited sites. This file is used for analyses requiring all positions, such as differential editing analysis, and will be referred to as DB2 in this study.

2.Editing_baseline_db_Gt10.rds: This file contains editing candidates with a coverage of ≥5. It is particularly useful for adjusting other filtering criteria, such as estimating consistency across sample groups or calculating global editing site counts and editing frequencies. This file will be referred to as DB3 in this study.

Editing sites per sample quantification

The number of mapped bases for each sample was obtained using Samtools stats. This value was then used to normalize the corresponding number of editing sites per sample. The normalization formula applied is as follows:

$$Normalized\ Editing\ Sites = \frac{Number\ of\ Editing\ Sites}{\frac{Mapped\ Bases}{10^6}}$$

This normalization ensures that the number of editing sites is scaled relative to sequencing depth, enabling more reliable comparisons between samples.

DB3 was used to count the number of editing sites, applying the following filtering criteria: editing sites present in at least 2 out of 3 biological replicates, a median total coverage of ≥10, and a median number of reads supporting editing sites of ≥5. All positions with an editing frequency ≠ 0 were then included in the count.

This filtering approach undoubtedly increases the potential inclusion of low-quality editing sites or false positives. However, assuming the error rate remains consistent across all samples, any observed differences between samples should primarily reflect true differences in editing sites, even if of lower quality.

Differentially Edited sites detection

Differential editing sites (DES) were identified using the DSS[81–83] package, implemented in an in-house script "7.0.Differential_RNA_Editing_DSS.R" with the smoothing option disabled. Originally developed for differential methylation (DM) detection, DSS employs a rigorous Wald test for beta-binomial distributions. The test statistics account for both biological variations (characterized by the dispersion parameter) and sequencing depth. Candidate editing sites from DB2 were used as input for this analysis. The log2 fold change (log2FC) was calculated using the following formula:

$$\text{Log2FC} = \log2(1) - \log2(2)$$

Gene expression analysis

The quantification was performed using Salmon v0.14.2[84] in mapping-based mode, providing an efficient and accurate method for transcript quantification. The following command line was used to execute Salmon:

```
"salmon quant --numBootstraps 20 -i /UCSC_GRCm38/SALMON_index/ -l A -1
/Trimmed/${Sample_name}_R1_paired.fastq.gz -2
/Trimmed/${Sample_name}_R2_paired.fastq.gz -p 25 -o /SALMON_expr/${Sample_name}
--validateMappings"
```

The Salmon outputs were imported into EdgeR[85] via the tximport[86] ackage, which produces gene-level estimated counts and an associated edgeR offset matrix. Differential analysis for gene counts was performed using the EdgeR[85], implemented in an in-house code. Significantly upregulated/downregulated genes were determined by abs(logFC)>0.5 and FDR < 0.05. The volcano plot was generated using the EnhancedVolcano R package[87].

Nanopore direct-RNAseq pre-processing

The pod5 files were basecalled using the ONT basecaller Dorado v0.7.0, with the models "rna004_130bps_hac@v5.0.0" and "rna004_130bps_hac@v5.0.0_m6A@v1" for the kit "SQK-RNA004". Basecalling was performed on a GPU (Tesla V100-SXM2-32GB).
The command line used is as follows:

```
"dorado basecaller --min-qscore 6 --emit-moves hac,m6A
/ont/raw/i0039410/data/1184237/pod5_pass/ --reference /UCSC_GRCm38/mm10.fa --
mm2-preset splice:uf:k14 > /ONT/Bams_dorado_Genome/File.bam"
```

--hac,m6A: Specifies the models used for basecalling. The hac model (rna004_130bps_hac@v5.0.0) is the high-accuracy model for standard basecalling, while the m6A model (rna004_130bps_hac@v5.0.0_m6A@v1) is used for detecting m6A RNA modifications. At the time of the initial analysis, the detection of inosine modifications was not available as an option in the modification detection settings.

--mm2-preset splice:uf:k14: Configures the minimap2 alignment preset for mapping RNA reads, optimized for spliced alignment[88].
Output bam files were sorted and indexed using samtools v1.5.

Nanopore m6a detection

The BAM files were processed to generate modification BED files using Modkit v0.3.1. For m6A calling, the parameters --filter-threshold A:0.8 and --mod-threshold m:0.99 were applied, as determined by the modification probability density plot and HeatMap generated using Modkit sample-probs output files [...].

Modkit sample-porbs command line:

```
"modkit sample-probs -t 20 --percentiles 0.1,0.5,0.95 -f 0.3 --hist --only-mapped --force --prefix ${S_name} -o /m6a_Res/${S_name}.bam"
```

Modkit pileup command line:

```
"modkit pileup -t 20 --log-filepath /m6a_Res/Pileup/${S_name}.log --sampling-frac 0.4 --max-depth 20000 --with-header --filter-threshold A:0.8 --mod-thresholds a:0.99 ${S_name}.bam /m6a_Res/Pileup/${S_name}.bed"
```

M6a preprocessing

Modkit sample-probs results revealed no discernible differences in m6A counts between METTL3-KO and control samples when using threshold values below 0.99 [...]. This finding suggests a high likelihood of false-positive m6A site detection at lower thresholds, or, less plausibly, the presence of residual methylation mediated by other methyltransferases or potential miscalling of m1A as m6A.

To discover potential m6A sites, we began by identifying differentially methylated (DM) candidates under the assumption that changes in methylation frequency highlight bona fide m6A modifications dependent on METTL3. We then performed two separate comparisons using METTL3-KO (untreated and LPS/IFN-γ 24 h) as the negative control. Specifically, we compared:

ADAR (untreated and LPS/IFN-γ 24 h) versus METTL3-KO (untreated and LPS/IFN-γ 24 h).

CTRL (untreated and LPS 24 h) versus METTL3-KO (untreated and LPS/IFN-γ 24 h).

These comparisons allowed us to pinpoint potential DM sites that differ between ADAR or CTRL samples and METTL3-KO under corresponding conditions [...]. These comparisons employed the R package DSS[81–83] within an in-house script, with the smoothing option disabled. While smoothing is designed for CpG island analyses, where m6A sites often exhibit strong spatial correlations, it can produce false positives in RNA data by labeling m6a site flanking regions as m6A-positive despite zero actual m6a read count.

For the DM analysis, genomic positions were initially filtered as follows:
Coverage Threshold: Only positions with a coverage of ≥10 reads across samples were retained.

Replicate and Sample Group Consistency: Candidate edited positions must be present in at least 2 out of 3 biological replicates, and in both sample groups being compared. Eliminating positions that showed no change between target and METTL3-KO samples yielded a final set of m6A candidate sites, including their genomic coordinates, coverage data, and log2 fold-change relative to the corresponding knockout samples. At this stage, no filtering was applied based on the number of modified reads supporting a methylated position or logFC; these thresholds will be established later, according to the specific requirements of downstream analyses.

In a second step, the m6A candidate sites identified in the previous comparisons were merged to generate a comprehensive list of potential m6A sites. This list was then used to retrieve corresponding positions from the BED methylation files (for ADAR-KO and CTRL samples), producing a consolidated dataset of potential m6A positions observed in 2 or more samples [...].

Notably, this approach also incorporates unmethylated positions overlapping putative m6A sites. The sites used for list building were filtered using the criteria $|Log2FC| \leq 0.5$ and $FDR < 0.05$, ensuring the selection of m6A sites that were either unmethylated or poorly methylated in METTL3-KO samples. Any additional filtering of these methylated positions was applied based on the specific requirements of subsequent analyses, ensuring data relevance and methodological consistency.

M6a and A-to-I Editing sites effect prediction and Annotation

The impact of editing sites was analyzed using the Ensembl Variant Effect Predictor (VEP)[89] and Homer[90], integrated into an in-house R script executed via the command line. M6A sites were annotated and profiled across gene body regions using ChIPseeker[91] and Homer[90]. The list of macrophages, double strand Response, phagocytosis makers downloaded from Mouse Genome Informatics using the following Gene Ontology terms: GO:0042116 (macrophages activation), GO:0006909 (phagocytosis), GO:0034340 (response to type I interferon), GO:0043331 (response to dsRNA).

M6a sites per sample quantification

For this analysis, m6A (DB1m6a) sites were selected based on criteria requiring a minimum total coverage of 10 reads and at least 5 reads supporting the m6A site. Although total coverage and the number of supporting reads may not always be sufficient to reliably distinguish true m6A sites from false positives, the error rate is expected to be consistent across the entire library of samples. Consequently, any observed changes, if present, should be attributed to genuine m6A sites. The number of m6A sites was then normalized using the same approach previously applied to editing sites.

M6a Motif analysis

m6A sites considered for the analysis were taken from untreated Ctrl samples (DB1m6a). The motif was tested, and identified sites were filtered using the following criteria: median coverage ≥ 10, median m6A frequency ≥ 5, and median minimum number of reads supporting m6A sites ≥ 5, using regular expressions ([AGT][AG]A[C][ACT]) for DRACH motif and ([AGT][AG]A[C][.]) for less strict DRACN motif.

A-to-I - m6a modification interplay

The editing and m6A sites used to study the potential relationship between the two modifications were initially analyzed only in Ctrl-24h. We selected Ctrl-24h post-stimulation because:

-Both enzymatic machineries (METTL3 and ADAR1) are fully functional, ensuring that both modifications can occur.

-Editing frequency peaks at 24 hours, making it the ideal time point to test whether a relationship between m6A and A-to-I editing exists.

-Furthermore, the same editing sites identified in Ctrl-24h were used for direct comparison with the corresponding edited regions in METTL3-KO, allowing us to assess how m6A depletion could affect editing levels.

Based on these assumptions, editing sites for the analysis were selected from DB2 using the following criteria:

Median coverage ≥ 20

Median number of reads supporting editing ≥ 5

Median editing frequency ≥ 0.05

The same filtering cutoffs were applied to m6A (DB1m6a) site selection.

For the final dataset, the distance between each editing site and the closest m6A site was calculated using distanceToNearest, GRanges's function[92]. Furthermore, the number of editing sites and the number of methylated sites per transcript feature were also included and utilized for a more detailed statistical model [(Table S5)].

Only modification events occurring in the 3' UTR were considered for the analysis. The distance and m6A level ranking, as well as the resulting classification, were set up based on quantiles calculated over both distance and m6A levels to ensure a systematic categorization"[72] (Fig. 22D).

Additional software

Figures presented in this work were partially created using Biorender.com and the GraphPad Prism 10.5.0. DeepL was used as an aid for the translation of the abstract from English to German.

3. Aim of the dissertation

Various studies have identified independent roles of m6A and A-to-I editing during macrophage activation by modulation of NF-κB signaling and macrophage polarization[62–64,66–68,93]. Moreover, m6A and A-to-I editing function independently in modifying endogenous RNAs to prevent dsRNA formation and innate immune sensing[26,33,34,51,52,94]. In addition to their related functional roles in macrophage activation and in self vs. foreign RNA discrimination, A-to-I editing and m6A sites share a common localization preference in the transcript's 3′ UTR[12,32,95]. Due to their overlapping function and localization, I asked whether the two RNA modifications modulate each other globally as well as on the single transcript level, and whether the interaction between the two RNA modifications coordinately promotes the pro-inflammatory activation and immune function of macrophages.

To address these questions, I utilized the mouse macrophage cell line RAW 264.7 (RAW) as a model system that resembles monocyte-derived macrophages. In order to study the effect of the absence of each modification, I created clonal knockout (KO) cell lines deficient of the RNA modifying enzyme ADAR1 for A-to-I editing depletion and METTL3 for m6A depletion. Using METTL3- and ADAR1-KO RAW cells as well as a small-molecule METTL3 inhibitor, I studied the impact of the two mRNA modifications on macrophage phenotype, activation and phagocytosis activity. By observing the temporal dynamics of the two mRNA modifications upon stimulation and mapping them at the transcript level, I studied the relationship and association between m6A and A-to-I editing sites to understand the interdependencies and co-regulation of these two RNA modifications.

4. Results

4.1 Impact of m6A and A-to-I editing on the immunological function of macrophages

4.1.1 RAW macrophages respond to pro-inflammatory LPS and IFN-γ stimulation

To confirm that the RAW macrophage cell line serves as a useful model to study RNA modifications during macrophage activation, I tested the response of wild-type RAW cells to pro-inflammatory stimulation. For this purpose, I stimulated resting RAW macrophages with a combination of LPS and IFN-γ and harvested RNA at different time points after treatment (0 h, 2 h, 12 h, and 24 h) for transcriptomic analysis. RNA was sequenced using Illumina next generation sequencing (NGS) and bioinformatic analysis was performed by Dr. Salvatore Di Giorgio (Fig. 4A).

In the gene expression analysis I observed tremendous changes in the expression of genes associated with macrophage activation (gene ontology [GO]:0042116) throughout the 24 h time course after pro-inflammatory stimulation. Genes were clustered in groups according to their temporal regulation and magnitude of response (Fig. 4B). The temporal trends of significantly differentially expressed macrophage activation genes are visible in the bar plots depicting log 2-fold-change (Log2FC) of gene expression (Fig. 4C). For instance, selected pro-inflammatory cytokines, i.e., *Tnfa* and Interferon-β1 (*Ifnb1*), showed low basal expression but rapid induction upon stimulation as seen in high expression levels 2 h post-LPS/IFN-γ treatment. I observed another group of genes, i.e. *Tlr1*, *Tlr3*, *Tlr6*, and *Tlr9,* involved in pathogen recognition[46], that was strongly expressed starting at 12 h post-treatment. Meanwhile, a third group of genes showed medium to high expression levels at rest while being repressed at different time points after stimulation. Examples include receptors regulating macrophage differentiation, migration and inflammation such as CX3C motif chemokine receptor 1 (*Cx3cr1),* triggering receptor expressed on myeloid cells 2 *(Trem2),* interleukin 1 receptor-like 1 *(Il1rl1)* and nuclear receptor subfamily 4 group A member 1 (*Nr4a1;* Fig. 4B-C). As demonstrated by the phased pro-inflammatory gene expression program of RAW macrophages in response to LPS and IFN-γ stimulation, I

concluded that the RAW cell line serves as a useful model for studying the role of RNA modifications in macrophage activation.

In addition to genes directly involved in macrophage activation, I investigated the expression of genes regulating m6A and A-to-I editing. Most genes associated with the m6A RNA modification were relatively stable or mildly up- and downregulated at selected time points after stimulation. This includes stable expression of the members of the core m6A-writer complex *Mettl3* and *Wtap* (not differentially expressed at any time point, hence, not depicted in Fig. 4D), mild upregulation of m6A readers *Fmr1, Igf2bp1* and *Hnrnpa1*, and mild downregulation of m6A readers *Hnrnpa2b1, Lrpprc*, and *Snd1*, m6A writer *METTL14*, and m6A eraser *Fto* at selected time points after stimulation (Fig. 4D). On the other hand, I expected interferon inducible *Adar1* to be upregulated after LPS and IFN-γ treatment[29]. Indeed, *Adar1* (also known as *Adar*) together with m6A reader *Igf2bp2* were the highest and most consistently upregulated genes at any time point after stimulation as compared to the resting state. In contrast, *Adar2* (also known as *Adarb1*) was downregulated 12 h and 24 h after treatment (Fig. 4D). As the expression levels of *Adar2* were overall relatively low (on average 60-fold lower than *Adar1;* Table S1) and no role of *Adar2* has been described in myeloid cells, I focused on the highly expressed A-to-I editing enzyme *Adar1* in this study. Considering the differential expression of *Adar1* and various m6A regulating enzymes during the time course of stimulation, I hypothesized a possible functional role of ADAR1-mediated A-to-I editing and METTL3-mediated m6A in macrophage activation.

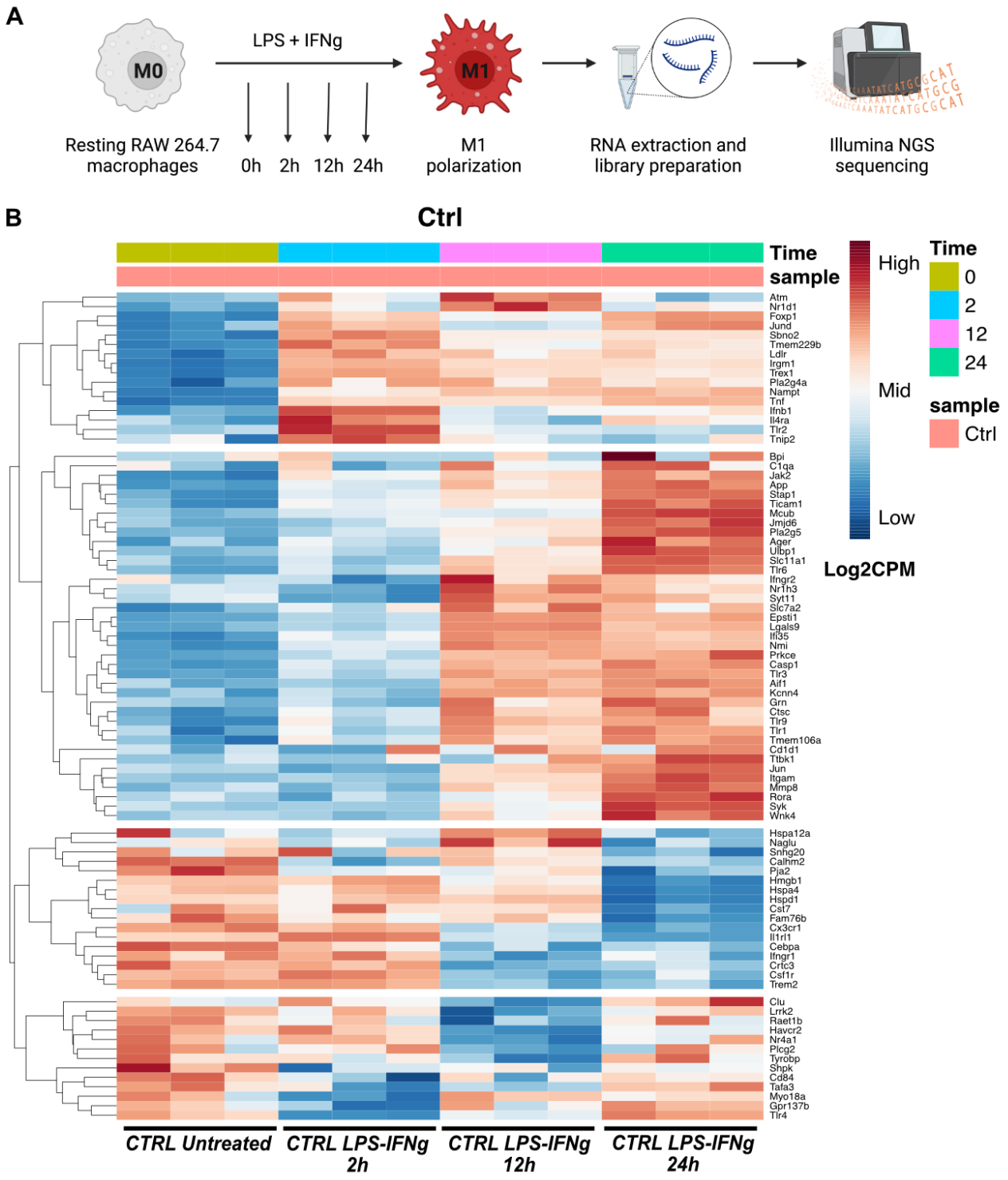

Figure 4. Response of RAW macrophages to pro-inflammatory stimulation. (continued on next page)

Figure 4, continued:

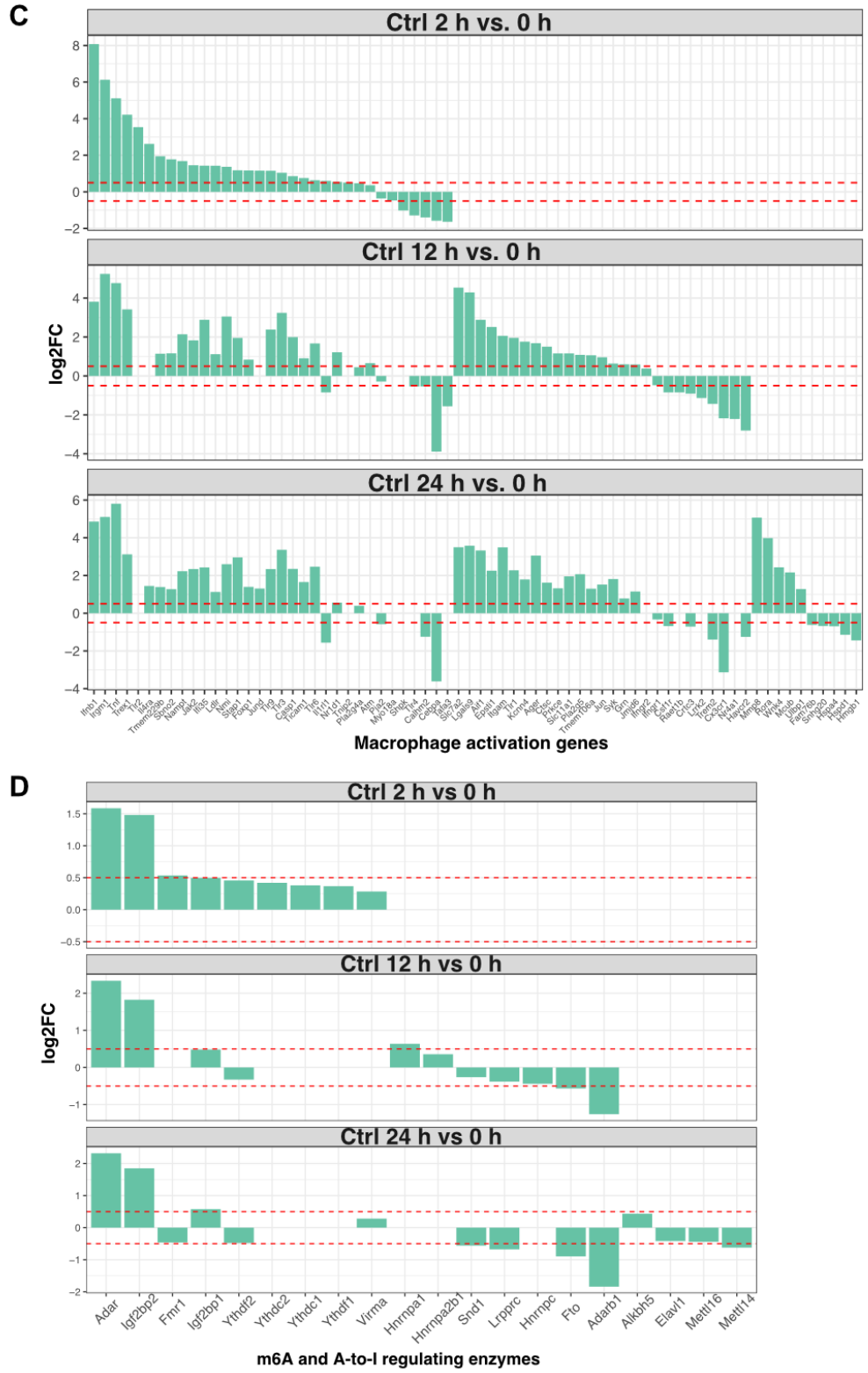

Figure 4. Response of RAW macrophages to pro-inflammatory stimulation (continued on next page).

Figure 4, continued: (A) Schematic representation of macrophage activation assay. **(B)** Transcriptomic expression (log2- counts per million reads [log2CPM]) of genes involved in macrophage activation (GO:0042116) 0 h, 2 h, 12 h, and 24 h after LPS/IFN-γ treatment in control RAW macrophages. Gene expression-based hierarchical clustering by Euclidean distance is illustrated by the dendrogram. **(C)** Changes in gene expression (Log2-fold change [Log2FC]) are depicted for differently expressed macrophage activation genes for specified comparisons. **(D)** Changes in gene expression (Log2FC) of differentially expressed genes regulating m6A and A-to-I RNA modifications are depicted for specified comparisons. **(C–D)** Statistical significance was defined by false discovery rate (FDR) < 0.05; the red lines mark |log2FC| = 0.5, defining the minimum limit for differential expression. **(B-D)** n=3; produced by Dr. Salvatore Di Giorgio.

4.1.2 Generation of ADAR1-KO and METTL3-KO cell lines

To study the role of m6A and A-to-I RNA modifications in macrophages, I created clonal ADAR1- and METTL3-KO RAW cell lines. First, I and Chih-Yuan Kao cloned non-targeting single guide RNAs (sgRNAs) and targeting sgRNAs for METTL3 and ADAR1 into the pSpCas9(BB)-2A-GFP (PX458; a gift from Feng Zhang) plasmid, encoding green fluorescent protein (GFP) and the Clustered Regularly Interspaced Short Palindromic Repeats (CRISPR)-associated protein 9 (Cas9). After I nucleofected RAW macrophages with the plasmid for transient GFP and sgRNA, GFP^+ cells were single-cell sorted. I tested colonies arising from single cell clones for successful ADAR1- and METTL3-KO by polymerase chain reaction (PCR) amplification and Sanger sequencing of targeted genomic regions to detect insertion-deletion mutations (indels). In case of allelic differences, PCR products were cloned into plasmid vectors and consecutively analyzed by Sanger sequencing. Additionally, I validated potential KO clones by Western blot to confirm the absence of protein and by an additional functional assay. Finally, the absence of RNA modification was analyzed by liquid chromatography with tandem mass spectrometry (LC-MS/MS; Fig. 5A, Fig. 6A). The control cell line (ctrl) was created by nucleofection of two plasmids encoding non-targeting sgRNAs and sorting of GFP^+ cells in bulk.

For the generation of ADAR1-KO cells, I designed a sgRNA targeting exon 2 that was shared by *Adar1* p110 and p150 isoforms. I confirmed the successful KO of ADAR1 in four clones by Sanger sequencing of the targeted region (Fig. 5B), Western blot (Fig. 5C) and absence of A-to-I editing in *Exoc1* mRNA (Fig. 5D). In LC-MS/MS analysis, I detected inosine

only in control cells after LPS and IFN-γ treatment while inosine levels were below the detection limit in all unstimulated and stimulated ADAR1-KO samples. This indicates that A-to-I editing increased upon stimulation selectively in the control but not in ADAR1-KO cells. However, LC-MS/MS was not sensitive enough for inosine detection in unstimulated samples (Fig. 5E). Nevertheless, by several other means, I demonstrated the successful generation of a RAW ADAR1–KO cell line.

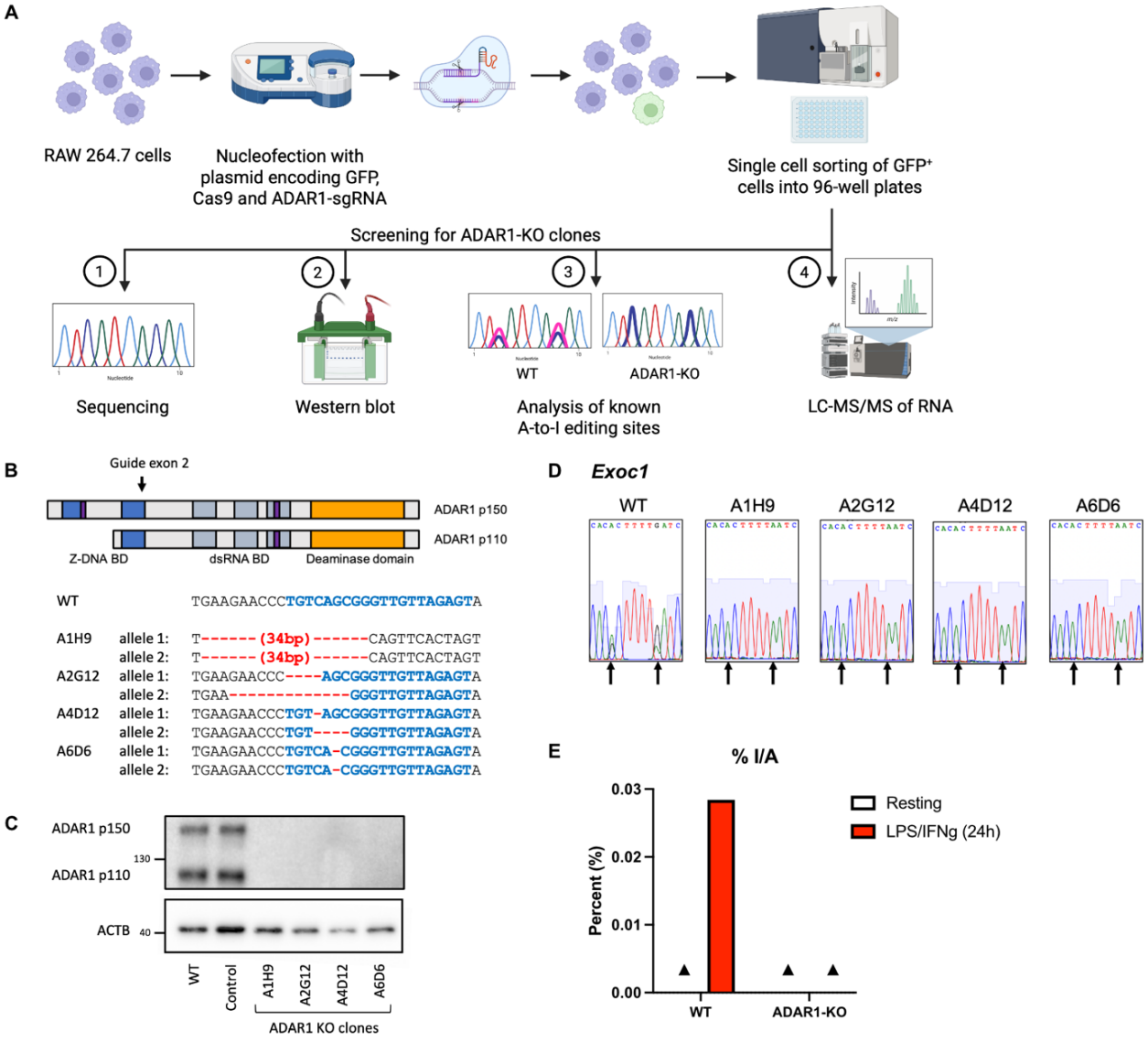

Figure 5. Creation of ADAR1-KO RAW macrophages. (A) Schematic representation of the workflow to generate ADAR1-KO RAW cells. **(B)** Depiction of sgRNA targeted region in *Adar1*. Clonal KO lines were analyzed for insertions or deletions in targeted region on the genomic level by PCR amplification, cloning of amplicons into plasmids and Sanger sequencing; BD: binding domain (continued on next page).

Figure 5, continued: (C) Western blot showing the absence of ADAR1 protein in ADAR1-KO lines. **(D)** RNA was isolated, reverse transcribed and a highly edited region of *Exoc1* was PCR-amplified. Absence of editing in ADAR1-KO clones was validated by Sanger sequencing. Sequencing chromatograms are displayed. **(E)** LC-MS/MS analysis of inosine (I) in poly-A enriched RNA; ▲ indicates when RNA modifications were below the detection limit; n=1.

The RAW METTL3-KO cell line was created using sgRNAs targeting *Mettl3* exon 1 and exon 3. I identified indels in *Mettl3* gene locus in six clones (Fig. 6B). Using an antibody against METTL3's catalytic subunit, I validated the absence of full and potential shorter METTL3 splice isoforms with a retained catalytic subunit[96] by Western blot (Fig. 6C). For functional confirmation of the METTL3-KO, I quantified mRNA levels of torsin 1A-interacting protein 2 (*Tor1aip2)* splice isoforms that are affected by the presence of m6A. While *Tor1aip2*'s long isoform is favored in the absence of m6A, the short isoform is favored in the presence of m6A[97]. Indeed, particularly the short *Tor1aip2* splice isoform was reduced and confirmed m6A depletion in the METTL3-KO clones (Fig. 6D). Additionally, LC-MS/MS analysis showed a strong depletion of m6A in the METTL3-KO samples (Fig. 6E right). Altogether, these data confirm the successful generation of a METTL3-KO cell line in RAW cells.

To detect if large differences between individual clones existed due to clonal heterogeneity or mutations, I submitted RNA of wild-type (WT), control, ADAR1-KO and METTL3-KO clones for Illumina RNA sequencing. In principal component analysis (PCA), control cells and WT cells clustered closely together while METTL3-KO and ADAR1-KO clones differed notably from them. Moreover, from this analysis I identified individual clones (METTL3-KO P3D8 and P4D5) as outliers that might carry non-specific mutation and I excluded them from further analysis in this study (Fig. 6F).

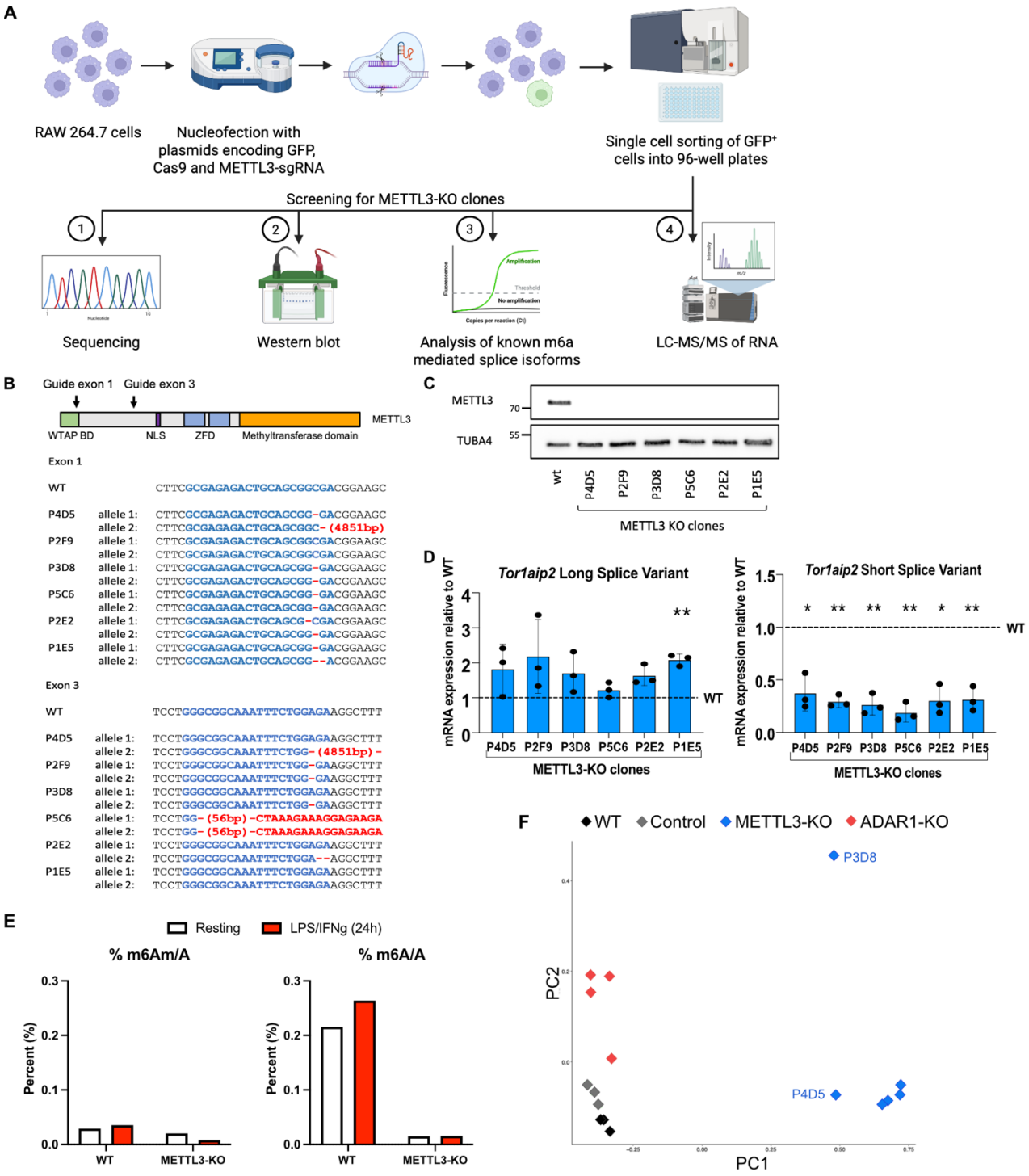

Figure 6. Creation of METTL3-KO RAW macrophages. (A) Schematic representation of the workflow to generate METTL3-KO RAW cells. **(B)** Depiction of sgRNA targeted regions in *Mettl3*. Clonal KO lines were analyzed for insertions or deletions in targeted region on the genomic level by PCR amplification, cloning of amplicons into plasmids and Sanger sequencing. **(C)** Western blot showing the absence of METTL3 protein in METTL3-KO lines (continued on next page).

Figure 6, continued: (D) Quantification of mRNA levels of m6A-dependent *Tor1aip2* splice isoforms by RT-qPCR with the long isoform known to be favored in the absence of m6A and the short isoform favored in the presence of m6A; n=3; Paired, two-tailed t test was performed between control and each KO clone; significance values are indicated as follows: ∗p < 0.05; ∗∗p < 0.01; ∗∗∗p < 0.001; ∗∗∗∗p < 0.0001; n=3. **(E)** LC-MS/MS analysis of poly-A enriched RNA for m6A levels and m6Am; m6Am is absent in mRNA and commonly used to control for rRNA contaminations; n=1. **(F)** RNA from WT, control, METTL3-KO and ADAR1-KO clones was analyzed by Illumina sequencing. Principal component analysis (PCA) was performed based on expressed genes and two outliers were identified among METTL3-KO clones (P3D8 and P4D5). **(F)**Produced by Dr. Salvatore Di Giorgio.

4.1.3 Mapping of mRNA modifications

After establishing METTL3- and ADAR1-KO cell lines, I used these KO lines as m6A- and inosine-free negative controls for calling and mapping the two RNA modifications. For identification of m6A, I performed direct RNA sequencing of poly-A RNA using Oxford Nanopore Technology (ONT) that was analyzed by Dr. Salvatore Di Giorgio. METTL3-dependent m6A sites were identified by differential methylation analysis (Fig. 7B), considering only sites where a site showed increased methylation in control or ADAR1-KO samples as compared to METTL3-KO samples while filtering out false positive signals that likely arise from noise and non-related RNA modifications (detailed filtering criteria are described in the methods). Using this analysis, I identified many m6A sites in the control and ADAR1-KO that were absent in the METTL3-KO (Fig. 7A-B). Interestingly, treatment of an ADAR1-KO clone (A6D6) with the small-molecule METTL3 inhibitor STM2457 (48 h) and LPS/IFN-γ (24 h; ADAR_KO_STM-24h) resulted in a major reduction in m6A levels; however, more residual m6A signal was detected as compared to the METTL3-KO samples (Fig. 7A). Closer analysis of the identified m6A sites revealed a strong sequence preference of the consensus DRACH motif (D=A, G or U; H=A, C or U; Fig. 7C-D), confirming the validity of identified m6A sites.

When calling inosine sites from the Nanopore sequencing data set, attempts to set adequate filtering criteria failed as no major distinction of inosine levels were observed in ADAR1-KO as compared to ADAR1-competent samples (Fig. 7E). Hence, we used the reliable Illumina sequencing data set to accurately identify A-to-I editing sites using REDItools. Here, A-to-I editing was identified from A-to-G mismatches that were absent in the ADAR1-KO conditions.

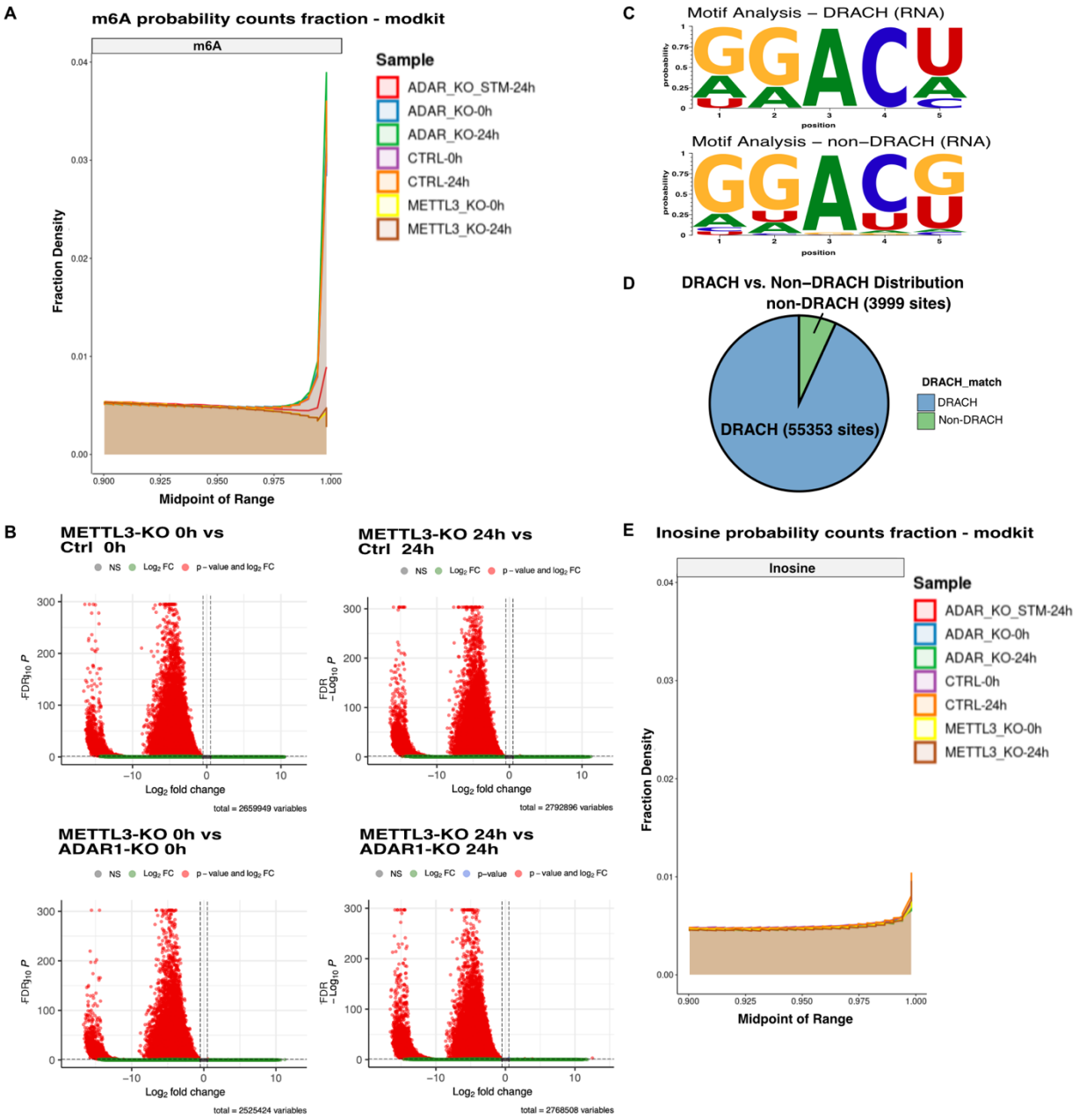

Figure 7. Calling of RNA modifications based on Nanopore sequencing. RNA from control, METTL3-KO and ADAR1-KO samples were sequenced by direct RNA Nanopore sequencing and analyzed for adenosine modifications. **(A)** m6A modification probabilities (output from the Modkit sample-probs analysis tool) indicate reduced m6A probabilities in the METTL3-KO as compared to other samples. **(B)** Differential methylation analysis between METTL3-KO samples with either control or ADAR1-KO samples identified differentially methylated sites that were considered true m6A sites. **(C)** Analysis of the preferred sequence motif of m6A sites (in unstimulated control cells). **(D)** Identification of sequence motifs as DRACH (D=A, G or U; H=A, C or U) and non-DRACH motifs. **(E)** A-to-I editing probabilities (output from the Modkit sample-probs analysis tool) allows no clear distinction between ADAR1-KO and other samples indicating unreliable A-to-I editing detection by this Nanopore data analysis. **(A-E)** n=3; produced by Dr. Salvatore Di Giorgio.

4.1.4 Loss of m6A and inosine impacts innate immune activation in the absence of an exogenous stimulus

Previous studies have reported a role of m6A and A-to-I editing in counteracting the formation of immunostimulatory dsRNA structures, thereby preventing type I IFN production and innate immune activation[26,33,34,94]. To test if such an innate immune response was induced in RAW macrophages upon m6A or inosine depletion, I monitored gene expression profiles characteristic of an interferon and dsRNA response. Contradictory to most published literature that demonstrates ISG induction and inflammation upon ADAR1 depletion[33,34,52], I observed a tendency of ADAR1-deficient macrophages to express reduced levels of type I interferon *Ifnb*, ISGs and genes involved in the dsRNA response as compared to the control macrophages (Fig. 8A, B, E).

In contrast, METTL3-KO cells exhibited the opposite phenotype with a tendency of increased *Ifnb* expression, type I IFN signaling and a dsRNA response in the absence of exogenous stimuli (Fig. 8C, D, E). To evaluate whether m6A depletion induces type I IFN expression also for a shorter time span, I treated RAW cells with the small-molecule METTL3 inhibitor STM2457. After 24 h, 48 h, and 72 h of METTL3 inhibition, *Ifnb* expression tended to increase as compared to DMSO-treated control cells (Fig. 8F). Overall, the observed induction of type I IFNs and innate immune activation upon m6A depletion is in line with m6A's role in preventing formation of dsRNA structures and consecutive activation of dsRNA sensors[26,94] or recognition of unmethylated RNAs by other TLRs[51].

4.1.5 Loss of m6A and inosine impairs macrophage IFN response upon pro-inflammatory stimulation

Next, I tested the response of the modification-deficient macrophages to pro-inflammatory stimulation presented by LPS and IFN-γ treatment. In control cells, I observed a peak in *Ifnb* levels 2 h after stimulation (Fig. 8G) that was accompanied by a type I IFN response as seen in the upregulation of several ISGs including *Isg15, Mda5 (=Ifih),* Z-DNA binding protein 1 *(Zbp1),* 2'-5'-oligoadenylate synthetase Like 1 *(Oasl1)* and *Oasl2* at time point 24 h after stimulation as compared to resting conditions (Fig. 8H). While ADAR1-KO cells induced *Ifnb* after stimulation comparable to stimulated control macrophages, their downstream interferon response 24 h after LPS/IFN- γ was dampened (Fig. 8I), similar to

the dampened ISG response observed in ADAR1-KO cells at resting state (as described above, Fig. 8A).

Surprisingly, LPS/IFN-γ-treated METTL3-KO cells lacked the characteristic peak in *Ifnb* expression after stimulation (Fig. 8G). This lack of *Ifnb* upregulation might either be explained by a direct effect of m6A modifications in regulating gene expression or by adaptations to constitutively elevated IFNB levels due to immune sensing of unmethylated RNAs. First, I asked if expression of cell surface receptors that are responsible for LPS and IFN-γ recognition was influenced by the loss of METTL3. I did not observe differential expression of *Ifngr1*, *Ifngr2*, and *Tlr4* in resting METTL3-KO as compared to resting control cells (Table S2-3). Alternatively, deficient *Ifnb* upregulation in METTL3-KO cells could be mediated by modulation of downstream signaling, epigenetic[99] or post-translational modifications[100] or by upregulation of negative *Ifnb* regulators NFKB Repressing Factor (NKRF)[101] or IRF2 assisted by interferon regulatory factor 2 binding protein 1 (IRF2BP1) and IRF2BP2[102,103] as their transcripts were upregulated in METTL3-KO cells at different time points (Table S2-S3).

Despite failure of rapid *Ifnb* induction upon pro-inflammatory stimulation, several ISGs were up- or downregulated in METTL3-KO as compared to control cells (Fig. 8J), demonstrating an influence of m6A on the response to LPS and IFN-γ stimulation and that METTL3-KO cells were capable to induce IFN-β-independent inflammatory processes. Among the differentially expressed IFN and dsRNA response genes, I found several genes with m6A and A-to-I editing sites (Fig. 8A-D, H-J). This suggests that m6A and A-to-I editing may directly regulate gene expression, independently of their indirect effects on the formation and recognition of unmodified RNA structures. A direct role of m6A in the regulation of macrophage pro-inflammatory response is further supported by the coordinated upregulation of m6A readers *Igf2bp1*, *Igf2bp2*, *Fmr1* and *Hnrnpa1*, and downregulation of m6A readers *Hnrnpa2b1, Lrpprc* and *Snd1* and eraser *Fto* during stimulation (Fig. 4D).

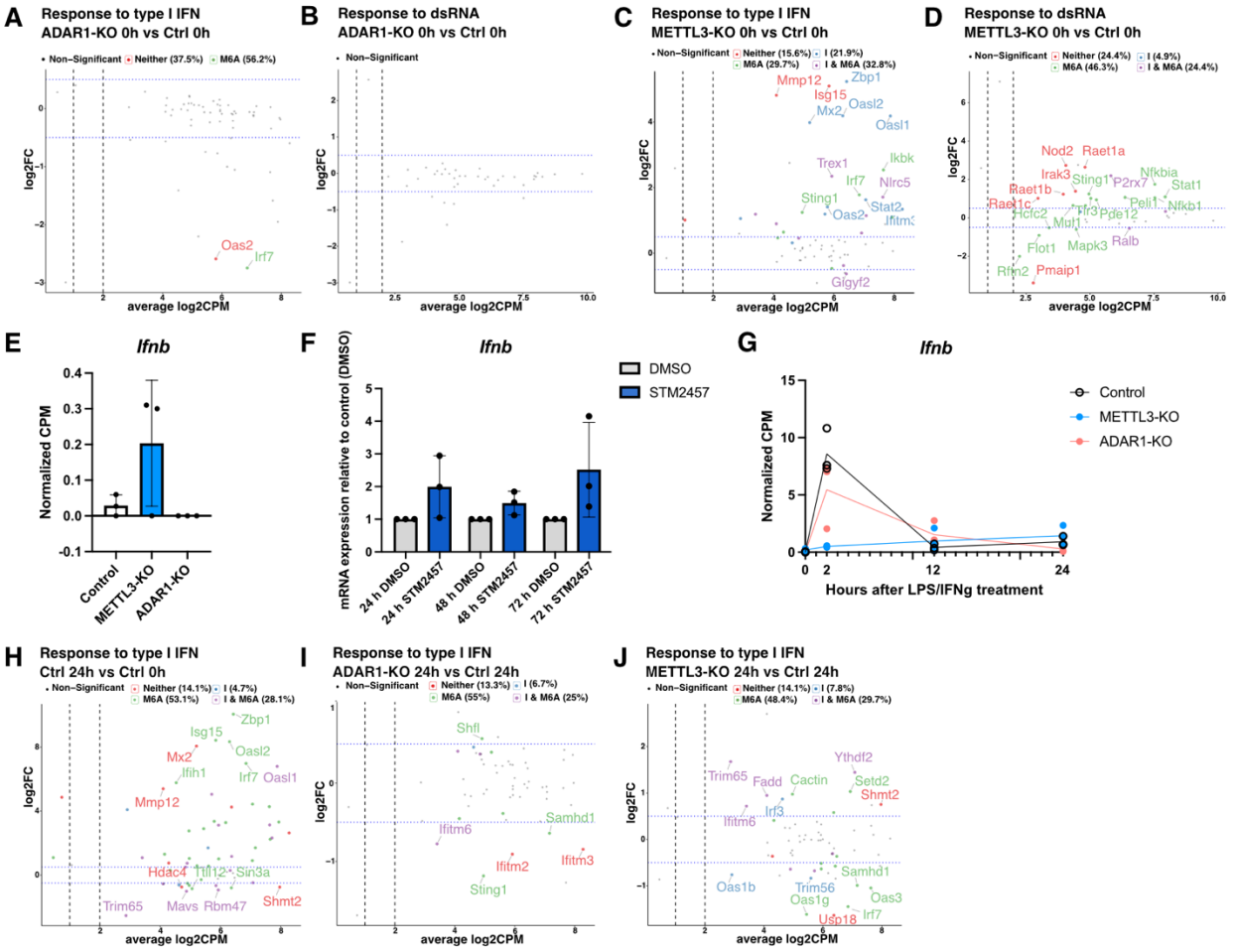

Figure 8. Changes in interferon and dsRNA responses upon depletion of RNA modifications. (A-D, H-J) Mean gene expression (average log 2 counts per million reads [log2CPM], x-axis) and changes in gene expression (log2FC, y-axis) between indicated comparisons of control, ADAR1-KO and METTL3-KO for genes involved in the response to type I interferons (GO:0034340) **(A, C, H-J)** and to dsRNA (GO:0043331) **(B, D)**. Genes are labeled according to presence of RNA modification sites and differential expression. The left vertical lines indicate log2CPM = 1: genes below are considered lowly expressed; the right vertical lines indicate log2CPM = 2: genes above are considered highly expressed; expression levels of genes with 1< log2CPM< 2 are regarded as moderate. The horizontal lines mark the limits for differential gene expression of |log2FC| = 0.5. **(E)** CPM of *Ifnb* reads obtained from Illumina sequencing data in control, METTL3-KO and ADAR1–KO RAW macrophages at rest. **(F)** *Ifnb* mRNA levels after 24 h, 48 h, and 72 h of METTL3 inhibition by STM2457 (10 μM) treatment. **(G)** CPM of *Ifnb* reads obtained from Illumina sequencing data in control, METTL3-KO and ADAR1–KO RAW macrophages at different time points after stimulation. **(A-J)** n=3; **(A-E & G-J)** produced by Dr. Salvatore Di Giorgio.

4.1.6 Importance of adenosine modifications in macrophage classical activation

To investigate the role of m6A and A-to-I editing in macrophage activation more closely, we analyzed the mRNA modification sites of transcripts that are functionally associated with macrophage activation and their gene expression changes upon METTL3 and ADAR1 depletion. I observed the induction of many genes involved in macrophage activation in control macrophages upon LPS and IFN-γ treatment with 76.6% of these differentially expressed genes carrying mRNA modification sites (Fig. 9A). Additionally, I noticed different gene expression patterns with a progressive downregulation of many macrophage activation markers and inflammatory cytokines in METTL3- and ADAR1-KO cells upon stimulation as compared to control macrophages at corresponding time points (Fig. 9B-D). Both observations indicate a role of m6A and A-to-I RNA editing in macrophage activation.

To test if transcriptomic defects during macrophage activation were also translated at the protein level, I assessed macrophage activation marker expression by flow cytometry (Fig. 10A). While resting macrophages showed mostly unchanged levels of activation markers in the absence of ADAR1 and METTL3, upon pro-inflammatory stimulation, METTL3-KO macrophages showed deficient upregulation of cell surface markers CD40, CD80, MHC II, beta-2-microglobulin (b2M; promoting MHC I cell surface expression and peptide binding[104,105]) and CD36 (Fig. 10B). Most apparent deficiencies included CD80 and MHC II expression, key molecules for antigen presentation and co-stimulation of T cells[57]. ADAR1-KO macrophages showed similar cell surface marker expression like control macrophages with only a tendency of mildly attenuated expression of selected markers such as CD80, MHC II, and b2M (Fig. 10B). Overall, these findings stress the crucial role of mRNA modifications, particularly of m6A, in enabling macrophages to fulfill their function during inflammation and communication with other players of the immune system.

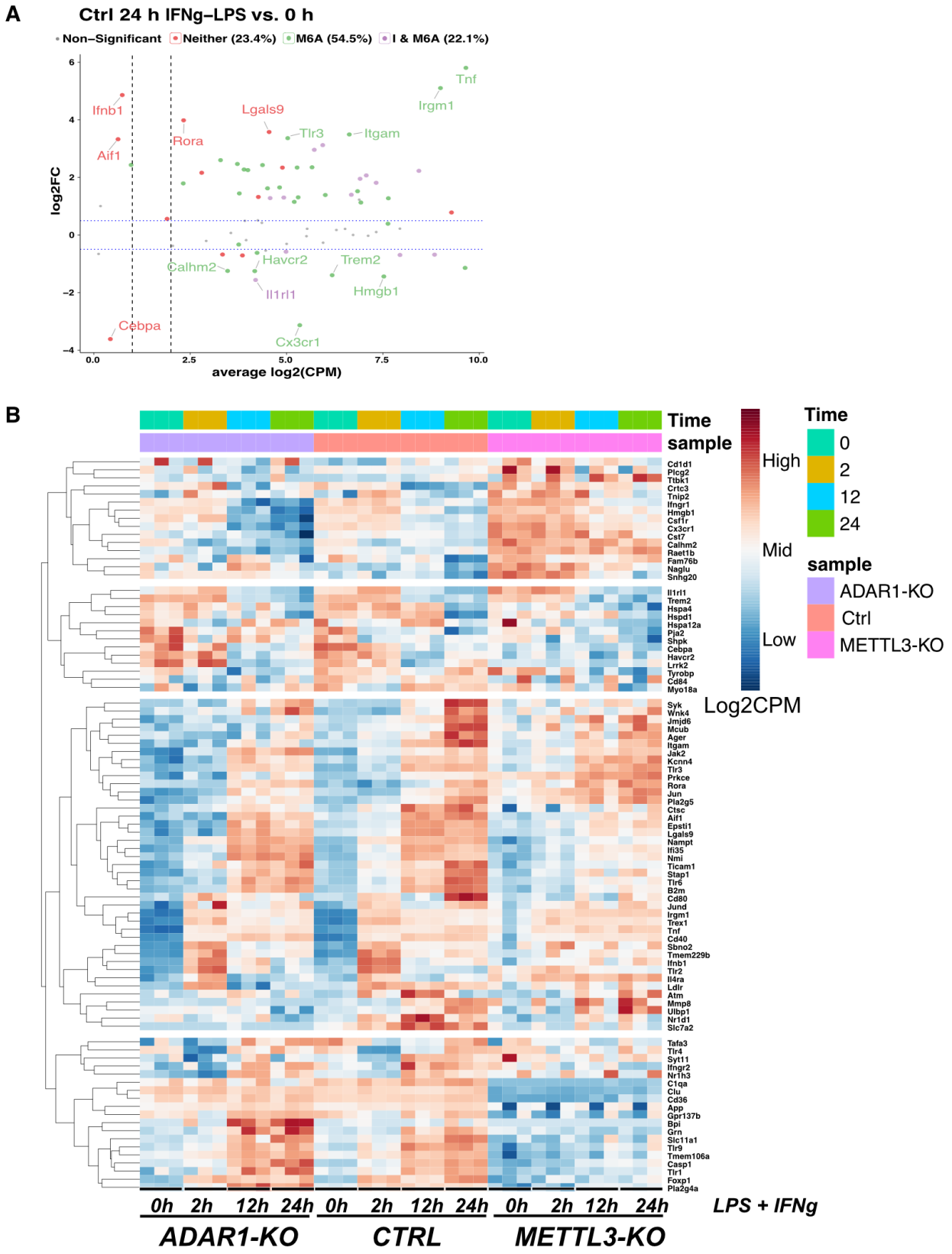

Figure 9. Transcriptomic changes in macrophage activation upon loss of METTL3 or ADAR1 in RAW macrophages (continued on next page).

Figure 9, continued:

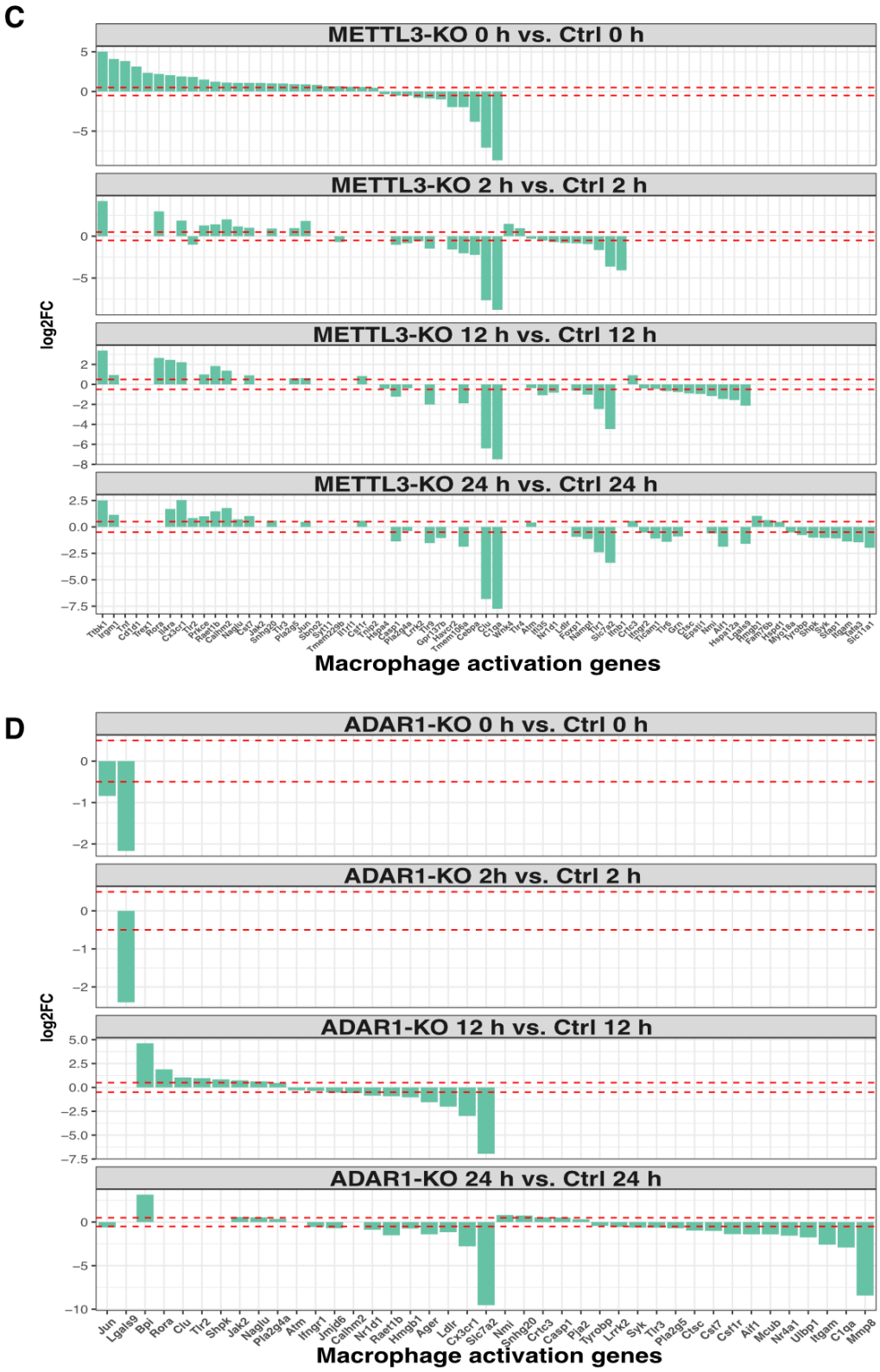

Figure 9, continued: Transcriptomic changes in macrophage activation upon loss of METTL3 or ADAR1 in RAW macrophages (continued on next page).

Figure 9, continued: (A) Mean gene expression (average log 2 counts per million reads [log2CPM], x-axis) and changes in gene expression (log2FC, y-axis) of macrophage activation markers (GO:0042116) between control samples 24 h post-LPS/IFN-γ treatment and unstimulated control samples. Genes are labeled according to presence of RNA modification sites and differential expression. The left vertical line indicates log2CPM = 1: genes below are considered lowly expressed; the right vertical line indicates log2CPM = 2: genes above are considered highly expressed; expression levels of genes with 1< log2CPM< 2 are regarded as moderate. The horizontal line marks the limits for differential gene expression of |log2FC| = 0.5. **(B)** Transcriptomic expression (log2-counts per million reads [CPM]) of macrophage activation genes 0 h, 2 h, 12 h, and 24 h after LPS/IFN-γ treatment in control, METTL3-KO and ADAR1-KO RAW macrophages. Gene expression-based hierarchical clustering by Euclidean distance is illustrated by the dendrogram. **(C-D)** Changes in gene expression (Log2FC) are depicted for differently expressed macrophage activation gene markers for METTL3-KO **(C)** and ADAR1-KO **(D)** as compared to control macrophages at respective time points. Statistical significance was defined by false discovery rate (FDR) < 0.05; the red lines mark |log2FC| = 0.5 defining the minimum limit for differential expression. **(A-D)** n=3; produced by Dr. Salvatore Di Giorgio.

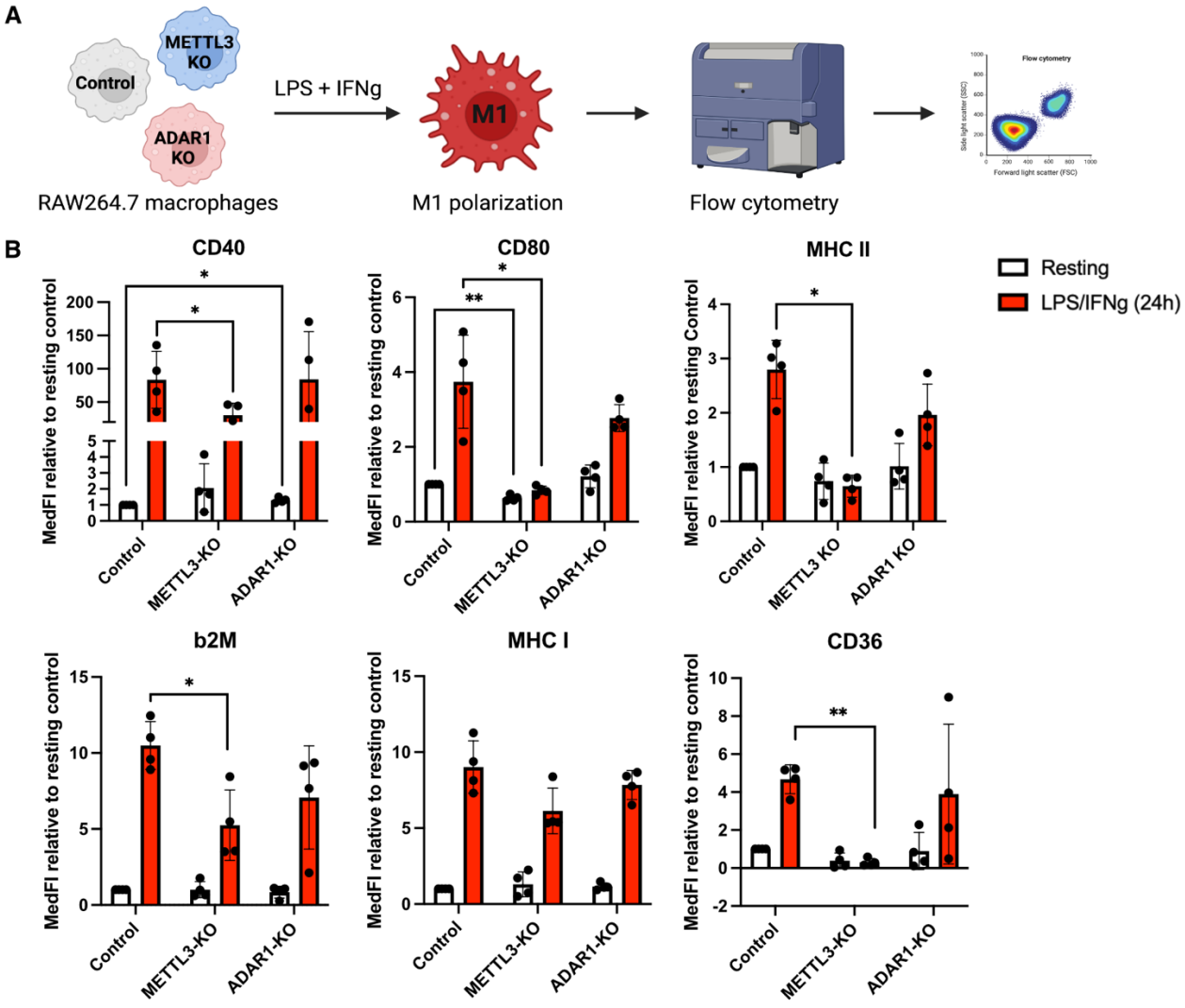

Figure 10. Macrophage activation marker expression upon ADAR1 and METTL3-KO and LPS and IFN-γ stimulation. (A) Schematic representation of the assay. **(B)** Flow cytometric analysis of activation-associated cell surface markers of control, METTL3-KO and ADAR1-KO RAW macrophages at rest and 24 h after LPS and IFN-γ treatment. Paired two-tailed t-tests were performed for each KO as compared to the control at corresponding treatments. Significance values are indicated as follows: ∗p < 0.05; ∗∗p < 0.01; ∗∗∗p < 0.001; ∗∗∗∗p < 0.0001; n=4.

4.1.7 METTL3 inhibition mimics the impaired macrophage activation observed in METTL3-KO cells

As I observed a substantial impairment of METTL3-deficient macrophages to upregulate activation markers, I wanted to test if these effects were specific to m6A depletion and could be recapitulated by short-time METTL3 inhibition using the small-molecule inhibitor STM2457. First, I treated METTL3-KO cells with the METTL3 inhibitor where I expected to observe no impact on macrophages' phenotype as m6A was already absent due to METTL3 KO. Indeed, surface markers of METTL3-KO cells remained unaffected by STM2457 treatment (Fig. 11). In contrast, when I treated control cells with the METTL3 inhibitor, they closely mimicked the phenotype of the full METTL3-KO as demonstrated by impaired CD40, MHC II, MHC I, b2M and CD36 upregulation upon pro-inflammatory stimulation (Fig. 11). Together, these findings validate that the impaired activation phenotype in METTL3-KO macrophages indeed depends on the m6A mRNA modification and that the small-molecule METTL3 inhibitor is a valuable tool to deplete m6A without genomic manipulation of a cell line.

As METTL3- and ADAR1-KO macrophages showed defects in macrophage activation, I asked whether there was an additive effect between inosine and m6A RNA modifications. To deplete both modifications from macrophages, I treated ADAR1-KO cells with the METTL3 inhibitor. Despite high variability between individual clones, ADAR1-KO cells treated with METTL3 inhibitor tended to further reduce activation markers CD80, MHC II, and b2M after stimulation as compared to DMSO-treated ADAR1-KO cells in response to LPS and IFN-γ treatment. The level of reduction in cell surface marker expression upon m6A depletion was similar in control and ADAR1-KO macrophages, indicating a dominant role of m6A on macrophage activation and a potential additive effect of m6A and inosine RNA modifications that would require further investigation (Fig. 11).

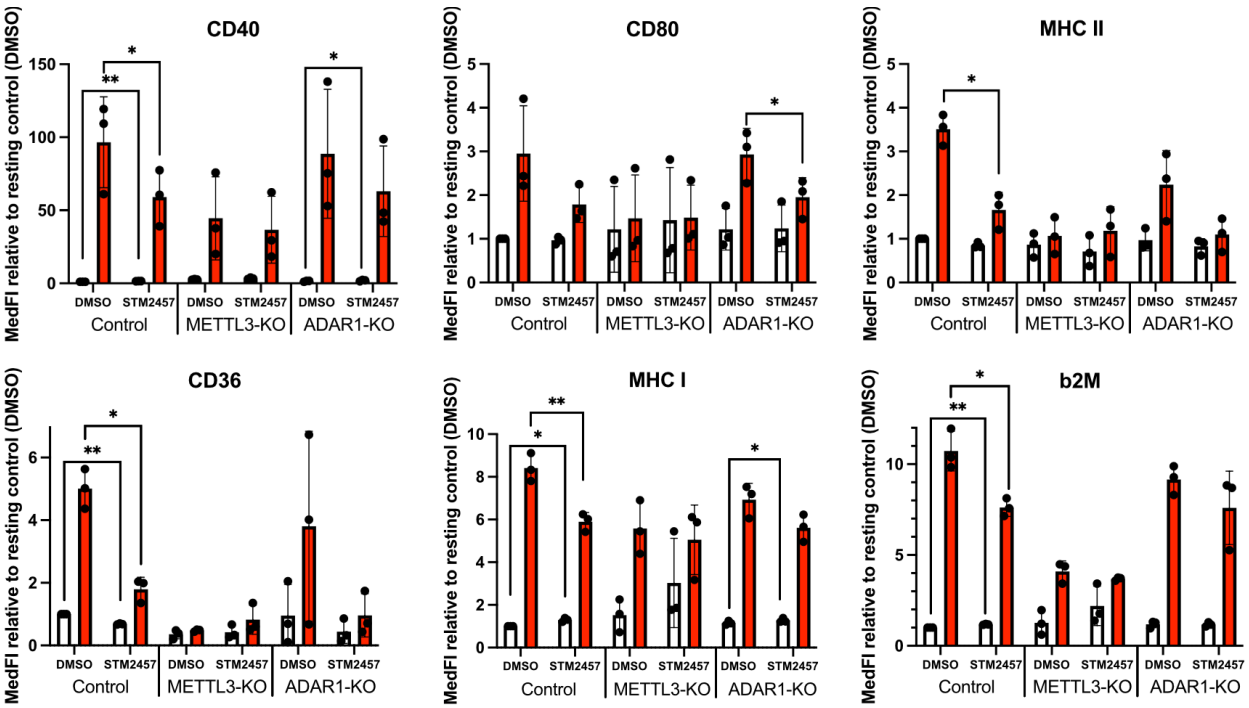

Figure 11. Macrophage activation marker expression upon treatment with METTL3 inhibitor. Control, METTL3-KO and ADAR1-KO RAW cells were treated with DMSO or small-molecule METTL3 inhibitor STM2457 (10 μM, 48 h). Expression of activation-associated cell surface markers was analyzed by flow cytometry at rest and 24 h after LPS and IFN-γ treatment. Paired two-tailed t-tests were performed comparing inhibitor treatment with DMSO treatment of corresponding cell lines and stimuli. Significance values are indicated as follows: ∗p < 0.05; ∗∗p < 0.01; ∗∗∗p < 0.001; ∗∗∗∗p < 0.0001; n=3.

4.1.8 m6A promotes activation in primary mouse macrophages

Next, I validated the observed role of m6A in the pro-inflammatory activation of macrophages in primary mouse macrophages. Cells collected from mouse bone marrow were differentiated into bone marrow-derived macrophages (BMDMs) *in vitro* by macrophage colony-stimulating factor (M-CSF). Six days into differentiation, I treated macrophages with the METTL3 inhibitor STM2457 or DMSO as negative control, followed by LPS and IFN-γ treatment on the seventh day (Fig. 12A). While primary macrophages generally induced activation marker expression upon pro-inflammatory stimulation, I observed a mild but significant attenuation in CD40, CD80 and CD69 expression after METTL3 inhibition as compared to DMSO-treated control macrophages (Fig. 12B). Notably,

treatment with M-CSF was described to favor macrophage polarization towards a M2-like phenotype[106]. Such pre-polarized macrophages might respond differently and their activation might be less m6A-dependent, explaining the less pronounced defect in macrophage activation of pre-polarized BMDMs upon m6A inhibition as compared to RAW cells. Despite observing a milder level of m6A-dependency, I conclude that the effect of m6A in macrophage activation is not limited to the RAW cell line model but also applies to primary macrophages.

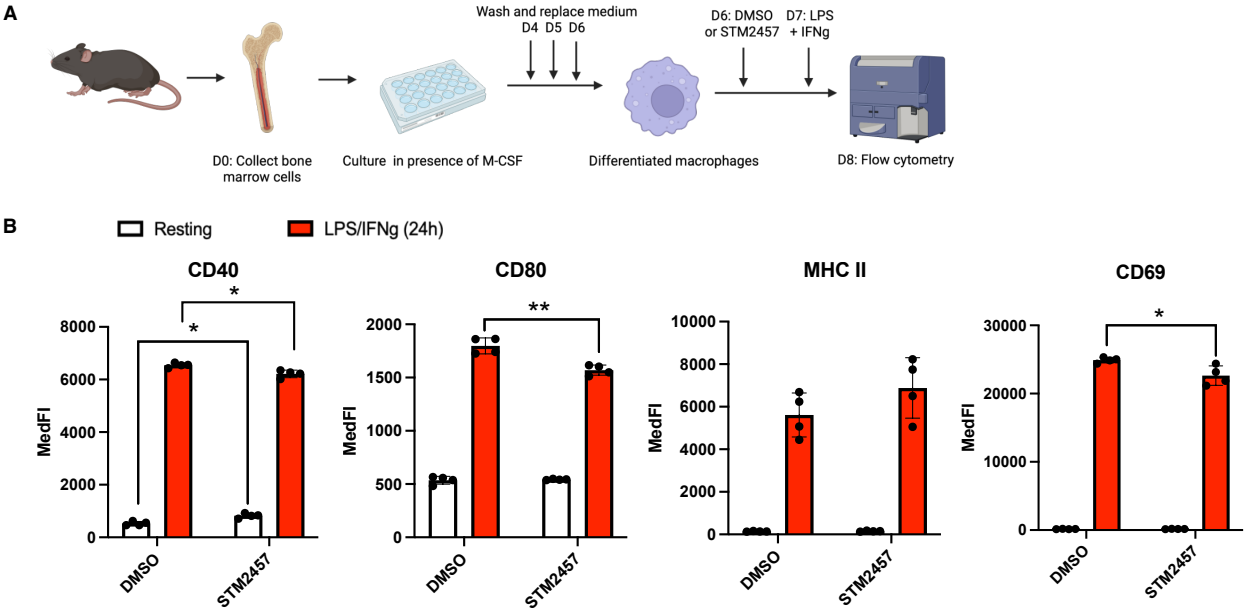

Figure 12. Macrophage activation marker expression in BMDMs upon METTL3 inhibition. (A) Schematic representation of BMDMs' differentiation and stimulation assay. **(B)** BMDMs were treated with DMSO or with the small-molecule METTL3 inhibitor STM2457 (10 µM, 48 h). Expression of activation-associated cell surface markers was analyzed by flow cytometry at rest and 24 h after LPS and IFN-γ treatment. Paired two-tailed t-tests were performed for corresponding conditions. Significance values are indicated as follows: ∗p < 0.05; ∗∗p < 0.01; ∗∗∗p < 0.001; ∗∗∗∗p < 0.0001; n=4.

4.1.9 RNA modifications drive macrophage activation in response to distinct pro-inflammatory stimuli

After establishing the impact of mRNA modifications in macrophage activation upon combinational LPS and IFN-γ stimulation, I asked whether m6A and A-to-I RNA modifications were similarly involved in regulating the response to other pro-inflammatory stimuli such as TLR agonists and IFN-γ that macrophages encounter during an infection. TLR

agonists represent PAMPs or their synthetic mimics that are characteristic for bacteria or other pathogens and recognized by TLRs to induce downstream NF-κB signaling. IFN-γ is a type II interferon that is typically produced by activated T and natural killer (NK) cells and initiates the JAK-Stat signaling cascade downstream of IFN-γ receptor 1/2 (IFNGR1/2) in macrophages, thereby inducing different signaling responses[107].

Among the previously monitored activating cell surface markers, TLR agonists had no effect on MHC I, MHC II and CD36 expression and only mildly induced CD40, CD80, and b2M. Despite this limitation, METTL3-KO macrophages partially recapitulated deficiency in CD80 and b2M upregulation in response to various TLR stimuli as compared to control macrophages (Fig. 13). To obtain a more comprehensive picture of m6A's role in TLR signaling, a direct target of TLR-mediated NF-κB signaling such as inflammatory cytokines could serve as a more suitable readout in the future. In contrast, I identified IFN-γ as the major driver of CD36, CD40, MHC II, MHC I and b2M induction. After IFN-γ treatment alone, particularly MHC II, CD36, and b2M expression was reduced in METTL3-KO as compared to control macrophages (Fig. 13). When testing the response of macrophages to TLR agonists and IFN-γ treatment during METTL3 inhibition by STM2457, I observed similar effects on impaired macrophage activation as in the full METTL3-KO cells (Fig. 14). Together, I conclude that m6A plays an important role in macrophage activation in response to a wide range of pro-inflammatory stimuli. However, it remains unclear to what extent the expression of involved cell surface receptors and signaling molecules is driven by m6A sites on specific transcripts or by the pre-activated state of METTL3-KO cells.

Simultaneously, ADAR1-KO macrophages treated with IFN-γ showed significantly reduced CD40, MHC II, MHC I, b2M and CD36 upregulation as compared to control macrophages (Fig. 13). This defect in ADAR1-KO macrophages' response to IFN-γ alone was higher as compared to treatment with different TLR agonists (Fig. 13) or previously described combined LPS/IFN-γ (Fig. 10B), suggesting that ADAR1's regulatory role in macrophage activation might be more specific to the IFN-γ signaling pathway and appears less involved in TLR signaling.

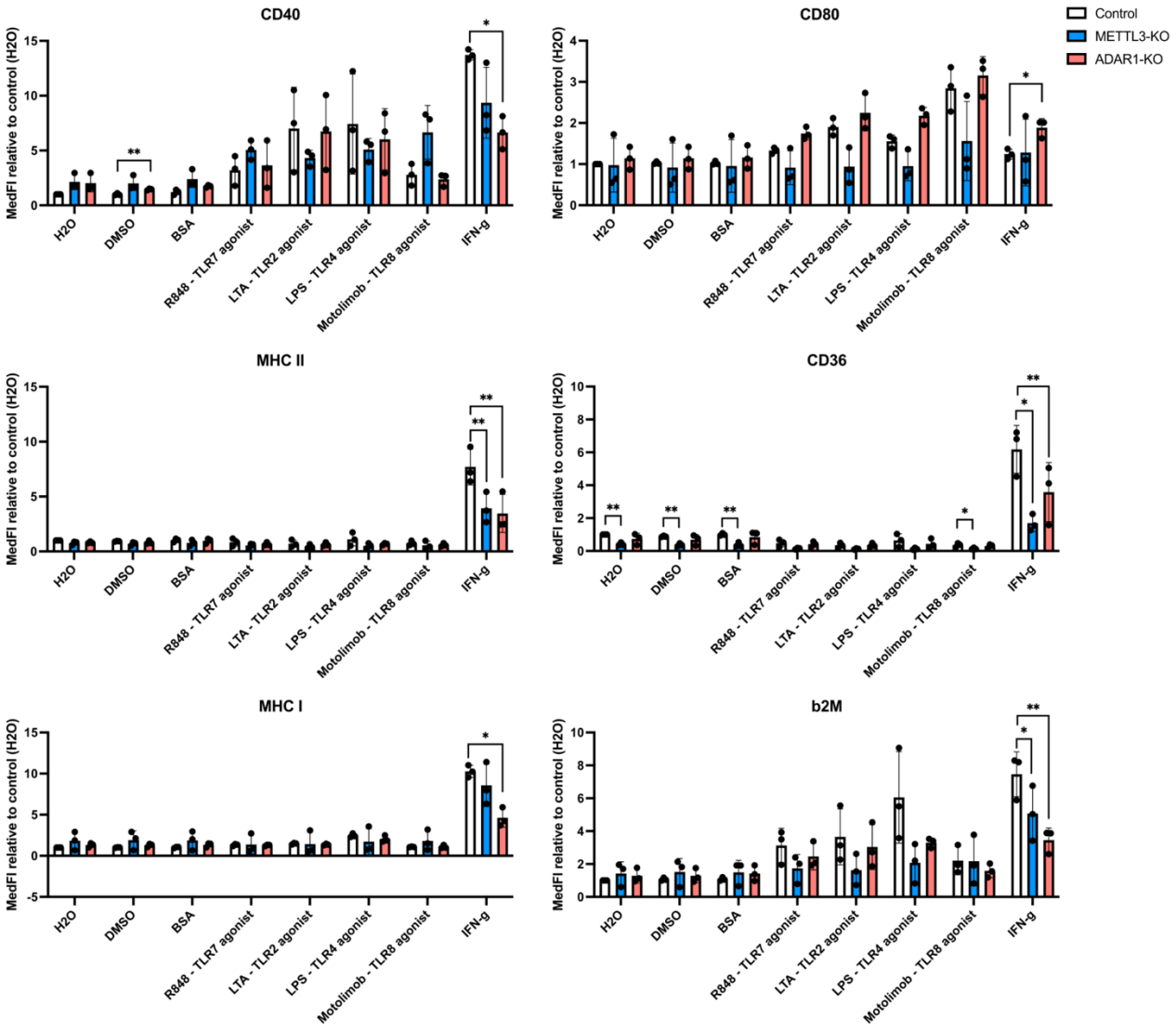

Figure 13. Macrophage activation marker expression upon treatment with various pro-inflammatory stimuli upon loss of METTL3 or ADAR1. Flow cytometric analysis of activation-associated cell surface markers in control, METTL3-KO and ADAR1-KO RAW macrophages 24 h after treatment with different TLR agonists or IFN-γ. Paired two-tailed t-tests were performed for each KO compared to the control at corresponding treatments. Significance values are indicated as follows: ∗p < 0.05; ∗∗p < 0.01; ∗∗∗p < 0.001; ∗∗∗∗p < 0.0001; n=3.

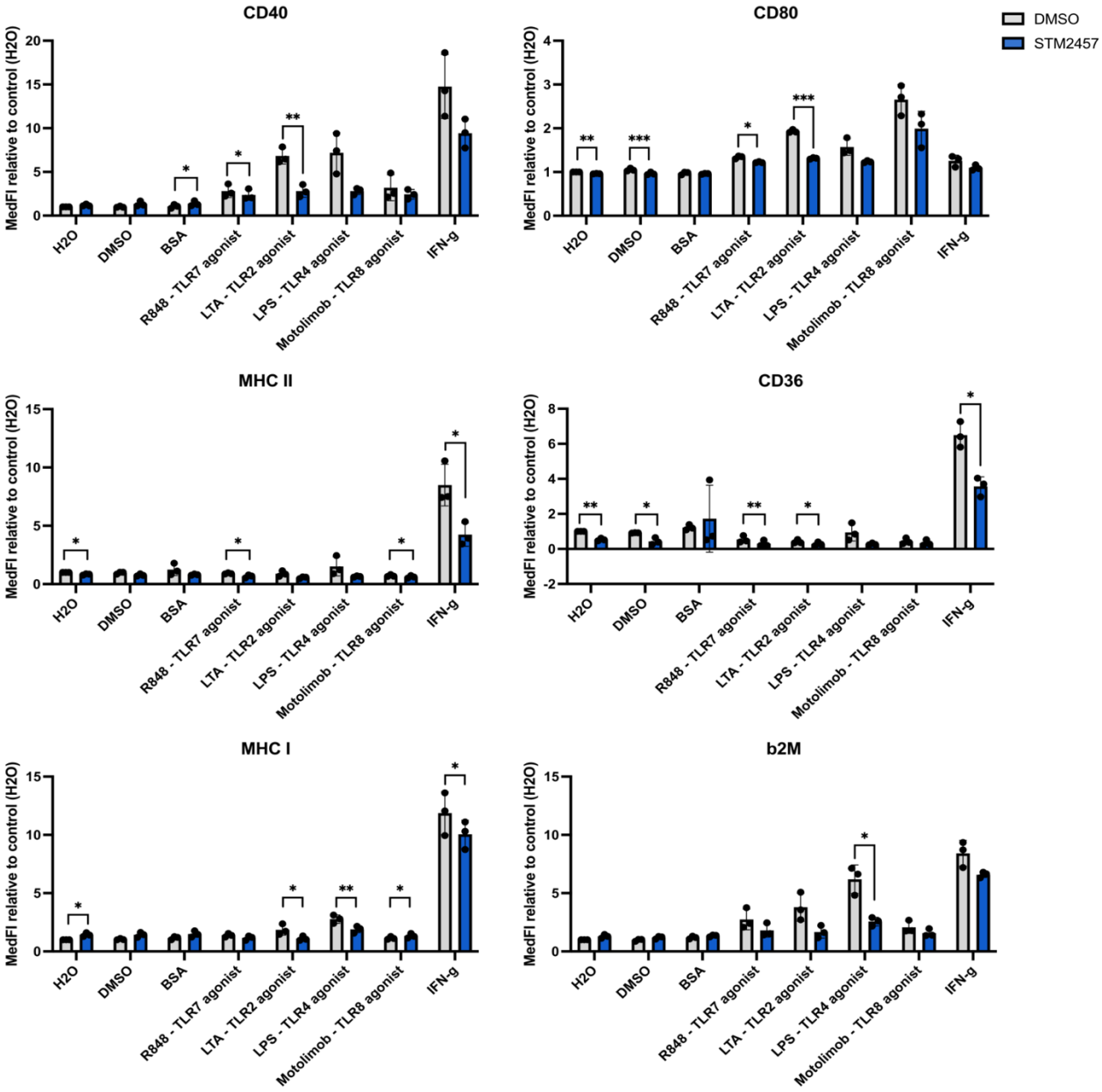

Figure 14. Macrophage activation marker expression upon treatment with various pro-inflammatory stimuli after METTL3 inhibition. Flow cytometric analysis of activation-associated cell surface markers of RAW cells treated with DMSO or METTL3 inhibitor STM2457 (10 µM, 48 h) and treatment with different TLR agonists or IFN-γ (24 h). Paired two-tailed t-tests were performed for corresponding treatments. Significance values are indicated as follows: ∗p < 0.05; ∗∗p < 0.01; ∗∗∗p < 0.001; ∗∗∗∗p < 0.0001; n=3.

4.1.10 RNA modifications affect anti-inflammatory surface marker expression

After highlighting the essential roles of both ADAR1 and METTL3 in driving macrophage pro-inflammatory activation, I tested if the RNA modifications also impact macrophages' response to anti-inflammatory stimuli. Exposure to anti-inflammatory cytokines IL-4 and IL-13 has been reported to induce M2 polarization in macrophages. Hence, I analyzed anti-inflammatory, M2-associated cell surface marker expression in resting and IL-4/IL-13-treated macrophages. Without exogenous stimulus, I observed a reduction of CD206 and CD200R expression in METTL3-KO as compared to control macrophages (Fig. 15), confirming a pre-activated and pro-inflammatory baseline state of METTL3-KO cells that is in line with previously-described innate immune activation by sensing of aberrant unmethylated RNAs (Fig. 8C-E). On the other hand, ADAR1-KO macrophages expressed increased levels of inhibitory receptor CD200R (Fig. 15), supporting their hypothesized dampened immune response and inflammatory state to cope with loss of ADAR1 (Fig. 8A, B, E).

When treating macrophages with IL-4 and IL-13, I detected no changes in cell surface markers in neither control, METTL3-KO nor ADAR1-KO cells as compared to their untreated state (Fig. 15). This observation indicates that the RAW macrophage cell line is not able to respond to anti-inflammatory stimulation by IL-4 and IL-13, potentially due to lack of corresponding cytokine receptor expression or blockage of downstream signaling cascades. Therefore, I was not able to study the role of m6A and A-to-I RNA modifications in the context of anti-inflammatory stimulation using RAW macrophages as a model system.

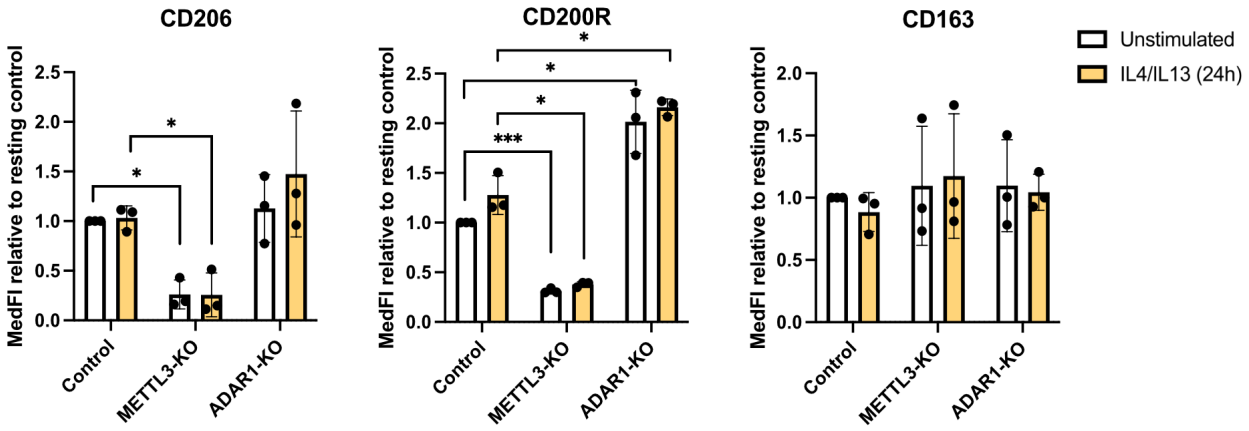

Figure 15. Macrophage M2 marker expression upon anti-inflammatory stimulation. Flow cytometric analysis of M2-associated cell surface markers in control, METTL3-KO and ADAR1-KO RAW macrophages at rest and 24 h after IL-4 and IL-13 treatment. Paired two-tailed t-tests were performed for each KO compared to the control at corresponding treatment. Significance values are indicated as follows: ∗p < 0.05; ∗∗p < 0.01; ∗∗∗p < 0.001; ∗∗∗∗p < 0.0001; n=3.

4.1.11 m6A modulates phagocytosis in non-stimulated macrophages

Phagocytosis of pathogens and cellular debris is a key function of macrophages. Pro-inflammatory stimulation induced differential expression of many genes regulating phagocytosis, many of their transcripts carrying m6A or A-to-I editing sites (Fig. 16A). Investigating phagocytosis related gene expression in the absence of m6A and inosine revealed deregulated gene expression at rest and after pro-inflammatory stimulation (Fig. 16B).

Next, I tested cell surface expression of phagocytosis receptors on macrophages that were found to be transcriptionally deregulated in the absence of RNA modifications (Fig. 16B, Table S2-S4). In line with transcriptomics data and in addition to above-described deficiency in scavenger receptor CD36 in METTL3-KO conditions (Fig. 10B), resting METTL3-KO macrophages tended to decrease Dectin 1 (=CLEC7A) while increasing TLR2 expression, the later potentially being linked to their described pre-activated state. Notably, these differences in Dectin 1 and TLR2 expression were lost after pro-inflammatory stimulation. Simultaneously, surface expression of these phagocytosis receptors was not impacted by loss of ADAR1 (Fig. 16C).

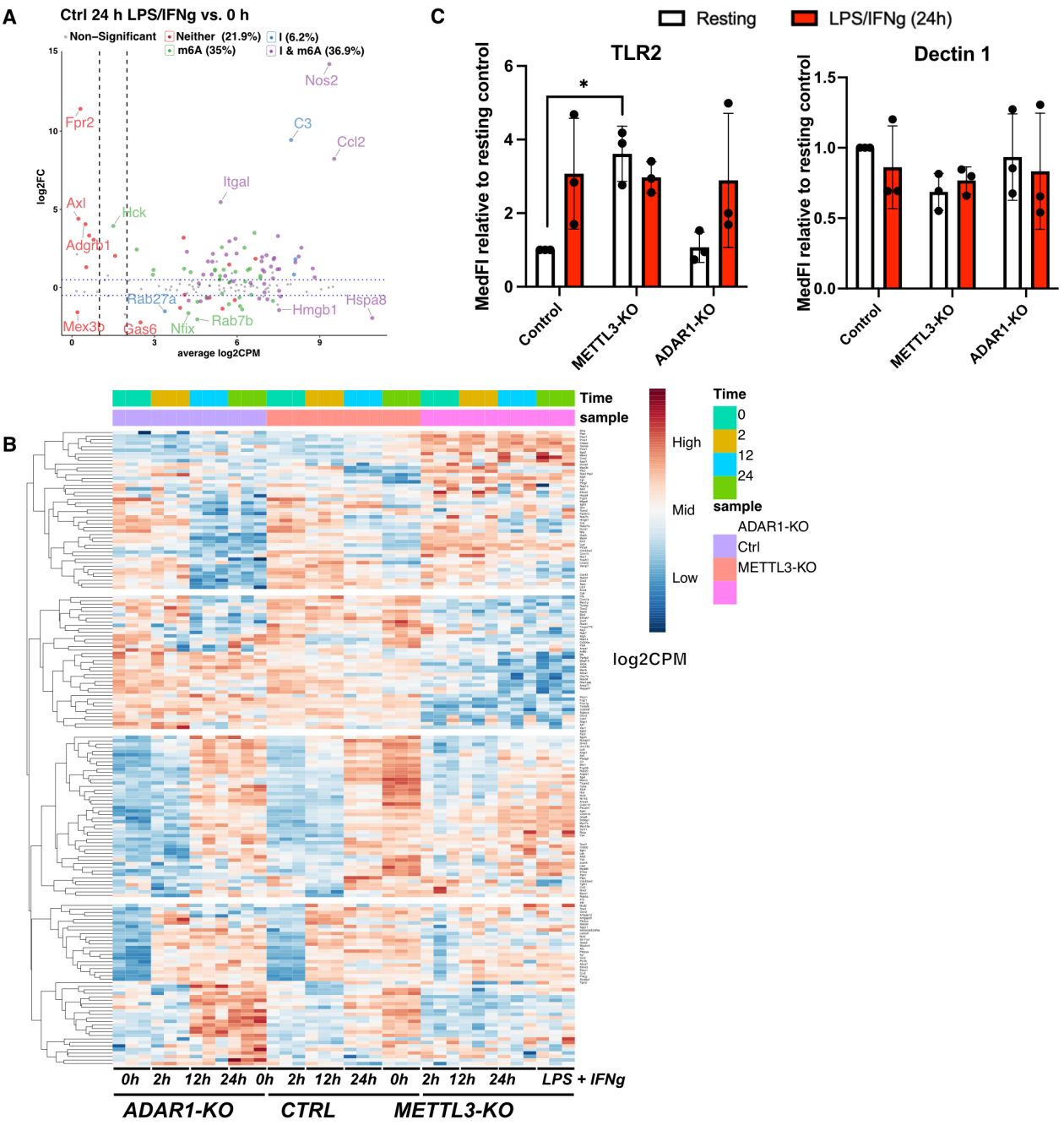

Figure 16. Impact of Adenosine mRNA modifications on Phagocytosis. (A) Mean gene expression (average log 2 counts per million reads [log2CPM], x-axis) and changes in gene expression (log2FC, y-axis) of phagocytosis associated genes (GO:0006909) between control samples 24 h after LPS/IFN-γ treatment and unstimulated control samples. Genes are labelled according to presence of RNA modification sites and differential expression. The left vertical line indicates log2CPM = 1: genes below are considered lowly expressed; the right vertical line indicates log2CPM = 2: genes above are considered highly expressed; expression levels of genes with 1< log2CPM< 2 are regarded as moderate. The horizontal line marks the limits for differential gene expression of |log2FC| = 0.5 (continued on next page).

Figure 16, continued: (B) Transcriptomic expression (log2-counts per million reads [CPM]) of phagocytosis associated genes 0 h, 2 h, 12 h, and 24 h after LPS/IFN-γ treatment in control, METTL3-KO and ADAR1-KO RAW macrophages. Gene expression-based hierarchical clustering by Euclidean distance is illustrated by the dendrogram. **(C)** Cell surface expression of phagocytosis receptors was assessed by flow cytometry. Paired two-tailed t-tests were performed for each KO compared to the control at corresponding treatment. Significance values are indicated as follows: ∗p < 0.05; ∗∗p < 0.01; ∗∗∗p < 0.001; ∗∗∗∗p < 0.0001; **(A-C)** n=3; **(A-B)** produced by Dr. Salvatore Di Giorgio.

To assess the functional contribution of RNA modifications on phagocytosis activity, I co-cultured unstimulated macrophages with a variety of different green-fluorescently labeled particles for uptake. Phagocytosis activity was assessed by flow cytometry, specifically by quantifying the percentage of green fluorescent cells (corresponding to cells that have phagocytosed particles) in the alive, single-cell population as well as their median fluorescent intensity (corresponding to the number of phagocytosed participles per phagocytosing cell; Fig. 17A).

First, I performed a bead-uptake assay using fluorescently labeled beads. While untreated ADAR1-KO macrophages showed similar phagocytosis activity of uncoated and LPS-coated beads like observed in control cells (Fig.17B-C), a significantly increased percentage of cells in the METTL3-KO population took up uncoated beads and more uncoated beads were phagocytosed per cell (Fig. 17B). However, this effect was not observed when analyzing uptake of LPS-coated beads (Fig. 17C).

Next, I repeated the phagocytosis assay using bacteria or zymosan (a component of yeast cell walls) labeled with a pH-sensitive green fluorophore (pHrodo Green) that fluoresces in the acidic endosome. As observed for the LPS-coated beads, for the Gram-negative Escherichia coli (*E. coli)* bacteria that naturally display LPS on their cell surface, I observed no significant difference in uptake between METTL3-KO, ADAR1-KO or control macrophages (Fig. 17D). When testing whether mRNA modifications affected the uptake of Gram-positive Staphylococcus aureus (*S. aureus)* bacteria that lack LPS, METTL3-KO macrophages possessed increased phagocytosis activity against *S. aureus*, as seen in elevated percentage of phagocytosing cells and increased number of *S. aureus* per cell as compared to control macrophages. ADAR1-KO cells showed only a minor increase in uptake of *S. aureus* particles per cell as compared to control conditions (Fig. 17E). In contrast, the per cell uptake

of zymosan particles was reduced in the METTL3-KO while unchanged in the ADAR1-KO as compared to control macrophages (Fig. 17F).

When testing phagocytosis activity after temporary METTL3 inhibition by treatment with STM2457 for 48 h, I observed increased phagocytosis of uncoated beads and decreased phagocytosis of zymosan upon m6A inhibition (Fig. 17G, K) similar to observations in METTL3-KO macrophages (Fig. 17B, F). Yet, temporary METTL3 inhibition did not change *S. aureus*, dampened *E. coli*, while enhancing LPS-coated bead uptake as compared to DMSO-treated control conditions (Fig. 17H-J), thereby differing from my observations in METTL3-KO cells (Fig. 17C-E). These differences might result from higher heterogeneity of METTL3-KO clones that lead to a larger spread in values, hence, less clearer results. Additionally, possible adaptations in METTL3-KO clones due to long-term loss of m6A could impact receptor expression and phagocytosis pathways. Nevertheless, together, my data suggests a role of mRNA modifications, particularly of m6A, in the phagocytosis activity of resting macrophages.

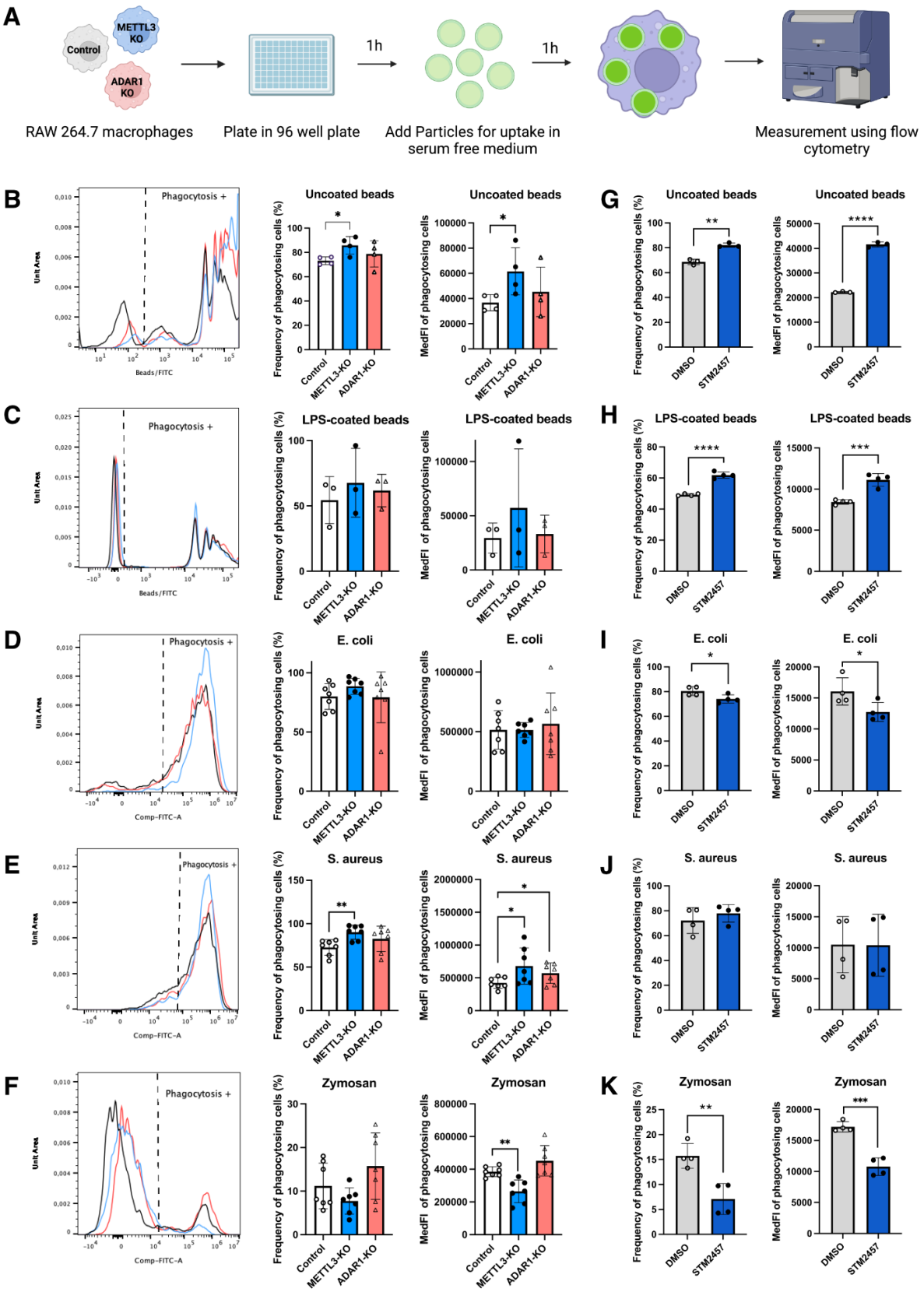

Figure 17. Phagocytosis by RAW macrophages without pre-treatment (continued on next page).

Figure 17, continued: (A) Schematic representation of phagocytosis assay. Phagocytosis assay of non-stimulated macrophages upon METTL3- or ADAR1-KO (**B-F**) or upon METTL3 inhibition by STM2457 (10 µM, 48 h; **G-K).** Phagocytosis of fluorescently labeled uncoated beads **(B, G)**, LPS-coated beads **(C, H)**, *E. coli* **(D, I)** *S. aureus* **(E, J)**, and Zymosan **(F, K). (B-F** Left) Exemplary histogram of the flow cytometric analysis depicting fluorescent signals of alive single cells. Gating of phagocytosis positive cells (based on fluorescent background signals of cells without fluorescent particles) is indicated. (**B-F** Middle/ **G-K** Left) Frequency of phagocytosis positive cells. (**B-K** Right) MedFI of phagocytosis positive cells. Two-tailed t-tests were performed for each condition as compared to the corresponding control. Significance values are indicated as follows: $*p < 0.05$; $**p < 0.01$; $***p < 0.001$; $****p < 0.0001$; **(B, I-K)** n=4; **(C, G, H)** n= 3; **(D-F)** n=7.

4.1.12 m6A and A-to-I impairs phagocytosis of pre-stimulated macrophages

Previously, I have observed deficient macrophage activation 24 h after pro-inflammatory stimulation in the absence of m6A or A-to-I RNA modifications as indicated by dampened expression of macrophage activation markers (Fig. 9-10). During an infection, macrophages might encounter pathogenic particles within a pro-inflammatory environment. To replicate such an inflammatory environment *in vitro*, I pre-treated macrophages for 24 h with LPS and IFN-γ before measuring their phagocytotic activity. While no significant change in uptake of uncoated or LPS-coated beads was observed for METTL3-KO macrophages (Fig. 18A-B), these cells showed deficient uptake of *E. coli*, *S. aureus*, and zymosan particles (Fig. 18C-E). Notably, after temporary METTL3 inhibition by METTL3 inhibitor treatment, m6A depletion induced deficient uptake of any particles tested (Fig. 18F-J), underlining a global role of m6A in enabling efficient phagocytosis during pro-inflammatory conditions. Similarly, ADAR1-KO macrophages showed impaired uptake of *S. aureus*, zymosan, and LPS-coated beads while uptake of *E. coli* and uncoated beads remained unaffected by the loss of ADAR1 (Fig. 18A-E). Together, the phagocytosis assay implies that ADAR1 and METTL3 differentially impact phagocytosis activity of macrophages depending on the activation state and presented stimulus. Thereby, RNA modifications were particularly important for efficient phagocytosis by pro-inflammatory macrophages likely by differential regulation of ligand recognition and endocytosis pathways.

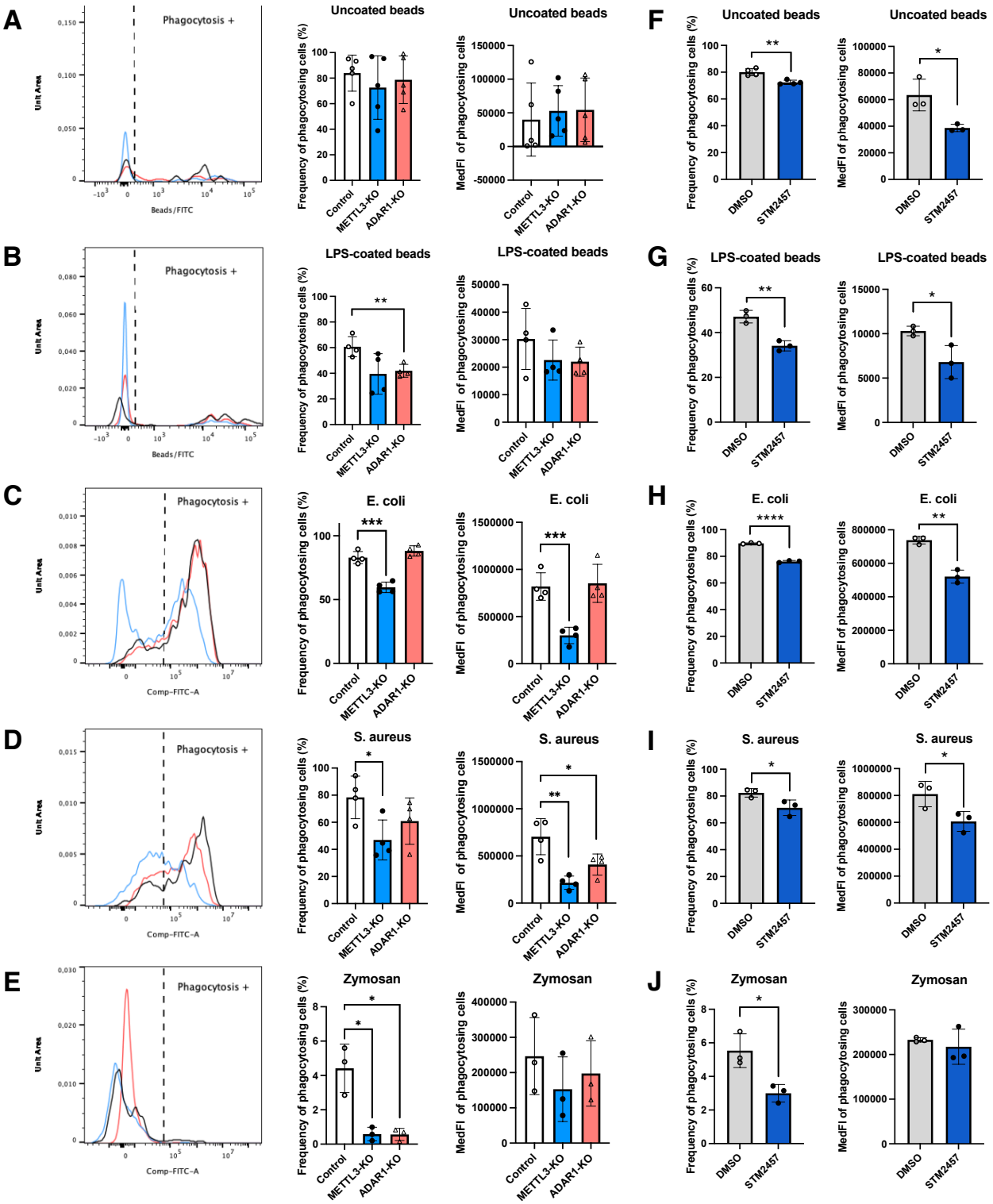

Figure 18. Phagocytosis by RAW macrophages pre-stimulated for 24 h with LPS and IFN-γ (continued on next page).

Figure 18, continued: Phagocytosis assay of macrophages pre-stimulated for 24 h with LPS and IFN-γ upon METTL3- or ADAR1-KO (**A-E**) or upon METTL3 inhibition by STM2457 (10 μM, 48 h; **F-J**). Phagocytosis of fluorescently labeled uncoated beads **(A, F)**, LPS-coated beads **(B, G)**, *E. coli* **(C, H)** *S. aureus* **(D, I)**, and Zymosan **(E, J). (A-E** Left) Exemplary histogram of the flow cytometric analysis depicting fluorescent signals of alive single cells. Gating of phagocytosis positive cells (based on fluorescent background signals of cells without fluorescent particles) is indicated. (**A-E** Middle/ **F-J** Left) Frequency of phagocytosis positive cells. (**A-J** Right) MedFI of phagocytosis positive cells. Unpaired two-tailed t-tests were performed for each KO or inhibitor treatment compared to the control. Significance values are indicated as follows: ∗p < 0.05; ∗∗p < 0.01; ∗∗∗p < 0.001; ∗∗∗∗p < 0.0001; **(A-D)** n=4; **(E-J)** n=4.

4.2 Interplay between m6A and A-to-I editing

4.2.1 Minor impact of ADAR1 on m6A levels in RAW macrophages

After demonstrating individual contributions of METTL3 and ADAR1 in macrophage activation and phagocytosis, I analyzed the possible interaction between the two RNA modifying enzymes and deposition of RNA modifications. First, I monitored how METTL3 expression behaved throughout pro-inflammatory stimulation and how this was affected by the loss of ADAR1-mediated A-to-I editing. *Mettl3* mRNA levels were relatively stable throughout macrophage stimulation with only mild fluctuations in control cells (between 3.7 and 4.3 log 2 counts per million reads [log2CPM] from Illumina sequencing data) and in ADAR1-KO macrophages (fluctuating between 3.9 and 4.9 log 2 CPM, Fig. 19A). Slightly increased *Mettl3* levels were observed at 12 h and 24 h after stimulation in the absence of ADAR1 as compared to control macrophages (Fig. 19A). While, METTL3 protein expression was mostly stable in both control and ADAR1-KO macrophages, I observed slightly reduced METTL3 expression in resting ADAR1-KO macrophages as compared to controls, yet, these differences were absent after stimulation (Fig. 19B-C).

Nanopore direct RNA sequencing was used to map and quantify m6A modifications transcriptome-wide. For this purpose, I focused on samples obtained at resting state and time point 24 h after LPS and IFN-γ stimulation, when the highest RNA editing levels were observed (Fig. 20D) and major differences in gene expression were detected (Fig. 4B-C). In the analysis, I observed a globally stable number of m6A sites in control macrophages, both

at rest and during pro-inflammatory conditions. Also, upon loss of ADAR1, the number of m6A events was not significantly changed. Only when comparing unstimulated and stimulated ADAR1-KO macrophages, a drop in m6A was observed after pro-inflammatory stimulation (Fig. 19D).

Based on my previous findings and the reported role of m6A in macrophages[62–64,93], I wondered if I could detect more pronounced changes in m6A levels in individual transcripts. However, in the results of the bioinformatic analysis, I identified only a limited number of genes with differentially methylated sites between resting and stimulated control macrophages (Fig. 19E). The mostly stable methylation levels at individual sites suggest that the effect of m6A during macrophage activation is not mediated by differential methylation but rather by differential expression of m6A readers (as shown in Fig. 4D) that could facilitate m6A's functional role in promoting macrophage activation.

When comparing resting control and ADAR1-KO macrophages, only three genes showed differentially methylated sites (Fig. 19F). Also 24 h after LPS and IFN-γ treatment, I identified less then 20 genes with differentially methylated sites, but all except for one of these genes showed m6A sites with reduced methylation levels in the ADAR1-KO as compared to the control cells (Fig. 19G). While ADAR1-mediated A-to-I editing might support m6A deposition in a small group of transcripts after pro-inflammatory stimulation, this effect does not seem of global important due to its rare incidence.

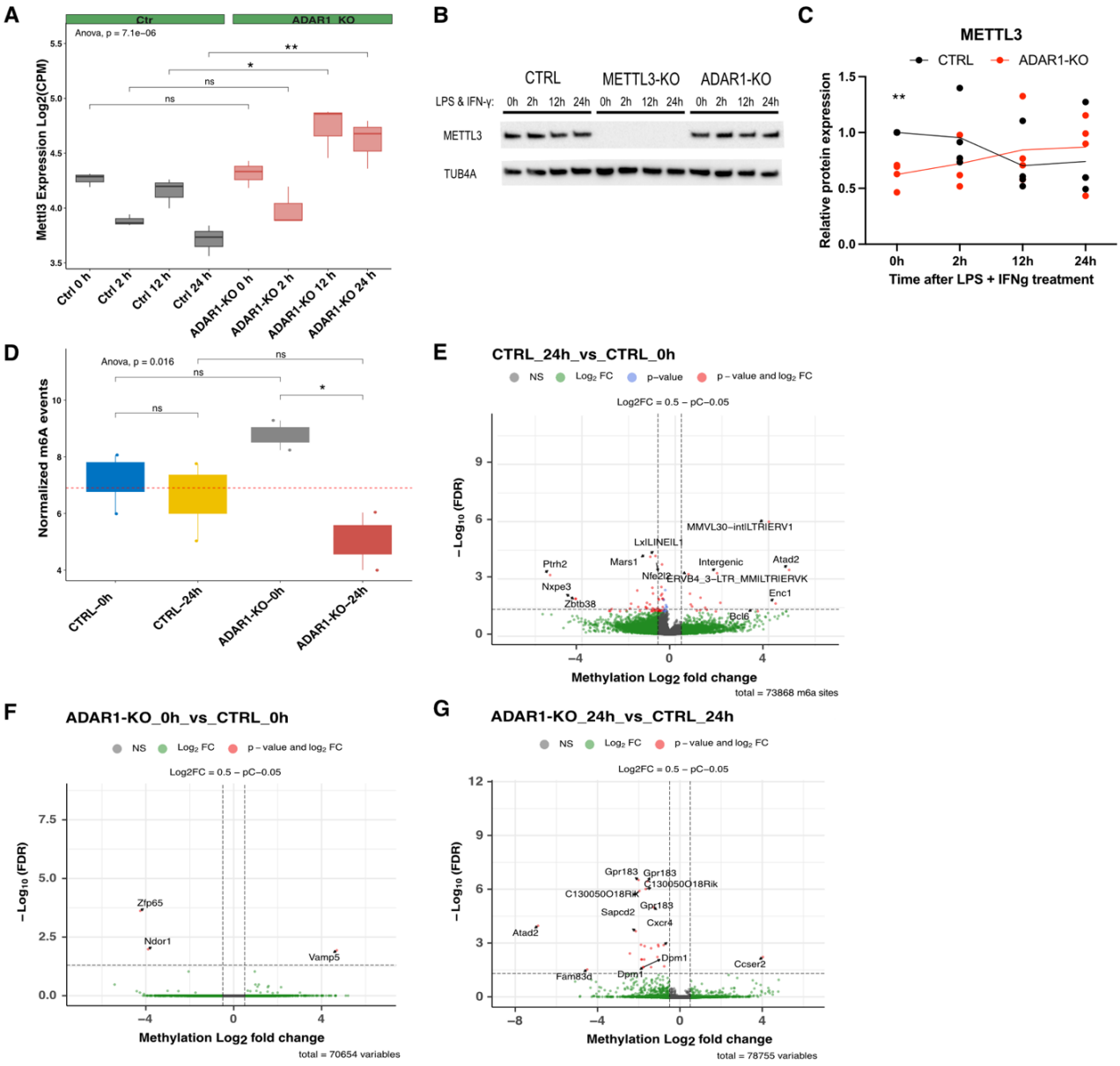

Figure 19. Impact of loss of ADAR1 on m6A levels during stimulation. (A) Transcript expression of *Mettl3* after LPS/IFN-γ treatment (0 h, 2 h, 12 h, and 24 h) in control and ADAR1-KO RAW macrophages. **(B)** Representative Western blot of METTL3 protein expression during the time course of stimulation. **(C)** Quantification of METTL3 protein levels; paired two-tailed t-tests were performed between control and ADAR1-KO cells at individual time points; n=4. **(D)** Number of m6a events in control and ADAR1-KO conditions normalized per million mapped bases. **(E-G)** The dots in volcano blots indicate individual differentially methylated sites (DMS) in control samples 24 h after LPS/IFN-γ treatment compared to untreated control samples **(E)**, in untreated ADAR1-KO compared to untreated control cells **(F)**, and in ADAR1-KO after 24 h of LPS/IFN-γ treatment compared to control samples after 24 h of LPS/IFN-γ treatment **(G).** The vertical lines mark the minimum limits for differential methylation of |log2FC| = 0.5; the horizontal lines depict the limit of the adjusted p-value of 0.05 (continued on next page).

Figure 19, continued: (A, D) statistical difference was determined by global ANOVA test and post hoc t-tests; significance values are indicated as follows: ∗p < 0.05; ∗∗p < 0.01; ∗∗∗p < 0.001; ∗∗∗∗p < 0.0001. **(A, D-G)**: n=3; produced by Dr. Salvatore Di Giorgio.

4.2.2 Loss of METTL3 impairs A-to-I editing

Conversely, I investigated the dynamics of ADAR1 expression during macrophage pro-inflammatory stimulation and the influence of METTL3-mediated m6A on A-to-I editing. The *Adar1* p150 isoform is interferon-inducible, hence, as expected, I observed the induction of *Adar1* in control and METTL3-KO macrophages in response to LPS and IFN-γ treatment. Increases in *Adar1* mRNA levels were observed as early as 2 h after pro-inflammatory stimulation and continued to rise at later time points (Fig. 20A). During unstimulated conditions, METTL3-KO cells expressed almost double the amount of *Adar1* transcript as compared to resting controls. Upon stimulation, differences in *Adar1* expression were no longer significant between control and METTL3-KO macrophages at any corresponding time point (Fig. 20A). A western blot confirmed the treatment-induced upregulation of ADAR1 that was mainly mediated by increased expression of the p150 isoform (Fig. 20B). Similar to mRNA levels, ADAR1 protein expression also increased during the time course of stimulation but with a delay as elevated ADAR1 was detected starting from 12 h after stimulation. While I observed equal ADAR1 levels between control and METTL3-KO macrophages at most time points, this was not the case 12 h after LPS and IFN-γ treatment. In control macrophages ADAR1 expression was higher and peaked 12 h after LPS and IFN-γ stimulation while METTL3-KO macrophages showed highest ADAR1 expression only after 24 h (Fig. 20B–C).

After observing rising ADAR1 levels after pro-inflammatory stimulation, I investigated if this was accompanied by increases in A-to-I editing. Indeed, after LPS/IFN-γ treatment, the number of detected editing events rose concordantly with ADAR1 protein levels, with highest levels detected 24 h after treatment. Globally, the number of editing events was comparable in corresponding time points between METTL3-KO and control macrophages (Fig. 20D). When comparing editing levels of specific sites, I observed that the majority of edited sites showed increased editing frequencies in control cells 24 h after pro-inflammatory stimulation (Fig. 20E) with mean editing levels increasing from approximately 10% (unstimulated) to 25% (24 h stimulation; Fig. 20F), confirming an RNA-editing

response induced by interferon-stimulated ADAR1 p150 expression[29]. Editing levels in METTL3-KO macrophages mimicked the control macrophages but mean editing levels reached only approximately 18% after 24 h of LPS/IFN-γ treatment indicating a defect in the A-to-I editing response during stimulation in the absence of m6A (Fig. 20G).

To better understand the changes in editing levels at individual positions in response to m6A, differential editing analysis was performed comparing control and METTL3-KO conditions. During unstimulated conditions, only minor differences between control and METTL3-KO cells were observed, with only 23 sites being either more or less edited between conditions (Fig. 20H). In contrast, when comparing editing levels 24 h after stimulation, the large proportion of sites were less edited in METTL3-KO as compared to control cells (Fig. 20I). Together, I identified a clear editing response to pro-inflammatory stimulation that is dampened in the absence of METTL3, indicating a functional role of m6A in ADAR1-mediated RNA editing.

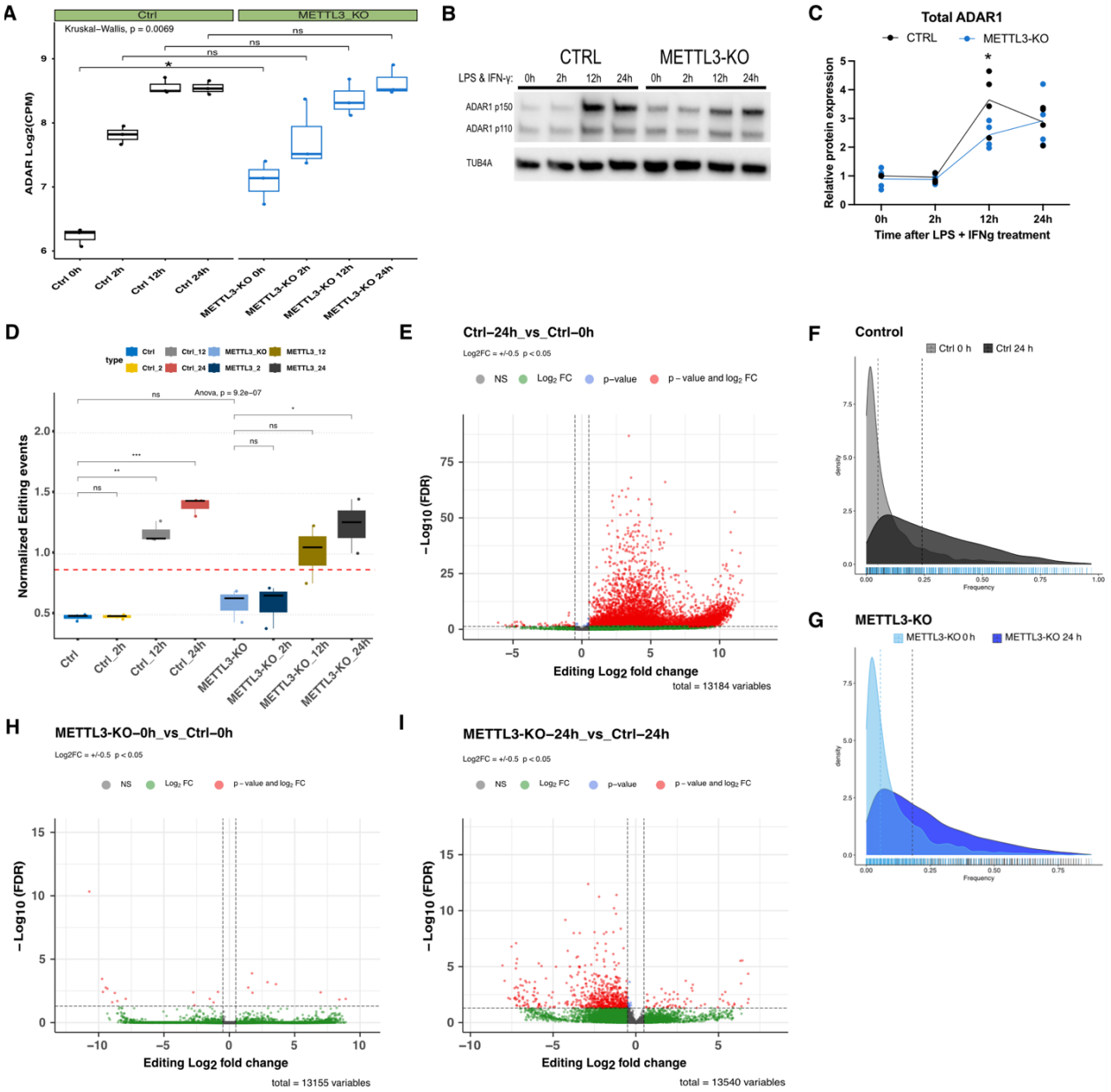

Figure 20. Impact of METTL3 on A-to-I editing during stimulation. (A) Transcript expression of *Adar1* after LPS/IFN-γ treatment (0 h, 2 h, 12 h, and 24 h) in control and METTL3-KO RAW macrophages. Statistical difference was determined by Krustkal-Wallis test. **(B)** Representative Western blot of ADAR1 protein expression during the time course of stimulation. **(C)** Quantification of total ADAR1 protein levels; paired two-tailed t-tests were performed between control and METTL3-KO conditions at individual time points; n=4. **(D)** Number of editing events in control and ADAR1-KO conditions that were normalized per million mapped bases; statistical difference was determined by global ANOVA test with pairwise comparisons by post hoc t-tests.**(E, H, I)** The dots in volcano blots indicate individual differentially edited sites in control samples 24 h after of LPS/IFN-γ treatment compared to untreated control samples **(E)**, in untreated METTL3-KO as compared to untreated control samples **(H)**, and in METTL3-KO 24 h after LPS/IFN-γ as compared to control samples 24 h after LPS/IFN-γ **(I)** (continued on next page).

Figure 20, continued: (E, H, I) The vertical lines mark the minimum limits for differential editing of |log2FC| = 0.5; the horizontal lines depict the limit of the adjusted p-value of 0.05. **(F-G)** Distribution of editing frequencies across sample conditions: control (untreated and 24 h after LPS/IFN-γ) **(F)**, and METTL3-KO (untreated and 24 h after LPS/IFN-γ) **(G)**; median editing frequencies are depicted as dashed lines. **(A, C, D)** Significance values are indicated as follows: ∗p < 0.05; ∗∗p < 0.01; ∗∗∗p < 0.001; ∗∗∗∗p < 0.0001. **(A, D-I)** n=3; produced by Dr. Salvatore Di Giorgio.

4.2.3 Direct effect of a m6A site on the *Adar1* transcripts on its splicing and translation

After observing a functional impact of METTL3 on A-to-I editing, I aimed to understand the interplay between the two RNA modifications. First, I asked if m6A influences *Adar1* directly by methylation of the *Adar1* transcript. Indeed, we identified known and novel m6A sites on *Adar1* mRNA including sites in the last exon and in the 3' UTR (Fig. 21A) that were reported to promote *Adar1*'s translation into protein. M6A's role in *Adar1* translation is supported by ribosome profiling performed Chih-Yuan Kao which showed decreased ribosome density, hence, decreased translation efficiency of *Adar1* in METTL3-KO macrophages 24 h after LPS and IFN-γ treatment (Fig. 21B), the time point when I also observed lower A-to-I editing levels in METTL3-KO cells (Fig. 20I).

We also found an additional set of m6A sites localized in exon 2 of *Adar1*. As exonic m6A sites were reported to affect splicing[16,19], I tested whether *Adar1*'s splicing was impaired in the absence of m6A. Indeed, alignment of Nanopore sequencing reads indicated slightly increased retention of intron 2-3 (found adjacent to exon 2 where m6A sites are missing in the METTL3-KO cells) in poly-A RNA from METTL3-KO cells. For quantification of splice variants, I quantified correctly spliced and mis-spliced (intron 2-3 retaining) *Adar1* isoforms in poly-A tailed RNA by RT-qPCR (Fig. 21C). I detected a tendency of increased levels of the intron-retained splice variant particularly after LPS and IFN-γ treatment in METTL3-KO as compared to control macrophages (Fig. 21D). Additionally, the ratio of mis-spliced over correctly spliced *Adar1* transcripts appeared to be elevated in unstimulated and stimulated METTL3-KO cells as compared to corresponding control cells (Fig. 21E).

Together, these findings indicate that m6A sites on the *Adar1* transcript may play a role in *Adar1* processing and translation, that might contribute to an overall decrease in A-

to-I editing in the absence of METTL3. However, as these effects did not strongly impair total ADAR1 protein levels (as shown by Western blot, Fig. 20B-C), I hypothesize that additional mechanisms are involved in the observed dependence of A-to-I editing on METTL3-mediated m6A.

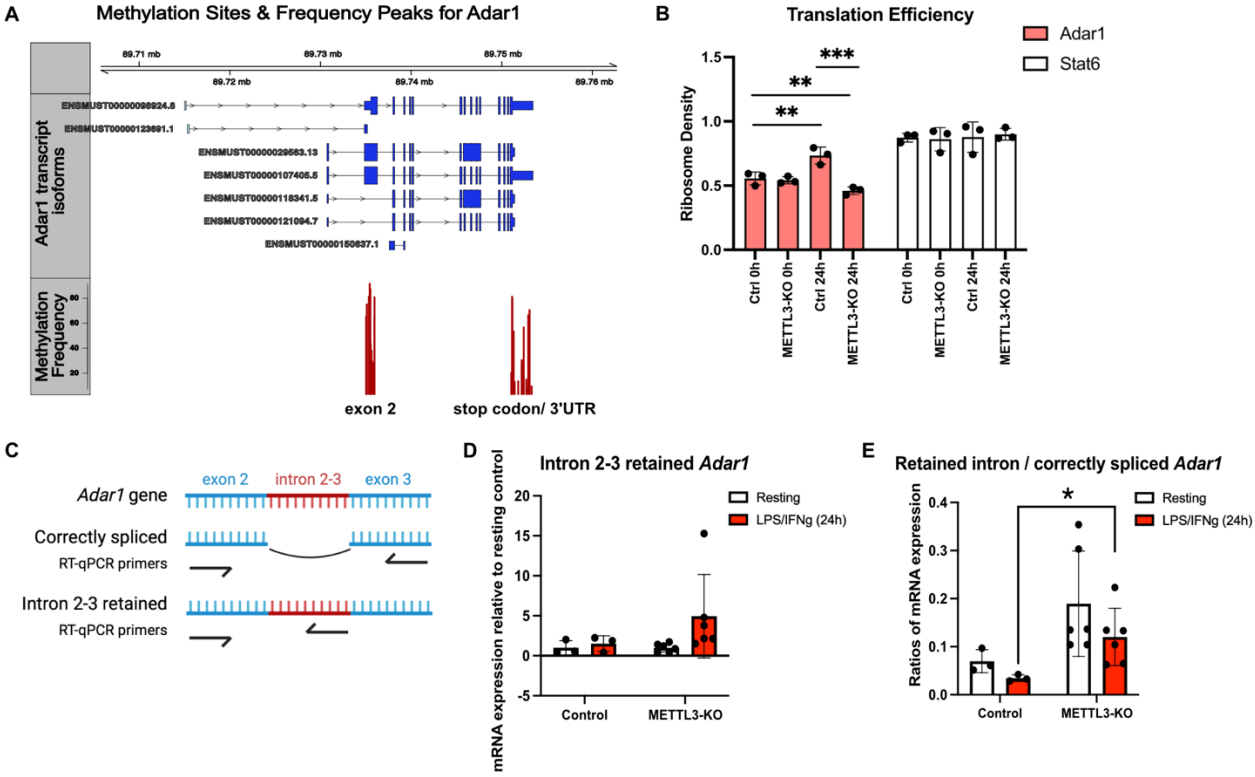

Figure 21. m6A site on *Adar1* transcript influences its mRNA metabolism. (A) Visualization of m6A sites on the *Adar1* transcript as identified by Nanopore direct RNA sequencing. **(B)** Ribosome sequencing showed the translation efficiency of *Adar1* and *Stat6* in resting control and METTL3-KO macrophages and 24 h after LPS and IFN-γ treatment; p-values based on one-way ANOVA. **(C)** Schematic representation of correctly spliced and aberrantly intron 2-3-retained *Adar1* splice isoforms and primers used for their detection by RT-qPCR. **(D)** Expression levels of poly-A-tailed *Adar1* transcripts with retained intron 2-3 as determined by RT-qPCR. **(E)** Ratio of intron 2-3 retained isoform as compared to correctly spliced isoform in poly-A-tailed RNA. **(D-E)** Unpaired two-tailed t-tests were performed for resting samples as well as stimulated samples. Significance values are indicated as follows: ∗p < 0.05; ∗∗p < 0.01; ∗∗∗p < 0.001; ∗∗∗∗p < 0.0001; n≥3. **(A)** Produced by Dr. Salvatore Di Giorgio. **(B)** Data produced by Chih-Yuan Kao.

4.2.4 Global interplay between m6A and A-to-I editing

To investigate an additional relationship between m6A and A-to-I editing levels, I focused on RNA modifications present in a single condition, namely, in control cells 24 h after LPS and IFN-γ stimulation, when editing was highest. When mapping RNA modifications, in a total of approximately 13,000 expressed genes, more than half carried an adenosine RNA modification site, with 2.8% carrying only A-to-I editing sites, 45.7% only m6A sites, and 11% exhibiting both m6A and A-to-I sites, while no modification sites were detected on the remaining 40.5% of expressed genes (Fig. 22A). Notably, genes with detectable RNA modifications were higher expressed than genes that appeared to be modification-free (Fig. 22B), suggesting a bias of more-efficient detection of RNA modifications in higher expressed genes or a potential role of the RNA modifications in transcript abundance and stability[18,108].

Despite different RNA substrate preference - METTL3 mostly modifying DRACH motifs in ssRNA and ADAR1 editing dsRNA – the localization of m6A and inosine overlaps in the transcript. I observed a similar distribution of the two modifications across the transcript body with enrichment in proximity to the transcription start site (TSS), 5’ UTR, 3’ UTR, and transcription termination site (TTS; Fig. 22C). The close proximity of the two RNA modifications makes a co-regulatory effect plausible.

Nanopore sequencing seemed a promising approach to map both m6A and inosine RNA modifications on full-length transcripts, thereby obtaining information on their co-dependency on the single transcript level. However, as demonstrated earlier, Nanopore base callers failed to reliably identify inosines on a transcript (Fig. 7E), making simultaneous detection of m6A and inosine impossible. As an alternative approach, we combined data from Nanopore sequencing for m6A and Illumina sequencing for inosine to analyze the relationship between the two mRNA modifications.

Focusing on the mRNA modifications in control macrophages 24 h after pro-inflammatory LPS and IFN-γ stimulation, we ranked the m6A and inosine sites in the 3’ UTR based on their distance into four equal quartiles (Q) and defined them as close (Q1), medium (Q2 & Q3), or far apart (Q4; Fig. 22D). Similarly, methylation levels were ranked into three

equal quantiles as low, medium and high. These classifications were used to establish an association between editing frequencies, m6A levels, and distances.

I observed a negative influence of highly methylated sites on A-to-I editing frequencies when in close proximity (<139 nt, Q1, Fig. 22E-F). When editing sites were at medium (139–1192 nt, Q2-Q3) or far distances (>1 192–10 000 nt, Q4) from m6A sites, I observed elevated editing frequencies associated with medium and highly methylated sites (Fig. 22E-F). A multiple regression model served as a more sophisticated model that statistically validated the identified associations (Table S5). Hence, I conclude, that m6A regulates A-to-I RNA editing on individual transcripts in a distance-dependent manner.

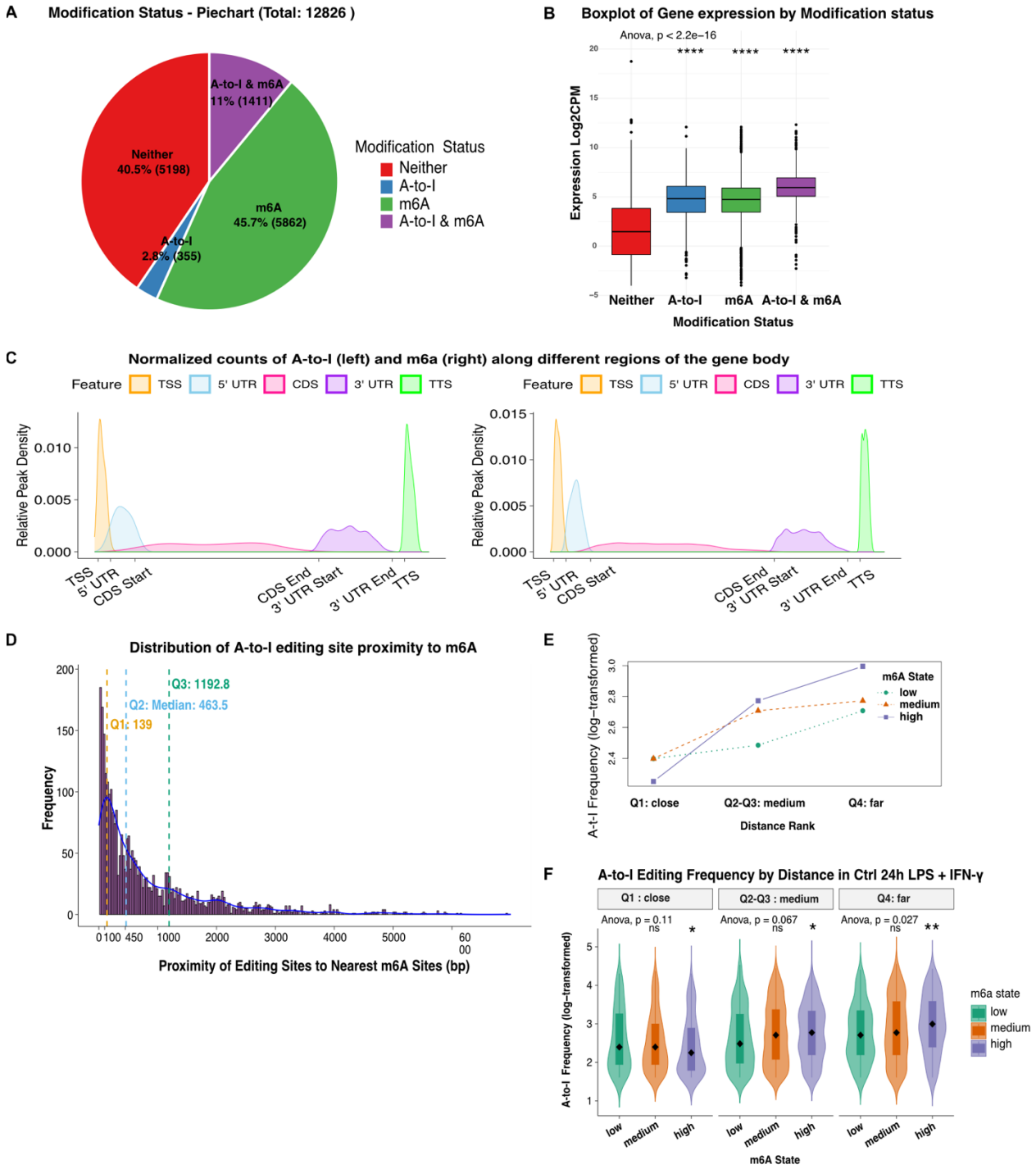

Figure 22. Global interdependencies between m6A and A-to-I. (A) Genes expressed in control samples 24 h after LPS/IFN-γ stimulation were categorized according to the type of mRNA modifications on their transcripts. **(B)** The gene expression levels of these categories were compared by global ANOVA and post-hoc t-test. **(C)** Localization of A-to-I and m6A modification sites across different transcript regions normalized to the length of each region. **(D)** Distribution of distances between A-to-I editing sites and their nearest m6A sites in the 3′ UTR. Vertical lines mark the 25th, 50th, and 75th percentiles (continued on next page).

Figure 22, continued: (E-F) These percentiles were used to categorize editing sites based on their distance to the nearest m6A site: close (≤25th percentile, Q1), medium (between 25th and 75th percentiles, Q2–Q3), and far (≥75th percentile, Q4). Each distance group was further divided according to their levels of m6A modifications at the corresponding m6A site (low, medium, or high)**.** A-to-I frequencies were then examined in each m6A and distance subgroup. **(E)** The plot depicts the association of editing frequency (log-transformed; y-axis) with m6A rank (marked by colors) and distance rank (close, medium, far; x-axis). **(F)** Differences between groups were analyzed by one-way ANOVA, followed by pairwise comparisons using post hoc t-tests. Significance values are indicated as follows: ∗p < 0.05; ∗∗p < 0.01; ∗∗∗p < 0.001; ∗∗∗∗p < 0.0001. **(A-F)** n=3; produced by Dr. Salvatore Di Giorgio.

4.2.5 m6A in guide RNAs improves targeted RNA editing

The positive association between m6A and A-to-I editing frequencies at long distances might be explained by m6A recruiting ADAR1 to a target transcript. Proposed mechanisms include but are not limited to common interacting proteins, for instance, binding of m6A readers to m6A but also to ADAR1[109], or remodeling of RNA structure, for instance, m6A stabilizing labile dsRNA structures[110,111]. To test this hypothesis, we used an artificial system to report targeted RNA editing. The reporter cell line encoded a truncated enhanced GFP (eGFP) where tryptophan (W) codon UGG at position 58 is mutated to a stop codon (UAG; W58X). Using a guide RNA complementary to the mutated region (also known as ASO[74,112]), endogenous ADAR1 is recruited to edit the stop codon to a restored tryptophan codon (UIG), and thereby restoring eGFP expression. Guide RNA-mediated ADAR1 editing can be assessed as eGFP expression by flow cytometry[74]. To determine the influence of m6A in ADAR1-recruitment and -editing, we used *in vitro* transcribed guides that were either unmodified or carried m6A at all A positions (Fig. 23A).

Upon lipofection of the gRNA, I observed that delivery of a m6A-containing guide RNA resulted in a 4-fold increase in ADAR1 recruitment and editing in comparison to unmodified guides as measured by eGFP expression. This difference was observed at various time points after guide delivery (Fig. 23B). Besides its relevance for therapeutical targeted RNA editing, this finding supports the hypothesis of m6A-assisted ADAR1 recruitment and editing, as the complementary methylated guide RNA might mimic a complementary transcript region at a distance from the editing site.

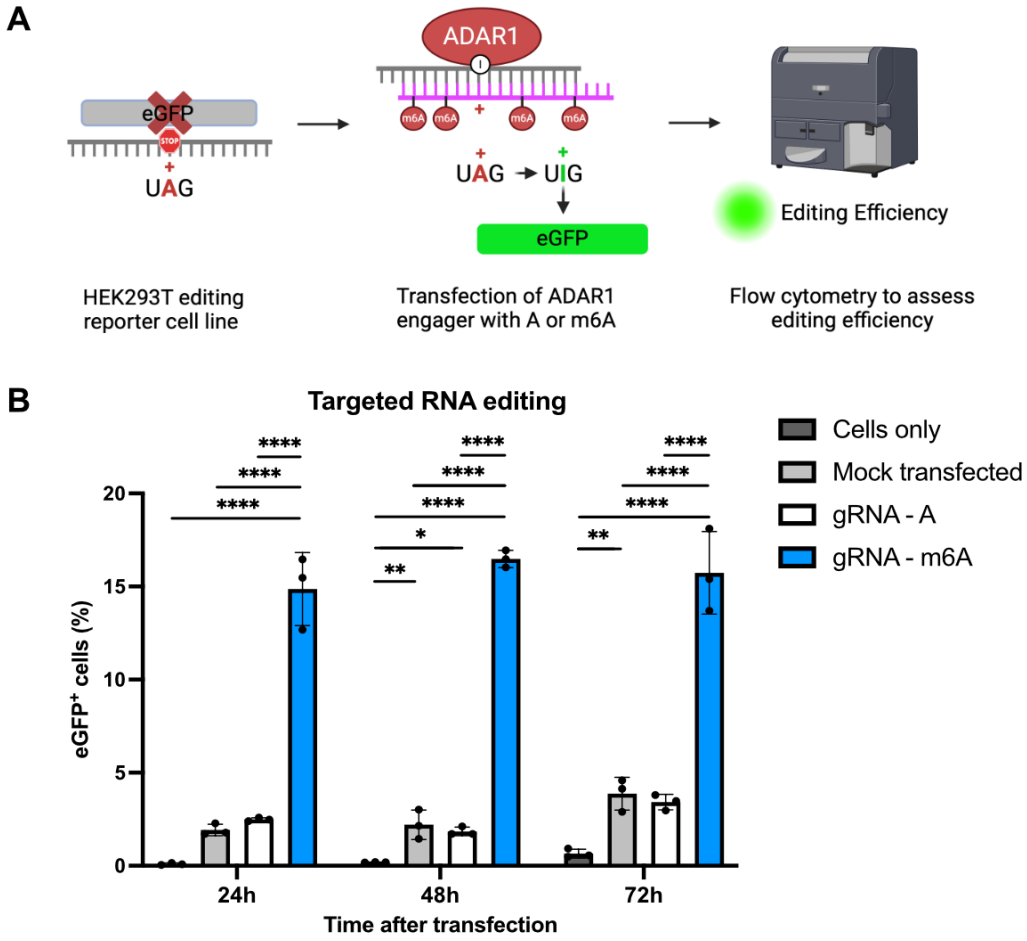

Figure 23. m6A in ADAR1-engaging guide RNA enhances targeted RNA editing. (A) Illustration of RNA-editing reporter assay to measure targeted RNA-editing by eGFP signal. **(B)** Analysis of targeted RNA editing after delivery of A or m6A containing guide RNAs assessed at different time points after transfection; n=3; statistical analysis by one-way ANOVA (multiple comparison) between conditions at individual time points. Significance values are indicated as follows: *p < 0.05; **p < 0.01; ***p < 0.001; ****p < 0.0001. **(B)** Data produced by Laura Pezzella.

5. Discussion

Immune cells that are on patrol throughout the body, constantly encounter different microenvironments, to which they must adapt. But even among immune cells, macrophages are unique in their high level of plasticity, which enables them to adapt rapidly to microenvironmental changes, thereby maintaining tissue homeostasis and protecting the body from external threats[55]. To fulfill this function, macrophages rely on their fine-tuned, coordinated, and fast responses that are mediated by transcriptional, translational and epitranscriptomic regulation. Epitranscriptomic modulations constitute an extraordinarily rapid and adaptive mechanism that drives macrophage activation and response to external stimuli[113–115]. While macrophages are commonly categorized as pro-inflammatory (M1) or anti-inflammatory (M2), macrophage polarization is very plastic, allowing a tailored, specific, and flexible phenotype that can acquire variable degrees of pro- and anti-inflammatory characteristics. This plasticity enables macrophages to precisely and efficiently fulfill their function in immune responses and tissue repair[55].

During my research, I studied the impact of mRNA modifications on the pro-inflammatory function of macrophages. I mostly applied stimulation by combined LPS and IFN-γ treatment to induce a pro-inflammatory, M1-like activation state in RAW macrophages *in vitro*. Upon stimulation, I observed a highly dynamic regulation of gene expression in different temporal clusters (Fig. 4B-C). Initially, macrophages rapidly induced primary response genes such as Ifnb1 and Tnf (Fig. 4B-C). This fast induction is facilitated by activation and nuclear translocation of constitutively expressed transcription factors[116] and induction of transcription elongation by the transcription initiation complex immediately after sensing the pro-inflammatory stimulus[117]. Next, primary response genes promoted the expression of downstream intermediate and late response genes as illustrated by gene clusters upregulated at time points 12 h and 24 h after stimulation (Fig. 4B-C), contributing to an orchestrated inflammatory response[116]. While at the later time points the continued expression of some primary response genes is facilitated by feed-forward mechanisms[116], negative feedback loops also become activated that repress translation of target mRNAs to promote the resolution of inflammation[118]. Interestingly, during the time course of

macrophage activation, m6A writers, readers and erasers and ADARs were differentially expressed as compared to resting conditions (Fig. 4D). Together with the identification of A-to-I and m6A sites in many genes involved in the innate immune response, macrophage activation and phagocytosis (Fig. 8H, 9A, 16A), this suggests an important role of mRNA modifications in the immune function of macrophages.

To assess the impact of A-to-I editing and m6A on macrophage activation, I generated RAW macrophages deficient in ADAR1 for A-to-I depletion (Fig. 5) and METTL3 for m6A depletion (Fig. 6). In many cell types, loss of ADAR1 and ADAR1-mediated A-to-I editing leads to increased levels of dsRNAs that are recognized by dsRNA sensors RIGI, MDA5, and PKR and induce innate immune responses[33,34,52–54,119]. Yet, contradictory to most published literature, I observed no innate immune activation upon loss of ADAR1 (Fig. 8A-B). A previous study suggests that only a very small subset of endogenous RNAs is responsible for MDA5 activation when not edited by ADAR1 p150[120]. However, the repertoire, expression and editing levels of these immunological endogenous RNAs might vary between cell types and tissues, with some cell types, possibly also macrophages, not inducing an interferon response upon loss of ADAR1[54].

In ADAR1-KO RAW macrophages, I did not only observe absence of innate immune activation, but an immunosuppressed phenotype as illustrated by a trend of reduced expression of type I IFNs and genes involved in dsRNA and IFN responses (Fig. 8A, B, E), as well as increased anti-inflammatory CD200R cell surface expression at resting state (Fig. 15)[121]. Hence, besides a potential lack of endogenous immunostimulatory dsRNAs, macrophages may have evolved alternative immunosuppressive mechanisms to cope with the loss of ADAR1, thereby avoiding innate immune activation. While the mechanism remains unknown, similar observations were made in other immune cells such as B cells[122] and NK cells (unpublished observation) that also showed a dampened immune response after loss of ADAR1. Potential mechanisms might involve deregulation of dsRNA recognition, downstream signaling pathways or interferon production. Disruption of GGNBP2, CNOT10, and CNOT11 that facilitate cytoplasmic accumulating and sensing of unedited transcripts by MDA5 in myeloid cells might result in observed loss of sensitivity to unedited transcripts[123].

Besides the dampened immune activation at resting state, ADAR1-KO macrophages also reduced expression of pro-inflammatory transcripts (Fig. 9B, D) and activating cell

surface markers (CD80 and MHC II; Fig. 10B) after LPS and IFN-γ treatment. Further, ADAR1-KO macrophages showed impaired phagocytosis activity against *S. aureus* and zymosan particles when pre-stimulated with LPS and IFN-γ (Fig. 18D-E). As many bacterial components are recognized by TLRs, I opted to test macrophages response to different TLR agonists as well as IFN-γ alone. While TLR signaling pathways converge at various stages with many shared signaling molecules to induce NF-κB signaling, IFN-γ signaling uses the distinct JAK-STAT signaling pathway, resulting in different downstream effects[107]. Such differences in downstream targets were illustrated by IFN-γ acting as a strong inducer of most measured activation markers, while TLR agonists induced no or only weak effects on the same markers. Despite this limitation, I observed pronounced activation defects of ADAR1-KO cells selectively after treatment with IFN-γ alone but not after exposure to individual TLR agonists (Fig. 13), indicating a specific role of ADAR1 in the response to IFN-γ. However, it remains unclear, whether the observed immunosuppressed phenotype results directly from the lack of ADAR1 editing-dependent or -independent functions.

On the other hand, when studying the effect of the m6A RNA modification, I identified a strong innate immune activation and inflammatory phenotype in m6A-depleted macrophages in the absence of exogenous stimuli. This is illustrated by transcriptional upregulation of dsRNA and type I IFN response genes (including ADAR1; Fig. 8C-D, 20A), reduced anti-inflammatory CD206 and CD200R cell surface expression (Fig. 15), and enhanced phagocytosis of beads and *S. aureus* in the absence of METTL3 (Fig. 17A, E). Such innate immune activation might be triggered by increased *Ifnb* expression (Fig. 8E-F), possibly due to loss of a destabilizing m6A site on the *Ifnb* transcript in the absence of METTL3[98]. Other studies have reported the recognition of unmethylated transcripts by innate immune receptors that induce downstream interferon and ISG production[51] potentially due to the formation of dsRNA structures by m6A depleted transcripts[26,124]. While these findings suggest that lack of m6A modifications induces innate immune activation, the true mechanism is not fully understood. Single m6A modifications are rather unlikely to counteract the formation of long stretches of dsRNAs. Additionally, the frequency of m6A in mature transcripts varies between sites but is typically below 20%[125]. Hence, it seems unlikely that the relatively low number of m6A sites and the low fraction of modified vs. unmodified copies of a transcript would prevent innate immune activation. Instead,

disruption of dsRNA structures or blockage of accessibility to innate immune sensors might depend on additional interacting proteins, such as RNA binding proteins that associate with m6A-decorated transcripts or the m6A writer complex that binds or scans along an RNA strand independently from effective m6A deposition, conceptually similar to observations of ADAR1's editing-independent repression of PKR and RIG-I[31,53].

Alternatively, innate immune activation might be related to m6A's role in transcript localization[20] and splicing[16,19,126,127]. In METTL3-KO cells, I observed increased levels of poly-adenylated mis-spliced *Adar1* isoforms that aberrantly retained an intron (Fig. 21C-E). Due to their poly-A tail, I hypothesize that the aberrantly spliced transcripts were transported into the cytoplasm where retained introns can form dsRNA structures and activate innate immune sensors[128]. The RNA-binding protein HNRNPM was found to bind LINEs within deep introns (more than 500 nt from the next exon) to prevent cryptic splicing and consecutive sensing of retained introns by dsRNA receptors[129]. While no association between HNRNPM and m6A is known, other HNRNP family members, specifically m6A readers HNRNPC and HNRNPA1, also bind deep introns[129] and regulate splicing[126,127]. In the context of these published reports, my observations of innate immune activation (Fig. 8C-D) and aberrant intron retention in the absence of m6A (Fig. 21 D-E) might hint towards m6A's role in regulating immunostimulatory cryptic splice products possibly through HNRNP family members. To confirm this hypothesis, future studies should investigate whether the loss of m6A induces globally aberrant splicing patterns and poly-A tailing of incompletely spliced transcripts, as well as the localization and mechanism of recognition of such aberrantly spliced transcripts by the innate immune system.

Beyond their role in preventing innate immune sensing, m6A RNA modifications have been reported to be crucial for regulating macrophage activation in response to various stimuli[63,64,66,124]. I identified m6A sites in more than half of the genes involved in macrophage inflammation, activation and phagocytosis (Fig. 8H, 9A, 16A). Many of these genes were differentially expressed upon pro-inflammatory stimulation (Fig. 8H, 9A, 16A) and upon loss of METTL3 (Fig. 8J, 9B-C, 16B), suggesting a regulatory role of m6A in the expression of genes involved in macrophage function. After combined LPS/IFN-γ treatment or IFN-γ treatment alone, I observed pronounced defects in cell surface expression of inflammatory and co-stimulatory molecules such as MHC I, MHC II, CD40 and CD80 (Fig. 10B, 11, 13, 14), that

provide essential signals for T cell activation[57]. Murine BMDMs partially phenocopied the impaired activation of RAW cells after m6A depletion and LPS/IFN-γ treatment, illustrating a conserved role of m6A in macrophage activation also in primary cells (Fig. 12B). These observations are in line with published results of m6A's role in directly regulating several different signaling molecules and activation markers in myeloid cells as reported for Stat1[62], MdyD88[130], Traf6[64], *CD40*, *CD80* and TIRAP[65]. Together, this data suggests a driving role of m6A in macrophages inflammatory function and in bridging innate with adaptive immunity to facilitate a comprehensive immune response.

m6A's role in pro-inflammatory activation and immune function is further illustrated by its impact on macrophage phagocytosis activity. After LPS and IFN-γ stimulation, macrophages treated with a METTL3 inhibitor phagocytosed fewer beads and pathogens, regardless of the specific ligands presented on the surface of the phagocytosed particle (Fig. 18F-J). Ligand-specific recognition or signaling might be influenced by loss of m6A, as demonstrated by partial m6A-dependent responses to TLR agonists (Fig. 13-14). However, the global defect of particle uptake hints towards a broader role of m6A in ligand-independent phagocytosis pathways that might involve cytoskeletal rearrangement for particle engulfment. Interestingly, mRNA of lymphocyte cytosolic protein 1 (*Lcp1*), a protein required for cytoplasmic rearrangement during phagocytosis[131], also contains m6A sites in my dataset, and is known to be stabilized by m6A reader HNRNPC[132], possibly playing a role in adequate phagocytosis in my experiment. Additionally, I identified a variety of other phagocytosis-related genes with m6A RNA modification sites (Fig. 16A), that might also contribute to differential regulation of phagocytosis upon m6A depletion.

Despite the here and previously described functional importance of m6A for macrophage function (Fig. 10, 17, 18) [62–64,66] and large changes in gene expression of m6A-modified transcripts during macrophage activation in control cells (Fig. 9A, 16A) or after METTL3-depletion (Fig. 9B-C, 16B), I observed only minor differences in methylation levels of individual m6A sites after pro-inflammatory stimulation in control macrophages (Fig. 19D-E). Hence, it seems that m6A's essential function in macrophage activation is not implemented by differential methylation. Instead, I and others have observed differential expression of m6A reader proteins, specifically of *Igf2bp2*[66], *Igf2bp1*, *Fmr1*, *Hnrnpa1*, *Snd1* and *Lrpprc*, upon pro-inflammatory stimulation (Fig. 4D), that can modulate various aspects

of RNA metabolism to induce functional changes[17,18,22,133]. Accordingly, differential regulation of m6A readers might mediate m6A's role in promoting full macrophage activation.

m6A levels also remained largely unaffected by the loss of ADAR1 (Fig. 19F-G), indicating that most m6A deposition occurs independent from ADAR1-mediated A-to-I editing. A previously reported A-to-I editing site on the *Mettl3* transcript[69] was absent in the murine RAW cell line, indicating no direct regulation of *Mettl3* expression by A-to-I editing. Additional reasons why m6A was mostly unaffected by A-to-I editing might be the order of m6A deposition and A-to-I editing that is influenced by the cellular localization of the RNA modifying enzymes. RNA methylation occurs co-transcriptionally in the nucleus[134], while the localization of ADAR1-mediated editing differs for the two ADAR1 isoforms with p110 localizing and editing co-transcriptionally in the nucleus and interferon inducible p150 isoform predominantly localizing to the cytoplasm where it performs most of its editing function[135,136]. Most editing events are induced after LPS/IFN-γ treatment and ADAR1 p150 induction (Fig. 20A-F), hence, are expected to occur in the cytoplasm where they cannot affect nuclear m6A deposition. This leaves only a small fraction of nuclear editing events paired with low editing incidences per site that could potentially influence m6A deposition. While the temporal hierarchy of nuclear editing and nuclear methylation remains unsolved, observing no major effect of ADAR1 depletion on m6A might indicate that m6A tends to occur prior to nuclear RNA editing, further explaining the absence of a strong impact of A-to-I depletion on m6A levels.

In contrast to the stable m6A levels, I identified a clear ADAR1-mediated RNA editing response 12 h and 24 h after LPS/IFN-γ treatment as compared to the resting state (Fig. 20D–F). I also identified METTL3-dependent differences in ADAR1-mediated editing with decreased editing in the absence of METTL3 in stimulated macrophages (Fig. 20 F, G, I). This finding strongly suggests a positive effect of m6A on ADAR1-mediated RNA editing, possibly caused by the direct effect of several m6A sites on the *Adar1* transcript leading to reduced translation efficiency[70] and mis-spliced *Adar1* isoforms due to m6A's role in splicing (Fig. 21)[19,126,127,137].

Additionally, I observed m6A's regulation of A-to-I editing on the transcript level by cross-referencing m6A sites obtained from Nanopore sequencing and A-to-I sites obtained

from Illumina sequencing. In line with previous findings[71], I observed a negative association between m6A and A-to-I editing when modification sites were in close proximity (≤139 nt apart; Fig. 22D-F). Reasons for this negative relationship at close distances include: (i) an A decorated with an m6A cannot be edited anymore[138] and vice versa, (ii) the two RNA modifications prefer different local sequence contexts (A-to-I editing with a mild preference of A or U as 5' neighbor of the edited site[139] while m6A occurs predominantly in DRACH motifs[9]), (iii) m6A might disrupt local dsRNA structure required for editing[25,26], and (iv) m6A writers or readers might occupy a transcript region and prevent ADAR1 from binding and editing in immediate vicinity of a m6A site.

In contrast, I observed a positive association between m6A and inosine when the two RNA modifications were at distances larger than 139 nt (Fig. 22 D-F). This can be explained by a variety of different but non-exclusive mechanisms that might depend on characteristics of the individual transcript: (i) m6A can increase stability of mRNA molecules[18,22,140]; the longer half-life of m6A-modified transcripts makes them more likely to be edited and detected, (ii) m6A promotes transport of mRNAs to the cytoplasm[20,133] where they can be edited by cytoplasmic ADAR1 p150, (iii) m6A might be stabilizing RNA secondary structure through RNA looping or folding, giving rise to dsRNA regions at a distance that can be edited[110,111], (iv) m6A might loosen perfect base pairing in the variable ds region in proximity to the editing site; imperfect base pairing in the variable ds region was found to promote ADAR1 editing[141,142], and (v) binding of m6A reader proteins might assist in ADAR1 recruitment as indicated by interactions of ADAR1 with m6A readers[109].

As we identified A-to-I and m6A sites using different data sets, and despite statistical evidence of their correlation, this cannot prove colocalization of the two RNA modifications on the same transcript. Hence, we used an artificial guide RNA that forms a dsRNA structure with its complementary target region to recruit ADAR1 for editing, thereby mimicking the back-looping of a distal complementary RNA region. When replacing unmodified adenosines in the guide RNA with m6A, I observed robustly increased targeted RNA editing (Fig. 23B). Together with the above-presented data, this observation indicates a possible structural or protein-mediated recruitment of ADAR1 towards m6A sites at a distance (even within an artificial setting). In the context of novel clinical approaches of targeted RNA editing[44,45],

designing m6A containing ADAR1-engaging guide RNAs might assist in improving therapeutic editing efficiencies.

Collectively, my findings provide novel insights into the interactions and dynamics of m6A and A-to-I editing and their functional impact on cells' transcriptional and phenotypic plasticity as demonstrated by the example of macrophages upon pro-inflammatory activation. Future investigations should help understand cell type and tissue-specific mechanisms of innate immune activation upon loss of m6A and A-to-I RNA modifications. Furthermore, it remains unclear whether the identified interplay and dynamics of m6A and A-to-I editing also apply in different cell types and organisms, as well as during physiological conditions. Demonstrating the association of m6A and A-to-I editing on the single-transcript level and understanding the underlying molecular mechanism can contribute to further advances in targeted RNA editing therapies.

6. Supplementary data

Table S1. Counts per million reads (CPM) of selected genes obtained from Illumina RNA sequencing (produced by Dr. Salvatore Di Giorgio)

Gene	Ctrl-1				Ctrl-2				Ctrl-3			
	0 h	2 h	12 h	24 h	0 h	2 h	12 h	24 h	0 h	2 h	12 h	24 h
Adar	77.94	247.28	418.41	404.02	67.12	202.77	361.66	348.49	80.18	225.95	357.64	371.08
Adarb1	6.59	5.06	2.62	1.59	7.89	5.23	3.03	2.53	6.88	5.41	3.25	1.84
Ifnb1	0.00	10.82	0.36	0.65	0.06	7.32	0.20	0.69	0.03	7.60	0.73	1.40
Gene	METTL3-KO-1				METTL3-KO-2				METTL3-KO-3			
	0 h	2 h	12 h	24 h	0 h	2 h	12 h	24 h	0 h	2 h	12 h	24 h
Adar	140.74	182.75	317.96	366.79	169.08	331.23	411.07	479.54	106.12	165.80	277.69	357.33
Adarb1	5.27	3.77	3.49	2.44	8.19	4.51	5.49	4.90	7.08	6.09	5.06	4.54
Ifnb1	0.30	0.43	0.67	0.64	0.00	0.56	2.11	2.34	0.31	0.52	0.14	1.32
Gene	ADAR1-KO-1				ADAR1-KO-2				ADAR1-KO-3			
	0 h	2 h	12 h	24 h	0 h	2 h	12 h	24 h	0 h	2 h	12 h	24 h
Adar	9.52	28.31	69.48	53.15	39.66	137.66	266.42	263.50	25.94	91.31	135.59	148.86
Adarb1	8.57	6.91	4.30	5.47	7.73	5.76	3.36	3.57	4.61	5.27	2.31	2.95
Ifnb1	0.00	2.05	0.75	0.08	0.00	7.02	1.07	0.65	0.00	7.29	2.76	0.15

Table S2. Extract of differential gene expression analysis comparing unstimulated METTL3-KO vs. unstimulated control macrophages (produced by Dr. Salvatore Di Giorgio)

Genes	ENSEMBLE ID	ENT	GT	logFC	logCPM	F-statistic	p value	FDR
Adar	ENSMUSG00000027951	56417	protein-coding	0.885	7.711	3.293	0.080	0.160
Ifnar1	ENSMUSG00000022967	15975	protein-coding	0.067	5.996	0.118	0.734	0.817
Ifnar2	ENSMUSG00000022971	15976	protein-coding	0.395	5.405	3.066	0.091	0.176
Irf2bp1	ENSMUSG00000044030	272359	protein-coding	0.129	4.179	0.658	0.424	0.554
Irf2bp2	ENSMUSG00000051495	270110	protein-coding	0.179	5.964	1.231	0.277	0.406
Nkrf	ENSMUSG00000044149	77286	protein-coding	0.590	4.877	19.273	1.472E-04	0.001
Lcp1	ENSMUSG00000021998	18826	protein-coding	0.362	9.825	5.025	0.033	0.081
Ifngr1	ENSMUSG00000020009	15979	protein-coding	0.201	3.760	2.489	0.126	0.226
Ifngr2	ENSMUSG00000022965	15980	protein-coding	0.037	5.534	0.068	0.796	0.862
Clec7a	ENSMUSG00000079293	56644	protein-coding	-6.095	0.924	33.234	2.169E-06	3.704E-05
Tlr2	ENSMUSG00000027995	24088	protein-coding	1.838	7.940	30.279	7.092E-06	9.476E-05
Cd36	ENSMUSG00000002944	12491	protein-coding	-13.545	7.287	75.769	2.308E-09	1.645E-07
Tlr4	ENSMUSG00000039005	21898	protein-coding	0.065	6.518	0.123	0.729	0.813

Table S3. Extract of differential gene expression analysis comparing METTL3-KO 24 h LPS/IFN-γ vs. control macrophages 24 h LPS/IFN-γ (produced by Dr. Salvatore Di Giorgio)

Genes	ENSEMBLE ID	ENT	GT	logFC	logCPM	F-statistic	p value	FDR
Adar	ENSMUSG00000027951	56417	protein-coding	0.099	7.711	0.042	0.838	0.886
Ifnar1	ENSMUSG00000022967	15975	protein-coding	0.002	5.996	6.880E-05	0.993	0.996
Ifnar2	ENSMUSG00000022971	15976	protein-coding	0.091	5.405	0.165	0.688	0.767
Irf2bp1	ENSMUSG00000044030	272359	protein-coding	0.672	4.179	17.105	2.929E-04	0.001
Irf2bp2	ENSMUSG00000051495	270110	protein-coding	0.706	5.964	18.493	1.878E-04	0.001
Nkrf	ENSMUSG00000044149	77286	protein-coding	0.574	4.877	18.070	2.147E-04	0.001
Lcp1	ENSMUSG00000021998	18826	protein-coding	-0.488	9.825	9.122	0.005	0.015
Ifngr1	ENSMUSG00000020009	15979	protein-coding	-0.072	3.760	0.308	0.584	0.677
Ifngr2	ENSMUSG00000022965	15980	protein-coding	-0.530	5.534	13.977	0.001	0.003
Clec7a	ENSMUSG00000079293	56644	protein-coding	-3.140	0.924	16.312	3.153E-04	0.001
Tlr2	ENSMUSG00000027995	24088	protein-coding	0.837	7.940	6.575	1.601E-02	0.038
Cd36	ENSMUSG00000002944	12491	protein-coding	-7.866	7.287	61.107	1.930E-08	5.012E-07
Tlr4	ENSMUSG00000039005	21898	protein-coding	-0.237	6.518	1.631	0.212	0.311

Table S4. Extract of differential gene expression analysis comparing unstimulated ADAR1-KO vs. unstimulated control macrophages (produced by Dr. Salvatore Di Giorgio)

Genes	ENSEMBLE ID	ENT	GT	logFC	logCPM	F-statistic	p value	FDR
Adar	ENSMUSG00000027951	56417	protein-coding	-1.585	7.711	10.090	0.004	0.236
Ifnar1	ENSMUSG00000022967	15975	protein-coding	-0.090	5.996	0.209	0.651	0.997
Ifnar2	ENSMUSG00000022971	15976	protein-coding	-0.063	5.405	0.077	0.783	1.000
Irf2bp1	ENSMUSG00000044030	272359	protein-coding	-0.154	4.179	0.929	0.344	0.969
Irf2bp2	ENSMUSG00000051495	270110	protein-coding	-0.031	5.964	0.037	0.848	1.000
Nkrf	ENSMUSG00000044149	77286	protein-coding	0.018	4.877	0.019	0.893	1.000
Lcp1	ENSMUSG00000021998	18826	protein-coding	-0.224	9.825	1.919	0.177	0.890
Ifngr1	ENSMUSG00000020009	15979	protein-coding	-0.115	3.760	0.819	0.373	0.975
Ifngr2	ENSMUSG00000022965	15980	protein-coding	-0.295	5.534	4.356	0.046	0.664
Clec7a	ENSMUSG00000079293	56644	protein-coding	0.803	0.924	2.686	0.111	0.821
Tlr2	ENSMUSG00000027995	24088	protein-coding	-0.824	7.940	6.311	0.018	0.479
Cd36	ENSMUSG00000002944	12491	protein-coding	0.008	7.287	1.335E-04	0.991	1.000
Tlr4	ENSMUSG00000039005	21898	protein-coding	-0.078	6.518	0.179	0.675	0.998

Table S5. Multiple regression model of association between A-to-I and m6A

Multiple regression analysis shows that the distance to the next m6a site and the both numbers of editing sites are major factors for editing frequency. Distinguishing 3' UTR and TSS regions from others, both stood out. The m6a editing frequency is also a relevant factor when considered in their interaction with region. Coverages are also associated with frequency, including their interaction with distance and number of editing sites. The table shows the full results from a multivariate regression model for log editing frequency (freq) with log transformed explanatory variables including distance (to next m6a), number of editing sites (N_ed), number of m6a editing sites (N_m6a), frequency of m6a (freq_m6a), coverages (cov and cov_m6a), and indicators for region (distinguishing between 3' UTR, TSS, and others). The model was selected from the full specification based on AIC (Akaike information criteria) scores allowing including pairwise interactions. All continuous variables where log transformed for variance stabilization, and entries with distances above 10000, coverages below 10 and frequencies below 5 were excluded. Multiple $R^2$is 0.31 (adjusted 0.30). Significance codes: *** ($p<0.001$), ** ($0.001 \leq p < 0.01$), * ($0.01 \leq p < 0.05$), . ($0.05 \leq p < 0.1$) (produced by Dr. Julia Brettschneider).

Coefficient	Estimate	SE	P-value
intercept	5.128	0.475	<2e-16 ***
distance	0.127	0.031	3.45e-05 ***
N_ed	-0.138	0.057	0.016 *
N_m6a	-0.122	0.034	0.000 ***
region 3'UTR	-0.490	0.221	0.026 *
region TTS	1.394	0.316	1.03e-05 ***
cov	-0.591	0.102	6.76e-09 ***
cov_m6a	-0.390	0.051	2.02e-14 ***
freq_m6a:region 3'UTR	0.083	0.035	0.016 *
freq_m6a:region TSS	-0.195	0.050	1.01e-4 ***
distance:cov	-0.230	0.006	3.74e-06 ***
distance:N_ed	-0.013	0.005	1.011 *
distance:N_m6a	0.018	0.005	4.07e-4 ***
cov:cov_m6a	0.095	0.011	< 2e-16 ***
cov:N_ed	0.017	0.009	0.052

PUBLISHED WORK AND CONTRIBUTIONS

Published work

Portions of the work described in this thesis were published as a preprint that is currently in revision at EMBO Journal:

Griesche, V. et al. m6A regulates ADAR1-mediated RNA editing during macrophage activation. 2025.01.28.635339 Preprint at https://doi.org/10.1101/2025.01.28.635339 (2025).

The methods, figures 4-10 and 16-23, and table S5 (including legends) were taken and adapted from the original manuscript and included in this thesis.

Contributions

Acknowledgement of the contribution to the presented work is given to:

Dr. Salvatore di Giorgio: Bioinformatic analysis of Illumina and Nanopore sequencing data and statistical analysis contributing to figures 4B-D, 6F, 7, 8A-E, G-J, 9, 16 A-B, 19A, D-G, 20 A, D-I, 21A, and 22, and tables S1-S4.

Dr. Julia Brettschneider: Statistical analysis of the multiple regression model table S4.

Chih-Yuan Kao: Processing and analysis of ribosome sequencing contributing to figure 21B and cloning to generate the plasmids to knock out METTL3.

Irem Tellioglu: Assisting in pre-processing of nanopore data.

Laura Pezzella, Dr. Jose Paulo Lorenzo, Annette Arnold and Dr. Riccardo Pecori: Experimental work, analysis and design of the experiment presented in figure 23.

Christina Mertens and Maria Moreira Pereira: Isolation of bone marrow cells from mice that were cultured by me for experiments involving BMDMs (Figure 12B).

Dr. Steffen Schmitt (DKFZ flow cytometry core facility): Fluorescence-activated cell sorting that contributing to the generation of the control, ADAR1-KO and METTL3-KO lines.

Next generation sequencing core facility: Illumina library preparation and sequencing.

REFERENCES

1. Amos, H. & Korn, M. 5-Methyl cytosine in the RNA of Escherichia coli. *Biochim. Biophys. Acta* **29**, 444–445 (1958).

2. Boccaletto, P. *et al.* MODOMICS: a database of RNA modification pathways. 2021 update. *Nucleic Acids Res.* **50**, D231–D235 (2022).

3. Shi, H., Chai, P., Jia, R. & Fan, X. Novel insight into the regulatory roles of diverse RNA modifications: Re-defining the bridge between transcription and translation. *Mol. Cancer* **19**, 78 (2020).

4. Delaunay, S., Helm, M. & Frye, M. RNA modifications in physiology and disease: towards clinical applications. *Nat. Rev. Genet.* **25**, 104–122 (2024).

5. Liu, J. *et al.* A METTL3–METTL14 complex mediates mammalian nuclear RNA N6-adenosine methylation. *Nat. Chem. Biol.* **10**, 93–95 (2014).

6. Wang, X. *et al.* Structural basis of N(6)-adenosine methylation by the METTL3-METTL14 complex. *Nature* **534**, 575–578 (2016).

7. Pendleton, K. E. *et al.* The U6 snRNA m6A Methyltransferase METTL16 Regulates SAM Synthetase Intron Retention. *Cell* **169**, 824-835.e14 (2017).

8. Warda, A. S. *et al.* Human METTL16 is a N6-methyladenosine (m6A) methyltransferase that targets pre-mRNAs and various non-coding RNAs. *EMBO Rep.* **18**, 2004–2014 (2017).

9. Dominissini, D. *et al.* Topology of the human and mouse m6A RNA methylomes revealed by m6A-seq. *Nature* **485**, 201–206 (2012).

10. Körtel, N. *et al.* Deep and accurate detection of m6A RNA modifications using miCLIP2 and m6Aboost machine learning. *Nucleic Acids Res.* **49**, e92–e92 (2021).

11. Liu, C. *et al.* Absolute quantification of single-base m6A methylation in the mammalian transcriptome using GLORI. *Nat. Biotechnol.* **41**, 355–366 (2023).

12. Ke, S. *et al.* A majority of m6A residues are in the last exons, allowing the potential for 3′ UTR regulation. *Genes Dev.* **29**, 2037–2053 (2015).

13. Wang, X. *et al.* N6-methyladenosine-dependent regulation of messenger RNA stability. *Nature* **505**, 117–120 (2014).

14. Meyer, K. D. *et al.* 5’ UTR m(6)A Promotes Cap-Independent Translation. *Cell* **163**, 999–1010 (2015).

15. Zhou, J. *et al.* Dynamic m6A mRNA methylation directs translational control of heat shock response. *Nature* **526**, 591–594 (2015).

16. Xiao, W. *et al.* Nuclear m(6)A Reader YTHDC1 Regulates mRNA Splicing. *Mol. Cell* **61**, 507–519 (2016).

17. Huang, H. *et al.* Recognition of RNA N6-methyladenosine by IGF2BP Proteins Enhances mRNA Stability and Translation. *Nat. Cell Biol.* **20**, 285–295 (2018).

18. Wang, H., Tang, A., Cui, Y., Gong, H. & Li, H. LRPPRC facilitates tumor progression and immune evasion through upregulation of m6A modification of PD-L1 mRNA in hepatocellular carcinoma. *Front. Immunol.* **14**, 1144774 (2023).

19. Alarcón, C. R. *et al.* HNRNPA2B1 Is a Mediator of m(6)A-Dependent Nuclear RNA Processing Events. *Cell* **162**, 1299–1308 (2015).

20. Roundtree, I. A. *et al.* YTHDC1 mediates nuclear export of N6-methyladenosine methylated mRNAs. *eLife* **6**, e31311 (2017).

21. Wang, X. *et al.* N6-methyladenosine Modulates Messenger RNA Translation Efficiency. *Cell* **161**, 1388–1399 (2015).

22. Baquero-Perez, B. *et al.* The Tudor SND1 protein is an m6A RNA reader essential for replication of Kaposi's sarcoma-associated herpesvirus. *eLife* **8**, e47261 (2019).

23. Zhang, F. *et al.* Fragile X mental retardation protein modulates the stability of its m6A-marked messenger RNA targets. *Hum. Mol. Genet.* **27**, 3936–3950 (2018).

24. Roost, C. *et al.* Structure and Thermodynamics of N6-Methyladenosine in RNA: A Spring-Loaded Base Modification. *J. Am. Chem. Soc.* **137**, 2107–2115 (2015).

25. Gao, Y. *et al.* m6A Modification Prevents Formation of Endogenous Double-Stranded RNAs and Deleterious Innate Immune Responses during Hematopoietic Development. *Immunity* **52**, 1007-1021.e8 (2020).

26. Qiu, W. *et al.* N6-methyladenosine RNA modification suppresses antiviral innate sensing pathways via reshaping double-stranded RNA. *Nat. Commun.* **12**, 1582 (2021).

27. Zheng, G. *et al.* ALKBH5 is a mammalian RNA demethylase that impacts RNA metabolism and mouse fertility. *Mol. Cell* **49**, 18–29 (2013).

28. Jia, G. *et al.* N6-Methyladenosine in nuclear RNA is a major substrate of the obesity-associated FTO. *Nat. Chem. Biol.* **7**, 885–887 (2011).

29. Savva, Y. A., Rieder, L. E. & Reenan, R. A. The ADAR protein family. *Genome Biol.* **13**, 252 (2012).

30. Tan, M. H. *et al.* Dynamic landscape and regulation of RNA editing in mammals. *Nature* **550**, 249–254 (2017).

31. Liang, Z., Goradia, A., Walkley, C. R. & Heraud-Farlow, J. E. Generation of a new Adar1p150 -/- mouse demonstrates isoform-specific roles in embryonic development and adult homeostasis. *RNA N. Y. N* **29**, 1325–1338 (2023).

32. Wulff, B.-E. & Nishikura, K. Substitutional A-to-I RNA editing. *Wiley Interdiscip. Rev. RNA* **1**, 90–101 (2010).

33. Pestal, K. *et al.* Isoforms of RNA-Editing Enzyme ADAR1 Independently Control Nucleic Acid Sensor MDA5-Driven Autoimmunity and Multi-organ Development. *Immunity* **43**, 933–944 (2015).

34. Mannion, N. M. *et al.* The RNA-Editing Enzyme ADAR1 Controls Innate Immune Responses to RNA. *Cell Rep.* **9**, 1482–1494 (2014).

35. Casati, B., Stamkopoulou, D., Tasakis, R. N. & Pecori, R. ADAR-Mediated RNA Editing and Its Therapeutic Potentials. in *Epitranscriptomics (eds. Jurga, S. & Barciszewski, J.)* 471–503 (Springer International Publishing, 2021).

36. Stefl, R. *et al.* The solution structure of the ADAR2 dsRBM-RNA complex reveals a sequence-specific readout of the minor groove. *Cell* **143**, 225–237 (2010).

37. Katrekar, D. *et al.* In vivo RNA editing of point mutations via RNA-guided adenosine deaminases. *Nat. Methods* **16**, 239–242 (2019).

38. Stafforst, T. & Schneider, M. F. An RNA-deaminase conjugate selectively repairs point mutations. *Angew. Chem. Int. Ed Engl.* **51**, 11166–11169 (2012).

39. Montiel-Gonzalez, M. F., Vallecillo-Viejo, I., Yudowski, G. A. & Rosenthal, J. J. C. Correction of mutations within the cystic fibrosis transmembrane conductance regulator by site-directed RNA editing. *Proc. Natl. Acad. Sci. U. S. A.* **110**, 18285–18290 (2013).

40. Cox, D. B. T. *et al.* RNA editing with CRISPR-Cas13. *Science* **358**, 1019–1027 (2017).

41. Rauch, S. *et al.* Programmable RNA-Guided RNA Effector Proteins Built from Human Parts. *Cell* **178**, 122-134.e12 (2019).

42. Merkle, T. *et al.* Precise RNA editing by recruiting endogenous ADARs with antisense oligonucleotides. *Nat. Biotechnol.* **37**, 133–138 (2019).

43. Qu, L. *et al.* Programmable RNA editing by recruiting endogenous ADAR using engineered RNAs. *Nat. Biotechnol.* **37**, 1059–1069 (2019).

44. Wave Life Sciences Ltd. *A Phase 1, Randomized, Double-Blind, Placebo-Controlled, Safety, Tolerability, and Pharmacokinetic Study of Single Ascending Doses and Multiple Doses of WVE-006 in Healthy Participants*. https://clinicaltrials.gov/study/NCT06186492 (2025).

45. Wave Life Sciences Announces First-Ever Therapeutic RNA Editing in Humans Achieved in RestorAATion-2 Trial of WVE-006 in Alpha-1 Antitrypsin Deficiency - Wave Life Sciences. https://ir.wavelifesciences.com/node/11731.

46. Uehata, T. & Takeuchi, O. RNA Recognition and Immunity—Innate Immune Sensing and Its Posttranscriptional Regulation Mechanisms. *Cells* **9**, 1701 (2020).

47. Bachellerie, J.-P. & Cavaillé, J. Small Nucleolar RNAs Guide the Ribose Methylations of Eukaryotic rRNAs. in *Modification and Editing of RNA* 255–272 (John Wiley & Sons, Ltd, 1998). doi:10.1128/9781555818296.ch13.

48. Bokar, J. A. & Rottman, F. M. Biosynthesis and Functions of Modified Nucleosides in Eukaryotic mRNA. in *Modification and Editing of RNA* 183–200 (John Wiley & Sons, Ltd, 1998). doi:10.1128/9781555818296.ch10.

49. Karikó, K., Ni, H., Capodici, J., Lamphier, M. & Weissman, D. mRNA is an endogenous ligand for Toll-like receptor 3. *J. Biol. Chem.* **279**, 12542–12550 (2004).

50. Weissman, D. *et al.* HIV gag mRNA transfection of dendritic cells (DC) delivers encoded antigen to MHC class I and II molecules, causes DC maturation, and induces a potent human in vitro primary immune response. *J. Immunol. Baltim. Md 1950* **165**, 4710–4717 (2000).

51. Karikó, K., Buckstein, M., Ni, H. & Weissman, D. Suppression of RNA recognition by Toll-like receptors: the impact of nucleoside modification and the evolutionary origin of RNA. *Immunity* **23**, 165–175 (2005).

52. Liddicoat, B. J. *et al.* RNA editing by ADAR1 prevents MDA5 sensing of endogenous dsRNA as nonself. *Science* **349**, 1115–1120 (2015).

53. Yang, S. *et al.* ADAR1 Limits RIG-I RNA Detection and Suppresses IFN Production Responding to Viral and Endogenous RNAs. *J. Immunol. Baltim. Md 1950* **193**, 3436–3445 (2014).

54. Chung, H. *et al.* Human ADAR1 Prevents Endogenous RNA from Triggering Translational Shutdown. *Cell* **172**, 811-824.e14 (2018).

55. Wynn, T. A., Chawla, A. & Pollard, J. W. Origins and Hallmarks of Macrophages: Development, Homeostasis, and Disease. *Nature* **496**, 445–455 (2013).

56. Wang, Y., Smith, W., Hao, D., He, B. & Kong, L. M1 and M2 macrophage polarization and potentially therapeutic naturally occurring compounds. *Int. Immunopharmacol.* **70**, 459–466 (2019).

57. Wang, R. *et al.* The interaction of innate immune and adaptive immune system. *MedComm* **5**, e714 (2024).

58. Hirayama, D., Iida, T. & Nakase, H. The Phagocytic Function of Macrophage-Enforcing Innate Immunity and Tissue Homeostasis. *Int. J. Mol. Sci.* **19**, 92 (2017).

59. Noy, R. & Pollard, J. W. Tumor-associated macrophages: from mechanisms to therapy. *Immunity* **41**, 49–61 (2014).

60. RNA modifications: importance in immune cell biology and related diseases | Signal Transduction and Targeted Therapy. https://www.nature.com/articles/s41392-022-01175-9.

61. Vu, L. P. *et al.* The N6-methyladenosine (m6A)-forming enzyme METTL3 controls myeloid differentiation of normal hematopoietic and leukemia cells. *Nat. Med.* **23**, 1369–1376 (2017).

62. Liu, Y. *et al.* The N6-methyladenosine (m6A)-forming enzyme METTL3 facilitates M1 macrophage polarization through the methylation of STAT1 mRNA. *Am. J. Physiol. Cell Physiol.* **317**, C762–C775 (2019).

63. Wang, J., Yan, S., Lu, H., Wang, S. & Xu, D. METTL3 Attenuates LPS-Induced Inflammatory Response in Macrophages via NF-κB Signaling Pathway. *Mediators Inflamm.* **2019**, 3120391 (2019).

64. Zong, X. *et al.* Mettl3 Deficiency Sustains Long-Chain Fatty Acid Absorption through Suppressing Traf6-Dependent Inflammation Response. *J. Immunol. Author Choice* **202**, 567–578 (2019).

65. Wang, H. *et al.* Mettl3-mediated mRNA m6A methylation promotes dendritic cell activation. *Nat. Commun.* **10**, 1898 (2019).

66. Wang, X. *et al.* The m6A Reader IGF2BP2 Regulates Macrophage Phenotypic Activation and Inflammatory Diseases by Stabilizing TSC1 and PPARγ. *Adv. Sci.* **8**, 2100209 (2021).

67. Cai, D., Sun, C., Murashita, T., Que, X. & Chen, S.-Y. ADAR1 Non-Editing Function in Macrophage Activation and Abdominal Aortic Aneurysm. *Circ. Res.* **132**, e78–e93 (2023).

68. Sun, C., Cai, D. & Chen, S.-Y. ADAR1 promotes systemic sclerosis via modulating classic macrophage activation. *Front. Immunol.* **13**, 1051254 (2022).

69. Li, Y. *et al.* RNA Editing Enzyme ADAR1 Regulates METTL3 in an Editing Dependent Manner to Promote Breast Cancer Progression via METTL3/ARHGAP5/YTHDF1 Axis. *Int. J. Mol. Sci.* **23**, 9656 (2022).

70. Tassinari, V. *et al.* ADAR1 is a new target of METTL3 and plays a pro-oncogenic role in glioblastoma by an editing-independent mechanism. *Genome Biol.* **22**, 51 (2021).

71. Xiang, J.-F. *et al.* N6-Methyladenosines Modulate A-to-I RNA Editing. *Mol. Cell* **69**, 126-135.e6 (2018).

72. Griesche, V. *et al.* m6A regulates ADAR1-mediated RNA editing during macrophage activation. 2025.01.28.635339 Preprint at https://doi.org/10.1101/2025.01.28.635339 (2025).

73. Perez-Garcia, V. *et al.* BAP1/ASXL complex modulation regulates epithelial-mesenchymal transition during trophoblast differentiation and invasion. *eLife* https://elifesciences.org/articles/63254/figures (2021) doi:10.7554/eLife.63254.

74. Montiel-González, M. F., Vallecillo-Viejo, I. C. & Rosenthal, J. J. C. An efficient system for selectively altering genetic information within mRNAs. *Nucleic Acids Res.* **44**, e157 (2016).

75. Love, M. I., Anders, S., Kim, V. & Huber, W. RNA-Seq workflow: gene-level exploratory analysis and differential expression. *F1000Research* **4**, 1070 (2015).

76. Bolger, A. M., Lohse, M. & Usadel, B. Trimmomatic: a flexible trimmer for Illumina sequence data. *Bioinforma. Oxf. Engl.* **30**, 2114–2120 (2014).

77. Dobin, A. *et al.* STAR: ultrafast universal RNA-seq aligner. *Bioinforma. Oxf. Engl.* **29**, 15–21 (2013).

78. Huber, W. *et al.* Orchestrating high-throughput genomic analysis with Bioconductor. *Nat. Methods* **12**, 115–121 (2015).

79. Li, H. *et al.* The Sequence Alignment/Map format and SAMtools. *Bioinformatics* **25**, 2078–2079 (2009).

80. Flati, T. *et al.* HPC-REDItools: a novel HPC-aware tool for improved large scale RNA-editing analysis. *BMC Bioinformatics* **21**, 353 (2020).

81. Feng, H., Conneely, K. N. & Wu, H. A Bayesian hierarchical model to detect differentially methylated loci from single nucleotide resolution sequencing data. *Nucleic Acids Res.* **42**, e69 (2014).

82. Park, Y. & Wu, H. Differential methylation analysis for BS-seq data under general experimental design. *Bioinformatics* **32**, 1446–1453 (2016).

83. Wu, H., Wang, C. & Wu, Z. A new shrinkage estimator for dispersion improves differential expression detection in RNA-seq data. *Biostat. Oxf. Engl.* **14**, 232–243 (2013).

84. Patro, R., Duggal, G., Love, M. I., Irizarry, R. A. & Kingsford, C. Salmon provides fast and bias-aware quantification of transcript expression. *Nat. Methods* **14**, 417–419 (2017).

85. Robinson, M. D., McCarthy, D. J. & Smyth, G. K. edgeR: a Bioconductor package for differential expression analysis of digital gene expression data. *Bioinforma. Oxf. Engl.* **26**, 139–140 (2010).

86. Soneson, C., Love, M. I. & Robinson, M. D. Differential analyses for RNA-seq: transcript-level estimates improve gene-level inferences. *F1000Research* **4**, 1521 (2015).

87. Lewis, M., B, K. & Rana, S. EnhancedVolcano: publication-ready volcano plots with enhanced colouring and labeling. https://bioconductor.org/packages/devel/bioc/vignettes/EnhancedVolcano/inst/doc/EnhancedVolcano.html (2024).

88. Li, H. Minimap2: pairwise alignment for nucleotide sequences. *Bioinformatics* **34**, 3094–3100 (2018).

89. McLaren, W. *et al.* The Ensembl Variant Effect Predictor. *Genome Biol.* **17**, 122 (2016).

90. Zhang, F. & Chen, J. Y. HOMER: a human organ-specific molecular electronic repository. *BMC Bioinformatics* **12**, S4 (2011).

91. Yu, G., Wang, L.-G. & He, Q.-Y. ChIPseeker: an R/Bioconductor package for ChIP peak annotation, comparison and visualization. *Bioinforma. Oxf. Engl.* **31**, 2382–2383 (2015).

92. Lawrence, M. *et al.* Software for computing and annotating genomic ranges. *PLoS Comput. Biol.* **9**, e1003118 (2013).

93. Tong, J. *et al.* Pooled CRISPR screening identifies m^6A as a positive regulator of macrophage activation. *Sci. Adv.* **7**, eabd4742 (2021).

94. Gao, Y. *et al.* m6A Modification Prevents Formation of Endogenous Double-Stranded RNAs and Deleterious Innate Immune Responses during Hematopoietic Development. *Immunity* **52**, 1007-1021.e8 (2020).

95. Meyer, K. D. *et al.* Comprehensive Analysis of mRNA Methylation Reveals Enrichment in 3′ UTRs and near Stop Codons. *Cell* **149**, 1635–1646 (2012).

96. Poh, H. X., Mirza, A. H., Pickering, B. F. & Jaffrey, S. R. Alternative splicing of METTL3 explains apparently METTL3-independent m6A modifications in mRNA. *PLoS Biol.* **20**, e3001683 (2022).

97. Wei, G. *et al.* Acute depletion of METTL3 implicates N6-methyladenosine in alternative intron/exon inclusion in the nascent transcriptome. *Genome Res.* **31**, 1395–1408 (2021).

98. Winkler, R. *et al.* m6A modification controls the innate immune response to infection by targeting type I interferons. *Nat. Immunol.* **20**, 173–182 (2019).

99. Gao, Z. *et al.* Single-nucleotide methylation specifically represses type I interferon in antiviral innate immunity. *J. Exp. Med.* **218**, e20201798 (2021).

100. Daman, A. W. & Josefowicz, S. Z. Epigenetic and transcriptional control of interferon-β. *J. Exp. Med.* **218**, e20210039 (2021).

101. Nourbakhsh, M. & Hauser, H. Constitutive silencing of IFN-beta promoter is mediated by NRF (NF-kappaB-repressing factor), a nuclear inhibitor of NF-kappaB. *EMBO J.* **18**, 6415–6425 (1999).

102. Childs, K. S. & Goodbourn, S. Identification of novel co-repressor molecules for Interferon Regulatory Factor-2. *Nucleic Acids Res.* **31**, 3016–3026 (2003).

103. Senger, K. *et al.* Gene Repression by Coactivator Repulsion. *Mol. Cell* **6**, 931–937 (2000).

104. Williams, D. B., Barber, B. H., Flavell, R. A. & Allen, H. Role of beta 2-microglobulin in the intracellular transport and surface expression of murine class I histocompatibility molecules. *J. Immunol.* **142**, 2796–2806 (1989).

105. Vitiello, A., Potter, T. A. & Sherman, L. A. The role of beta 2-microglobulin in peptide binding by class I molecules. *Science* **250**, 1423–1426 (1990).

106. Fleetwood, A. J., Lawrence, T., Hamilton, J. A. & Cook, A. D. Granulocyte-Macrophage Colony-Stimulating Factor (CSF) and Macrophage CSF-Dependent Macrophage Phenotypes Display Differences in Cytokine Profiles and Transcription Factor Activities: Implications for CSF Blockade in Inflammation1. *J. Immunol.* **178**, 5245–5252 (2007).

107. Li, M. *et al.* Signaling pathways in macrophages: molecular mechanisms and therapeutic targets. *MedComm* **4**, e349 (2023).

108. Huang, H. *et al.* Recognition of RNA N6-methyladenosine by IGF2BP Proteins Enhances mRNA Stability and Translation. *Nat. Cell Biol.* **20**, 285–295 (2018).

109. Vukić, D. *et al.* Distinct interactomes of ADAR1 nuclear and cytoplasmic protein isoforms and their responses to interferon induction. *Nucleic Acids Res.* **52**, 14184–14204 (2024).

110. Jones, A. N., Tikhaia, E., Mourão, A. & Sattler, M. Structural effects of m6A modification of the Xist A-repeat AUCG tetraloop and its recognition by YTHDC1. *Nucleic Acids Res.* **50**, 2350–2362 (2022).

111. Liu, B. *et al.* A potentially abundant junctional RNA motif stabilized by m6A and Mg2+. *Nat. Commun.* **9**, 2761 (2018).

112. Monian, P. *et al.* Endogenous ADAR-mediated RNA editing in non-human primates using stereopure chemically modified oligonucleotides. *Nat. Biotechnol.* **40**, 1093–1102 (2022).

113. Pinello, N. *et al.* Dynamic changes in RNA m6A and 5 hmC influence gene expression programs during macrophage differentiation and polarisation. *Cell. Mol. Life Sci.* **81**, 229 (2024).

114. Alqassim, E. Y. *et al.* RNA editing enzyme APOBEC3A promotes pro-inflammatory M1 macrophage polarization. *Commun. Biol.* **4**, 102 (2021).

115. Rayon-Estrada, V. *et al.* Epitranscriptomic profiling across cell types reveals associations between APOBEC1-mediated RNA editing, gene expression outcomes, and cellular function. *Proc. Natl. Acad. Sci.* **114**, 13296–13301 (2017).

116. Medzhitov, R. & Horng, T. Transcriptional control of the inflammatory response. *Nat. Rev. Immunol.* **9**, 692–703 (2009).

117. Hargreaves, D. C., Horng, T. & Medzhitov, R. Control of inducible gene expression by signal-dependent transcriptional elongation. *Cell* **138**, 129–145 (2009).

118. Schott, J. *et al.* Translational regulation of specific mRNAs controls feedback inhibition and survival during macrophage activation. *PLoS Genet.* **10**, e1004368 (2014).

119. McAllister, C. S., Taghavi, N. & Samuel, C. E. Protein Kinase PKR Amplification of Interferon β Induction Occurs through Initiation Factor eIF-2α-mediated Translational Control. *J. Biol. Chem.* **287**, 36384–36392 (2012).

120. Sun, T. *et al.* A Small Subset of Cytosolic dsRNAs Must Be Edited by ADAR1 to Evade MDA5-Mediated Autoimmunity. 2022.08.29.505707 Preprint at https://doi.org/10.1101/2022.08.29.505707 (2022).

121. Koning, N. *et al.* Expression of the Inhibitory CD200 Receptor Is Associated with Alternative Macrophage Activation. *J. Innate Immun.* **2**, 195–200 (2010).

122. Pecori, R. *et al.* ADAR1-mediated RNA editing promotes B cell lymphomagenesis. *iScience* **26**, 106864 (2023).

123. Heraud-Farlow, J. E. *et al.* GGNBP2 regulates MDA5 sensing triggered by self double-stranded RNA following loss of ADAR1 editing. *Sci. Immunol.* **9**, eadk0412 (2024).

124. Gao, Y. *et al.* m6A Modification Prevents Formation of Endogenous Double-Stranded RNAs and Deleterious Innate Immune Responses during Hematopoietic Development. *Immunity* **52**, 1007-1021.e8 (2020).

125. Murakami, S. & Jaffrey, S. R. Hidden codes in mRNA: Control of gene expression by m6A. *Mol. Cell* **82**, 2236–2251 (2022).

126. Huang, X.-T. *et al.* HNRNPC impedes m6A-dependent anti-metastatic alternative splicing events in pancreatic ductal adenocarcinoma. *Cancer Lett.* **518**, 196–206 (2021).

127. Loh, T. J. *et al.* CD44 alternative splicing and hnRNP A1 expression are associated with the metastasis of breast cancer. *Oncol. Rep.* **34**, 1231–1238 (2015).

128. Bowling, E. A. *et al.* Spliceosome-targeted therapies trigger an antiviral immune response in triple-negative breast cancer. *Cell* **184**, 384-403.e21 (2021).

129. Zheng, R. *et al.* hnRNPM protects against the dsRNA-mediated interferon response by repressing LINE-associated cryptic splicing. *Mol. Cell* **84**, 2087-2103.e8 (2024).

130. Zheng, Y. *et al.* Mettl14 mediates the inflammatory response of macrophages in atherosclerosis through the NF-κB/IL-6 signaling pathway. *Cell. Mol. Life Sci. CMLS* **79**, 311 (2022).

131. Morley, S. C. The Actin-Bundling Protein L-Plastin: A Critical Regulator of Immune Cell Function. *Int. J. Cell Biol.* **2012**, 935173 (2012).

132. Xie, W. *et al.* m6A Reader HNRNPC Facilitates Adipogenesis by Regulating Cytoskeletal Remodeling through Enhanced Lcp1 mRNA Stability. *Aging Dis.* **16**, 1080–1098 (2024).

133. Edens, B. M. *et al.* FMRP Modulates Neural Differentiation through m6A-Dependent mRNA Nuclear Export. *Cell Rep.* **28**, 845-854.e5 (2019).

134. Sendinc, E. & Shi, Y. RNA m6A methylation across the transcriptome. *Mol. Cell* **83**, 428–441 (2023).

135. Patterson, J. B. & Samuel, C. E. Expression and regulation by interferon of a double-stranded-RNA-specific adenosine deaminase from human cells: evidence for two forms of the deaminase. *Mol. Cell. Biol.* **15**, 5376–5388 (1995).

136. Desterro, J. M. P. *et al.* Dynamic association of RNA-editing enzymes with the nucleolus. *J. Cell Sci.* **116**, 1805–1818 (2003).

137. Xiao, W. *et al.* Nuclear m(6)A Reader YTHDC1 Regulates mRNA Splicing. *Mol. Cell* **61**, 507–519 (2016).

138. Véliz, E. A., Easterwood, L. M. & Beal, P. A. Substrate analogues for an RNA-editing adenosine deaminase: mechanistic investigation and inhibitor design. *J. Am. Chem. Soc.* **125**, 10867–10876 (2003).

139. Polson, A. G. & Bass, B. L. Preferential selection of adenosines for modification by double-stranded RNA adenosine deaminase. *EMBO J.* **13**, 5701–5711 (1994).

140. Huang, H. *et al.* Recognition of RNA N6-methyladenosine by IGF2BP Proteins Enhances mRNA Stability and Translation. *Nat. Cell Biol.* **20**, 285–295 (2018).

141. Uzonyi, A. *et al.* Deciphering the principles of the RNA editing code via large-scale systematic probing. *Mol. Cell* **81**, 2374-2387.e3 (2021).

142. Tian, N. *et al.* A structural determinant required for RNA editing. *Nucleic Acids Res.* **39**, 5669–5681 (2011).

APPENDIX A. MATERIALS

Table A1. Oligonucleotides

Name	Sequence	Purpose
sgRNA_METTL3-exon1	ggctttatatatcttgtggaaaggacgaaagGCGAGAGATTGCAGCGGCGAgtttt agagctagaaatagcaagttaaaat	Guide RNA for METTL3-KO to clone into px458
sgRNA_METTL3-exon3	ggctttatatatcttgtggaaaggacgaaagGGGCGGCAAATTTCTGGAGAgtttt agagctagaaatagcaagttaaaat	Guide RNA for METTL3-KO to clone into px458
VG3_sgRNA_mNT_unmod_g1	ggctttatatatcttgtggaaaggacgaaaGCTTTCACGGAGGTTCGACGgtttt agagctagaaatagcaagttaaaat	non-targetting control guide RNA for mouse to clone into PX458 vector
VG4_sgRNA_mNT_unmod_g2	ggctttatatatcttgtggaaaggacgaaagATGTTGCAGTTCGGCTCGATgtttt agagctagaaatagcaagttaaaat	2nd non-targetting control guide RNA for mouse to clone into PX458 vector
VG6_mMETTL3ex1_fw	GGCGTCCTCGTGAGAATTAGA	Primer for amplification and sequencing of Indel in METTL3 exon 1 forward
VG7_mMETTL3ex1_rv	TTGGTGTGGTGTTACGCTTG	Primer for amplification and sequencing of Indel in METTL3 exon 1 reverse
VG8_mMETTL3ex3_fw	ATGGCAGACAGCTTGGAGTG	Primer for amplification and sequencing of Indel in METTL3 exon 3 forward
VG9_mMETTL3ex3_rv	ACACTGACTGGACTGACCCT	Primer for amplification and sequencing of Indel in METTL3 exon 3 reverse
VG17_sgRNA_Adar1ko_ex2-1340	ggctttatatatcttgtggaaaggacgaaagACTCTAACAACCCGCTGACAgtttt agagctagaaatagcaagttaaaat	Guide RNA for ADAR1-KO to clone into px458
VG18_Adar1_ex2_fw	GACGGACAAGAAGCGTGAGA	Primer for amplification and sequencing of Indel in METTL3 exon 2 forward
VG19_Adar1_in2-3_rv	ACCAAGACAGCGTAAGAGCC	Primer for amplification and sequencing of Indel in METTL3 exon 2 reverse
VG23_Exoc8_B1r2fw_ad1edit	GAAACTTAGTAACTGAGTAGAG	detect ADAR1 editing site (mouse, sine element: ADAR1 specific editing site
VG24_Exoc8_B1r2rv_ad1edit	CCCTACTCAACAACCTGAAG	detect ADAR1 editing site (mouse, sine element: ADAR1 specific editing site

eGFP_W58X_IVT_fw	AAGCTAATACGACTCACTATAGGTGAATAGTATAACAATATGC	PCR amplification for IVT
eGFP_W58X_IVT_rv	AAACTACCTGTTCCATGG	PCR amplification for IVT
VGq3_mYthdc1_ex_rv	TGGTCTCTGGTGAAACTCAGG	RT qPCR
VGq7_mCPH_fw	ATGGTCAACCCCACCGTG	RT qPCR
VGq8_mCPH_rv	TTCTTGCTGTCTTTGGAACTTTGTC	RT qPCR
VGq13_Tor1aip2_long_ex-junction_fw	TCTGGACCTATGGTTCCGTG	RT qPCR
VGq14_Tor1aip2_long_ex-junction_rv	GCTGGGCTGGGGAAGAATAG	RT qPCR
VGq17_Tor1aip2_short_ex3_fw	TGGGTCTGCTTCTGTGGTCT	RT qPCR
VGq18_Tor1aip2_short_ex3_rv	CAAGAGGGGCCAGGTAGTTC	RT qPCR
VGq37_Ifnb_fw	CAGCTCCAAGAAAGGACGAAC	RT qPCR
VGq38_Ifnb_rv	GGCAGTGTAACTCTTCTGCAT	RT qPCR
VGq50_mAdar1_ex2_fw	GATGCCCTCCTTCTACAGCC	RT qPCR
VGq51_mAdar1_ex3_rv	ATTCCCGCCCATTGATGACA	RT qPCR
VGq52_mAdar1_in2-3_rv	TCTGGGCAGTCTCTTACCGA	RT qPCR
RiboSeq_qPCR_reaction_fw	GTTCAGAGTTCTACAGTCCGA	RT qPCR
RiboSeq_qPCR_reaction_rv	CCTTGGCACCCGAGAATTCCA	RT qPCR

Table A2. Kits and reagents

Name	Product Number	Supplier
10 mM dNTP solution	N0447	NEB
12% Mini-PROTEAN® TGX™ Precast Protein Gels, 15-well	4561046	Bio-Rad
16 % Formaldehyde Solution	28908	Thermo Fisher Scientific
2-Mercaptoethanol	M3148	Sigma-Aldrich
4–15% Mini-PROTEAN TGX precast protein gels, 12-well	4561085	Bio-Rad
4–15% Mini-PROTEAN® TGX™ Precast Protein Gels, 15-well, 15 µl	4561086	Bio-Rad
50x TAE buffer	A1691	ITW Reagents
Accutase	A6964	Sigma-Aldrich
Agarose	A9539	Sigma-Aldrich
Agencourt RNAClean XP beads	A63987	Beckman
Agilent RNA 6000 Nano Kit	NC1783726	Agilent
Amaxa Cell Line Nucleofactor Kit V	VCA-1003	Lonza
Amersham Protran 0.45 NC nitrocellulose Western blotting membrane	10600002	Cytiva
ammonium acetate	A2706	Sigma-Aldrich
Ampicillin Sodium Salt	A9518	Sigma-Aldrich
ApaLI	R0507S	NEB
BbsI	R0539S	NEB
BglII	R0144S	NEB
Bovine Serum Albumin	A9418	Sigma-Aldrich
Cell Lysis Buffer (10x)	9803	cell signaling
CloneJET PCR Cloning Kit	K1232	Thermo Fisher Scientific
CloneJET PCR Cloning Kit	K1232	Thermo Fisher Scientific
cOmplete, Mini, EDTA-free Protease Inhibitor Cocktail	11836170001	Roche
CutSmart Buffer	B9000	NEB
Cycloheximide	8682.3	Roth
Direct RNA Sequencing Kit	SQK-RNA002	Oxford Nanopore
Direct RNA Sequencing Kit	SQK-RNA004	ONT
Direct-zol RNA Miniprep	R2050	Zymo research
DMSO	D2650	Sigma-Aldrich

DTT	10197777001	Sigma-Aldrich
Dulbecco Modified Eagle-Medium (DMEM) - high glucose	D6429	Sigma-Aldrich
ECL™ Start Western Blotting Detection Reagent	RPN3243	Cytiva
EDTA	46-034-CI	corning
Ethanol	32205	Sigma-Aldrich
FCS	10270-106	Gibco
Flow Cell Wash Kit	EXP-WSH004	ONT
Gel Loading Dye, Purple (6X)	B7024S	NEB
Glycin	3908.2	Roth
GlycoBlue	AM9515	Ambion
HEPES	15630-056	gibco
Human-Mouse-Rat riboPOOL Kit	dp-K096-53	siTOOLs
IFN-gamma, rec. Murine	315-05	PeproTech
IL-13, rec. Murine	210-13	PeproTech
IL-4, rec. Murine	214-14-5	PeproTech
iTaq Universal SYBR® Green Supermix	1725121	Bio-Rad
IVTpro T7 mRNA Synthesis Kit	6144	Takara
L-Glutamin (200 mM)	25030-024	Gibco
Latex beads, carboxylate-modified polystyrene, fluorescent yellow-green	L4655	Sigma-Aldrich
LB broth with agar	L2897	Sigma-Aldrich
LB broth with agar	L3022	Sigma-Aldrich
Lipofectamine 2000	11668019	Thermo Fisher Scientific
Lipopolysaccharide	L2630	Sigma-Aldrich
mCherry-T2A-eGFP W58X reporter plasmid	-	Gift from Dr. Joshua Rosenthal
Methanol	32213	Sigma-Aldrich
Midori Green Advance DNAstain	617004	Biozym
Monarch Clean UP RNA Kit	T2040	NEB
Motolimod (Synonyms: VTX-2337; VTX-378) (TLR8 agonist)	HY-13773	MCE
Mouse GM-CSF Recombinant Protein		PeproTech
N6-Methyl-ATP	NU-1101	Jena Bioscience
NEBNext Multiplex Small RNA Library Prep Kit	E7300	NEB

NEBNext Poly(A) mRNA Magnetic Isolation Module (NEB)	E7490L	NEB
NEBNext® Quick Ligation Reaction Buffer (NEB B6058)	NEB B6058	NEB
NEBNext® Quick Ligation Reaction Buffer (NEB B6058)	NEB B6058	NEB
NEBuffer 2.1	B7202S	NEB
NEBuilder HiFi DNA Assembly Cloning Kit	E5520S	NEB
NP-40	I8896	Sigma-Aldrich
nuclease free water	AM9937	ambion
Nuclease free water	AM9937	Thermo Fisher Scientific
NucleoSpin Gel and PCR Clean-up Kit	11992242	Macherey-Nagel
NucleoSpin Plasmid (NoLid), Mini Kit	740.499.250	Macherey-Nagel
PBS	D8537	Sigma-Aldrich
Penicillin-Streptomycin	P4333	Sigma-Aldrich
pENTER-U6	K4945-00	Addgene
phenol: chloroform: isoamyl alcohol	A0944	AppliChem
phenylmethylsulfonyl fluoride solution	93482	Sigma-Aldrich
pHrodo Green E. coli Bioparticles	P35366	Thermo Fisher Scientific
pHrodo Green S. aureus BioParticles	P35367	Thermo Fisher Scientific
pHrodo Green Zymosan BioParticles	P35365	Thermo Fisher Scientific
Pierce™ BCA Protein Assay Kit	23225	Thermo Fisher Scientific
Poly(I:C) LMW	tlrl-picw	InvivoGen
Polynucleotide Kinase	M0201S	NEB
PromethION RNA Flow Cell	FLO-PRO004RA	ONT
ProtoScript First Strand cDNA Synthesis Kit	E6300L	NEB
pSpCas9(BB)-2A-GFP (PX458)	48138	Addgene
PureLink™ HiPure Plasmid Maxiprep Kit	K210007	Thermo Fisher Scientific
Purified LTA-SA (TLR2 agonist)	tlrl-pslta	InvivoGen
puromycin	A11138-03	Gibco
Q5 High-Fidelity DNA Polymerase	M0491L	NEB
Qubit dsDNA HS Assay Kit	Q32851	Thermo Fisher Scientific
QuickCip	M0525	NEB
QuickExtract DNA Extraction Solution	QE0905T	Lucigen

R848 (Resiquimod) (mouse TLR7 agonist)	tlrl-r848-1	InvivoGen
Rapid DNA Dephos + Ligation Kit	4898117001	Roche
Recombinant Mouse IFN-β1 (carrier-free)	581302	Biolegend
Recombinant Murine M-CSF	315-02	PeproTech
RNase I	AM2294	Ambion
RNAse-free DNAse I	M0303	NEB
RNaseOUT™ rekombinanter Ribonuklease-Hemmer	10777019	Thermo Fisher Scientific
Rneasy Mini Kit	74104	Qiagen
RPMI-1640	R8758	Sigma-Aldrich
SDS	L3771	Sigma-Aldrich
skim milk	42590.01	Serva
Sodium chloride	s/3160/65	Thermo Fisher Scientific
STM2457	HY-134836	MedChemExpress
SuperScript™ III Reverse Transcriptase	18080044	Invitrogen
SuperSignal™ West Femto Maximum Sensitivity Substrat	34095	Thermo Fisher Scientific
SybrGreen master mix	A25742	Applied Biosystems
T4 DNA Ligase 2M U/ml (NEB M0202)	M0202	NEB
Topo™ TA Cloning™ Kit	450030	Invitrogen
Triton-X	T9284	Sigma-Aldrich
Trizma base (Tris-base)	T1503	Sigma-Aldrich
TURBO DNA-free Kit-50 reactions	AM1907	Thermo Fisher Scientific
Tween 20	P9416	Sigma-Aldrich

Table A3. Antibodies and staining

Name	Product Number	Supplier	Dilution	Application
Propodium iodide	BMS500PI	Invitrogen	1:1000	FACS
CD200 Receptor - PerCP-eFluor™ 710	46-5201-82	Thermo Fisher Scientific	1:200	FACs
CD163 - APC/Fire 810	155309	Biolegend	1:200	FACs
CD206 (MMR) - APC	17-2061-82	Thermo Fisher Scientific	1:200	FACS
CD40 - APC/fire	124632	Biologend	1:200	FACS
CD80 - PE	553769	BD	1:400	FACS
CD36 - APC	102611	Biologend	1:200	FACS
DAPI (4',6-Diamidino-2-Phenylindole)	422801	Biolegend	1:1000	FACs
LIVE/DEAD™ Fixable Violet Dead Cell Stain Kit	L34964	Thermo Fisher Scientific	1:1000	FACS
CD86 - Brilliant Violet 510	105039	Biolegend	1:200	FACs
CD369 (Dectin-1/CLEC7A) - PE	144303	biolegend	1:400	FACS
CD282 (TLR2) - APC	153005	biolegend	1:200	FACS
I-A/I-E - FITC	107605	Biolegend	1:200	FACS
β2-microglobulin - APC	154505	Biolegend	1:200	FACS
H-2 - PE	125505	Biolegend	1:400	FACS
Anti-beta-actin	A5441	Sigma-Aldrich	1:5000	WB
anti-ADAR 1	sc-73408	Santa cruz	1:500	WB
Anti-alpha Tubulin	ab4074	abcam	1:5000	WB
Anti-METTL3 antibody	ab195352	Abcam	1:1000	WB
goat anti mouse - HRP (H+L)	170-6516	Bio-Rad	1:5000	WB
goat anti rabbit-HRP (H+L)	170-6515	Bio-Rad	1:5000	WB

Table A4. Homemade buffers

Buffer	Ingredients
LC-MS/MS digestion buffer	- 0.6 U NP1 = nuclease P1 from P. citrinum - 0.2 U PDE = snake venom phosphodiesterase from *C. adamanteus* - 0.2 U CIP/BIP = bovine intestine phosphatase - 10 U Benzo = benzonase - 200 ng PS = Pentostatin - 500 ng THU = Tetrahydrouridine - 5 mM Tris (pH 8) + 1 mM MgCl2

10X Running Buffer (TGS)	30.3 g Tris-Base (Trizma) 144 g Glycine 10 g SDS Dissolve in 800 mL water. Adjust final volume to 1 L
10X Transfer buffer (TG)	30.3 g Tris-Base (Trizma) 144 g Glycine Dissolve in 800 mL water. Adjust final volume to 1 L
1X Transfer buffer	Add 100 mL 10x Transfer buffer + 200 mL Methanol + 700 mL water
10X TBS	24.2 g Tris-Base (Trizma) 80 g NaCl Dissolve in 800 mL water pH to 7.6 with 12 N HCl Adjust final volume to 1 L
TBS-T(ween) 0.1%	Add 100 mL 10X TBS to 899 mL water + 1 mL Tween 20 (100%).
Blocking buffer	5 % Milk in TBS-T 0.1% or 5% BSA in TBS-T 0.1%
FACS buffer	2 % FCS in PBS
Sorting buffer	2 % FCS in PBS, 25 mM HEPES, 2mM EDTA
4X Laemli buffer	2.5 ml 1.0 M Tris-HCl, pH 6.8 4.0 ml 10% SDS 40 ml glycerol 0.02 g/100mL bromophenol blue 100 µL 2-mercaptoethanol Adjust final volume to 10 ml with distilled water
Polysome lysis buffer	20 mM Tris-HCl buffer pH 7.4 10 mM MgCl2 200 mM KCl 1 % NP-40 100 µg/ml cycloheximide 2 mM DTT 1 tablet EDTA-free Roche cOmplete Mini Protease Inhibitor per 10 ml

Table A5. Devices

Name	Supplier
LSM 710 confocal microscope	Carl Zeiss
2100 Bioanalyzer Systems	Agilent
BD FACS Canto II	BD
Cytek Aurora Spectral Flow Cytometer	BD
BD Aria 3	BD
ChemiDoc Imaging System	Bio-Rad
CFX Connect Real-Time System	Bio-Rad
C1000 Touch Thermal Cycler	Bio-Rad
C1000 Touch Thermal Cycler	Bio-Rad
PowerPac Basic	Bio-Rad
Thermo Fisher Scientificblock TS basic	Cell Media
Centrifuge 5427R	Eppendorf
Centrifuge 5920 R	Eppendorf
NuAire incubator	ibs tecnomara
NovaSeq 6000 Sequencing System	Illumina
NextSeq550 device	Illumina
Ecotron Bacterial shaker	Infors HT
Nucleofector® II Device	Lonza
neoLabLine rotator	Neo Lab
Promethion 24 Sequencing Device	ONT
Vortex genie 2	Scientific Industries
Nanodrop spectrophotometer	Thermo Fisher Scientific
Multiskan FC	Thermo Fisher Scientific
Safe 2020 Class II Biological Safety Cabinet	Thermo Fisher Scientific